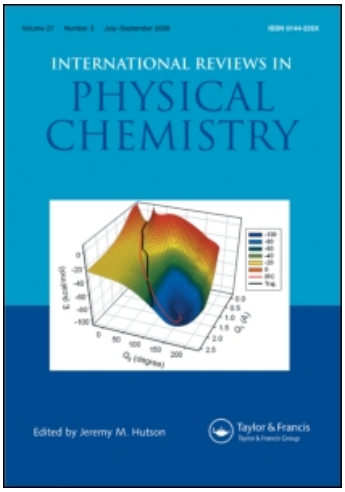

International Reviews in Physical Chemistry
Publication details, including instructions for authors and subscription information:
http://www.informaworld.com/smpp/title~content=t713724383

Tunnelling of heavy particles in the low temperature chemistry

V. A. Benderskii[a]; V. I. Goldanskii[a]
[a] Russian Academy of Sciences, Institute of Chemical Physics, Moscow, Russia

To cite this Article Benderskii, V. A. and Goldanskii, V. I.(1992) 'Tunnelling of heavy particles in the low temperature chemistry', International Reviews in Physical Chemistry, 11: 1, 1 — 70
To link to this Article: DOI: 10.1080/01442359209353265
URL: http://dx.doi.org/10.1080/01442359209353265

INTERNATIONAL REVIEWS IN PHYSICAL CHEMISTRY, 1992, VOL. 11, NO. 1, 1–70

Tunnelling of heavy particles in the low temperature chemistry

by V. A. BENDERSKII and V. I. GOLDANSKII

Russian Academy of Sciences, Institute of Chemical Physics, Moscow, Russia

The quantum dynamics of cryochemical solid-state reactions in the region of the low-temperature limit for the rate constant is considered in the framework of multidimensional nuclear tunnelling when low-frequency displacements of heavy particles lead to the formation of reaction complexes with high barrier transparency.

1. Introduction

The Arrhenius temperature dependence $K(T)$ of the rate constant is a universal law of chemical kinetics. The basic concept underlying this law treats a chemical conversion as surmounting a potential barrier of height V_0 between the states of reactants and products. Since in condensed media the transition occurs in thermal equilibrium, and the barrier height is much over the mean thermal energy ($V_0 \gg k_B T$), the transition probability is small and proportional to the population of the excited reactant states near the barrier top, i.e. $\exp(-V_0/k_B T)$. It follows from the Arrhenius law that even when the activation energies are quite small, the chemical reaction rates become non-observable at sufficiently low temperatures. For example, if $V_0 = 1\,\text{kcal(mol)}^{-1}$ and the prefactor has a typical value $k_0 = 10^{13}\,\text{s}^{-1}$, then $K(T) < 10^{-9}\,\text{s}^{-1}$ at $T \leqslant 10\,\text{K}$.

The advance of quantum mechanics not only ascertained the nature of chemical bonding and provided the description of the reaction potential energy surfaces (PES) (see, eg. [1]), but also revealed the possibility of tunnelling through a barrier. Wigner [2] was the first to note that the tunnelling near the barrier top increases the pre-exponential factor of the rate constant. Bell had shown in a series of papers [3–5] on proton transfer in liquids, that tunnelling reduces the apparent activation energy

$$E_a = k_B T^2 \partial \ln K / \partial T. \tag{1.1}$$

whereas the isotope H/D effect increases as the temperature drops. Similar effects have been observed later in the gas-phase reactions [6]. In those papers the nuclear tunnelling was considered as an effect, inherent in the thermally excited states, which leads merely to corrections to the Arrhenius law.

In 1959 one of the authors [7] showed for the first time that tunnelling from the ground state plays the major role in the transition at sufficiently low temperatures when the populations of the excited states are exponentially small. The rate constant becomes independent of the temperature and reaches its low-temperature limit K_0†. According

† In [3] the transition over the truncated parabolic barrier ($V(Q) = 0$ at $Q > d$ was considered, d is the barrier width at $E = 0$). The possibility of existence of the low-temperature limit, pointed out in this paper, was based on the incorrect assumption of finite barrier transparency at $E = 0$. As shown in [7], the latter is due to the zero-point vibrations in the initial state.

0144-235X/92 $3·00

to [7], the turnover between this limit and the Arrhenius region occurs at the characteristic cross-over temperature, depending on the barrier height and the mass of the tunnelling particle:

$$k_B T_c = r(\hbar^2 V_0/2md^2)^{1/2}, \tag{1.2}$$

where d is the barrier width, r is the factor of the order of 1, depending on the barrier shape.† The low-temperature limit is connected to V_0 and T_c by the following relation:

$$K_c = AK_0 \exp(-V_0/k_B T_c), \tag{1.3}$$

where the coefficient $A \cong k_B T_c/V_0$ characterizes the reduction of $K(T)$ in the intermediate region between the Arrhenius law and the low-temperature plateau.

The experimental studies, performed since the 1970s, have confirmed the two basic consequences of the tunnelling concept, pointed out in [7], namely the existence of the low-temperature rate constant limit and the cross-over temperature bordering this limit and the Arrhenius dependence. By now the low temperature limit has been found for more than 50 chemical reactions, and the number of examples grows steadily. This question has been systematically elucidated in [8–11]. In the present review the main attention is focused on the molecular-dynamical models developed intensively of late.

2. Quantum low-temperature limit and cross-over temperature

As noted before, the rate constant results from averaging the transition probability $w(E)$ as follows:

$$K = z_0^{-1} \int_0^\infty \rho(E) w(E) \exp(-E/k_B T)\, dE, \tag{2.1}$$

where Z_0 is the partition function in the initial state and $\rho(E)$ is the energy level density in its spectrum. In the semiclassical approximation the probability of surmounting the barrier $V(Q)$ along the reaction coordinate Q per unit energy interval at $E < V_0$ is given by

$$w(E) = (2\pi\hbar)^{-1} \exp\left[-\frac{2}{\hbar} S(E)\right], \qquad S(E) = \int_{Q_1(E)}^{Q_2(E)} \{2m[V(Q) - E]\}^{1/2}\, dQ, \tag{2.2}$$

where Q_1 and Q_2 are the turning points i.e. the borders of the classically unavailable energy regions, in which $V(Q_1) = V(Q_2) = E$ (figure 1 (*a*)). When $E > V_0$, $w(E) \cong 1$. It follows from (2.1) and (2.2) that:

$$K/K_0 = \frac{1}{K_B T} \int_0^{V_0} \exp\left[-\frac{E}{K_B T} - \frac{2}{\hbar} S(E)\right] dE + \exp\left(-\frac{V_0}{k_B T}\right). \tag{2.3}$$

The second term in (2.3) accounts for the usual Arrhenius dependence, coming from the thermally activated over-barrier transitions, while the first term describes tunnelling. Approximating the barrier near its top by a parabola and, consequently, determining a characteristic upside-down barrier frequency ω_B:

$$V(Q) = V_0 - \frac{m\omega_B^2}{2} Q^2, \tag{2.4}$$

† For the rectangle, parabolic and triangle barriers and for the adiabatic parabolic terms r equals 1/2, $2/\pi$, 3/4 and 1, respectively.

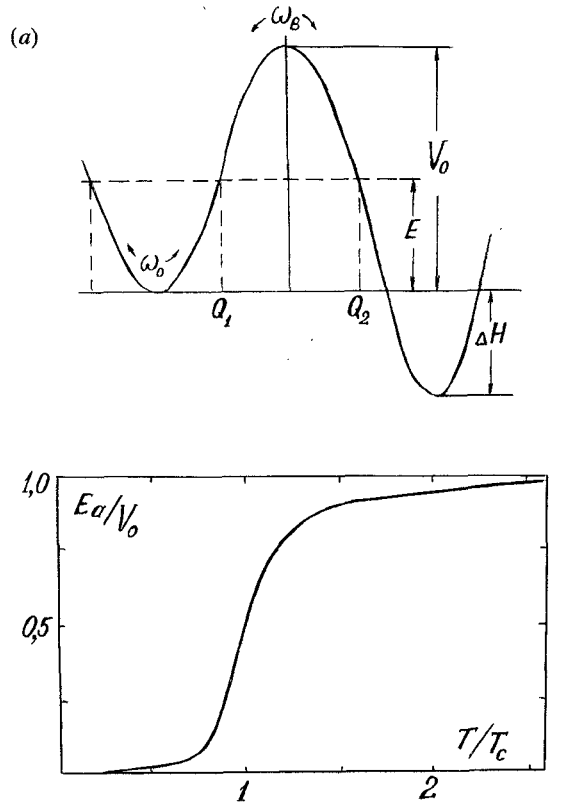

Figure 1. (*a*) Tunnelling throughout a one-dimensional barrier along the coordinate of exoergic reaction. $Q_1(E)$, $Q_2(E)$ are the turning points, ω_0 and ω_B frequencies of vibrations at the minimum of the term and in the upside-down barrier. (*b*) Apparent activation energy plotted against temperature, T_c is cross-over temperature. Parabolic barrier, $V_0/k_BT_c=30$. With the zero-point vibrations taken into account the energy is marked off from the $\hbar\omega_0/2$ level, in the Arrhenius region $E_a=V_0-\hbar\omega_0/2$.

one finds that the relative contributions of sub- and overbarrier transition are determined by the dimensionless parameter ξ:

$$\xi=\frac{\delta}{\lambda}=\left(\frac{2k_BT}{\hbar\omega_B}\right)^{1/2}, \tag{2.5}$$

which equals the ratio of the zero vibration amplitude in the upside-down barrier ($\delta^2=\hbar/m\omega_B$) and the thermal de Broglie wavelength ($\lambda=\hbar/(2mk_BT)^{1/2}$). The classical region $\xi\gg1$ corresponds to the Arrhenius law where $E_a=V_0$. In the quantum region ($\xi<1$) $K(T)$ passes on to the low temperature limit where $E_a=0$ and $K=K_c$ (figure 1 (*b*)). The apparent activation energy is determined by the narrow region of energies where the sum $E/k_BT+2S(E)/\hbar$ has a minimum, corresponding to the equation [12]:

$$\frac{\hbar}{k_BT}=\int_{Q_1(E_a)}^{Q_2(E_a)}\left[\frac{2m}{V(Q)-E_a}\right]^{1/2}\mathrm{d}Q. \tag{2.6}$$

The right-hand side of (2.6) is the period of vibration in the upside-down barrier $\tau(E_a) = \hbar/k_B T$. In terms of the apparent activation energy from (2.6), the rate constant can be expressed as

$$K/K_0 = \exp\left[-\frac{2}{\hbar}S(E_a)\right]\exp\left(-\frac{E_a}{k_B T}\right), \tag{2.7}$$

which demonstrates that tunnelling reduces both the activation energy and prefactor. The low values of the prefactor formally correspond to the large negative entropy of the activation:

$$\Delta S^{\neq} = -\frac{2}{\hbar}k_B S(E_a). \tag{2.8}$$

Although the reasons of its appearance have nothing to do with the change of initial partition function [1], typical values of $K_c = 10^{-1}$–10^{-5} correspond to $-\Delta S_c^{\neq} = 65$ $-83\,\text{kcal}\,(\text{mol})^{-1}$. Since in the solid-state reaction only the vibrational degrees of freedom take place, the negative values of the activation entropy mean the increase of the frequencies in the transition state, compared to the initial state ($\omega_k^{\neq} - \omega_k^{i} > 0$). For classical vibrations ($\hbar\omega/2k_B T \ll 1$) $\Delta S^{\neq}$ is given by

$$\Delta S^{\neq} = -k_B \sum_{k=1}^{N} \ln\frac{\omega_k^{\neq}}{\omega_k^{i}}, \tag{2.9}$$

where N is the number of changing-frequency vibrations. For $(\omega_k^{\neq} - \omega_k^{i})/\omega_k^{i} \ll 1$, the above-mentioned values of $\Delta S^{\neq}$ would correspond to the tremendous number of the classical degrees of freedom involved in the transition ($N > 10^2$), and in the quantum region N has to be even greater. The increase of frequencies would mean the increase in the barrier height due to the higher zero-point energies in the transition state. For this reason, the cooperative mechanism of solid-state cryochemical reactions could not be considered as an alternative to the tunnelling.

The values T_c and K_c/K_0 calculated for the tunnelling transfer of the H atom throughout the parabolic barrier are represented in table 1, illustrating the role of the tunnelling length which is a new parameter in the chemical kinetics specific for the low temperature reactions which does not enter the Arrhenius law. The variation of this length leads to the change in $K(T)$ at $T < T_c$ by 10–15 orders of magnitude.

As follows from (2.3), the Arrhenius region is separated from the low-temperature plateau by a sufficiently wide intermediate region ($\Delta T \cong 1/2\ T_c$), in which the change in $K(T)$ is relatively small (by $\cong V_0/k_B T$ times). For the quantitative description it is necessary to examine the change in the character of motion which accounts for the behaviour of the prefactor near T_c. At $T \gg T_c$ when $E_a = V_0$ the classical transition *via* the saddle-point occurs. When approaching T_c, the contribution of quantum fluctuations increases, compared to the thermal energy, which leads to the growth of the contribution of thermally activated particles possessing energies slightly lower than the barrier height and tunnelling throughout the rest of the barrier. For such transitions the tunnelling probabilities are not exponentially small and the semiclassical approximation (2.2) breaks down. Both effects increase K_0, as compared to the prefactor in the classical transition state theory K_{TST}^0:

$$K_0 = K_{TST}^0 f_q(T). \tag{2.10}$$

The tunnelling factor increases near T_c and equals unity at $T \gg T_c$.

Table 1. T_c and K_c/K_0 values for surmounting a static parabolic barrier by hydrogen atom.

V_0|d, Å kcal (mol)$^{-1}$	0·4	0·6	0·8	1·0	1·2	1·4	1·6	1·8
6	432 $9{\cdot}2\times10^{-4}$	288 $2{\cdot}8\times10^{-5}$	216 $8{\cdot}5\times10^{-7}$	173 $2{\cdot}6\times10^{-8}$	144 $7{\cdot}9\times10^{-10}$	123 $2{\cdot}4\times10^{-11}$	108 $7{\cdot}2\times10^{-13}$	96 $2{\cdot}2\times10^{-14}$
8	499 $3{\cdot}1\times10^{-4}$	333 $5{\cdot}5\times10^{-6}$	250 $9{\cdot}8\times10^{-8}$	199 $1{\cdot}7\times10^{-9}$	166 $3{\cdot}1\times10^{-11}$	142 $5{\cdot}5\times10^{-13}$	124 $9{\cdot}6\times10^{-15}$	110 $1{\cdot}7\times10^{-16}$
10	558 $1{\cdot}2\times10^{-4}$	372 $1{\cdot}3\times10^{-6}$	279 $1{\cdot}5\times10^{-8}$	223 $1{\cdot}6\times10^{-10}$	186 $1{\cdot}8\times10^{-12}$	159 $1{\cdot}9\times10^{-14}$	139 $2{\cdot}1\times10^{-16}$	124 $2{\cdot}3\times10^{-18}$
12	611 $5{\cdot}1\times10^{-5}$	407 $3{\cdot}6\times10^{-7}$	305 $2{\cdot}6\times10^{-9}$	224 $1{\cdot}9\times10^{-11}$	204 $1{\cdot}3\times10^{-13}$	175 $9{\cdot}5\times10^{-16}$	153 $6{\cdot}8\times10^{-18}$	136 $4{\cdot}9\times10^{-20}$

In the classical transition state theory the rate constant is determined by the statistically averaged flux of particles with the energy $E=P^2/2m+V(Q)$ across the dividing surface in the phase space (P,Q):

$$K=\int_0^\infty \frac{p}{m}\exp\left[-\frac{E(P,Q)}{k_BT}\right]\theta(E-V_0)\,dP. \tag{2.11}$$

The presence of the step function $\theta(E-V_0)$, equal to 0 and 1 at $E<V_0$ and $E\geqslant V_0$, respectively, implies the possibility of the over-barrier transition solely. In the variables (E,t), instead of (P,Q), the frequency factor is introduced by normalizing the distribution function [13]:

$$K_0^{-1}=\frac{1}{k_BT}\int_0^\infty t(E)\exp\left(-\frac{E}{k_BT}\right)dE. \tag{2.12}$$

The sojourn time in the reactant valley $t(E)$ at $V_0\gg k_BT$ equals the vibration period in the initial state $2\pi/\omega_0$ and corresponds to the closed classical trajectories at $E<V_0$ in this valley. Expression (2.1), in contrast to (2.11), incorporates the tunnelling trajectories for which the transition probability is finite when $E<V_0$. Near the cross-over point there arises a new extremal trajectory named instanton, for which the total action $S_L(E)=S(E)+E/k_BT$ ($S(E)$ is defined in (2.3)) is less than the classical one $\hbar V_0/k_BT$. Unlike the classical motion, the tunnelling occurs instantaneously in real time (the term instanton originates from this fact), while in imaginary time it is a vibration with the period $\hbar/k_BT$, as determined by (2.6). Imaginary-time finite trajectory of the over-barrier transition corresponds to the dwelling near the unstable equilibrium positions of the upside-down potential (the minima of initial and final states). Therefore, the change in dynamics of motion near T_c consists of the appearance of the instanton in exchange for the trivial saddle-trajectory [14]. As shown in [15], the appearance of the instanton is similar to the second-order phase transition. Because of the sharp variation of K_0 the intermediate region of $K(T)$ turns out to be quite narrow

$$\left(\Delta T\lesssim\tfrac{1}{2}T_c\frac{k_BT_c}{V_0}\right).$$

The previous discussion of $K(T)$ clearly does not take into account the interaction of reactants with the medium, like in the usual transition state theory. According to Kramers' idea [16], this interaction can be incorporated by introducing a random force along with a friction coefficient γ into the equation of motion. The general solution of the Kramers' problem has been obtained in [17]. As shown recently [18, 19], the value of γ comes from the coupling coefficients characterizing the interaction of the reaction coordinate with the medium coordinates. This coupling ensures the settling of the thermal equilibrium and changes the character of motion across the saddle-point from the free translational one to the spatial diffusion when $\gamma/\omega\gg 1$. The Kramers' problem has been generalized to the temperatures near cross-over point $T\cong T_c$ by many authors (see, e.g. [20–24] and review [25]). The presence of friction reduces the rate constant (at $T>T_c$) by the factor ω_R/ω_B, as prescribed by the following relation:

$$K(T)=f_q\frac{\omega_0}{\omega_B}\exp\left(-\frac{V_0}{k_BT}\right), \tag{2.13}$$

where ω_R is the Kramers' frequency:

$$\omega_R=\omega_B[(1+\alpha^2)^{1/2}-\alpha],\qquad \alpha=\frac{\gamma}{2\omega_B}. \tag{2.14}$$

ω_0 is the frequency of the Q vibrations in the initial state. The cross-over temperature drops as the friction increases:

$$k_B T_c = \frac{\hbar \omega_R}{2\pi}. \tag{2.15}$$

At small γ the tunnelling factor f_q is described immediately by the relationship for the parabolic barrier [26]:

$$f_q = \frac{\omega_B \sinh(\hbar\omega_0/2k_B T)}{\omega_0 \sin(\hbar\omega_B/2k_B T)}, \qquad T > T_c. \tag{2.16}$$

As γ increases, the intermediate region widens due to both the decrease in T_c and, at the same time, increase in f_q. The numerically calculated $K(T)$ for the model cubic potential

$$V(Q) = \frac{27}{4} V_0 \frac{Q^2}{d^2}\left(1 - \frac{Q}{d}\right) \tag{2.17}$$

is represented in figure 2 for different γs [23]. The increase in γ affects only the prefactor in the classical region but exponentially reduces the transition probability in the

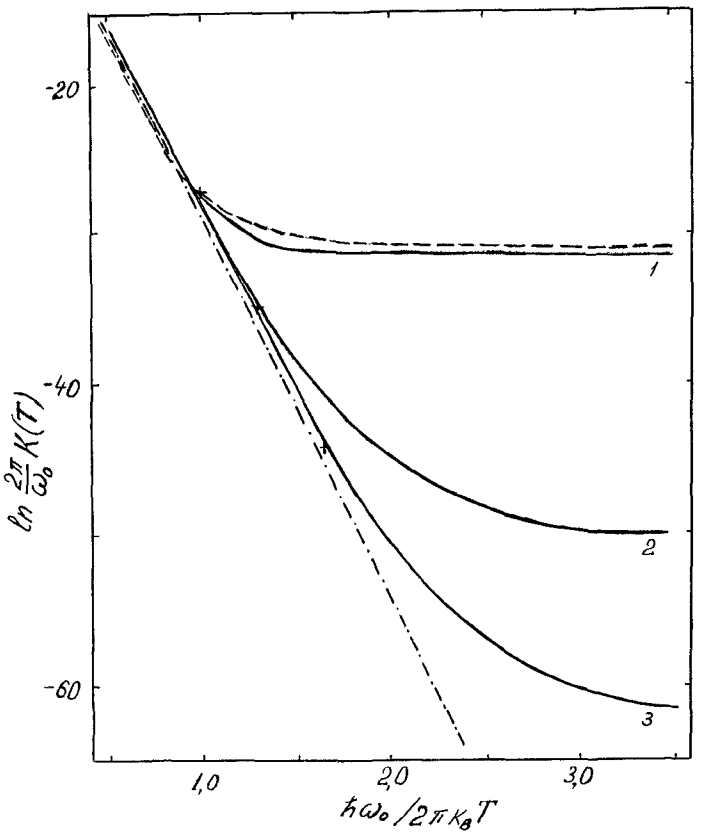

Figure 2. The temperature dependence of the decay rate in a metastable state (cubic potential (2·17)) for different coefficients of frequency-independent friction [23]. $V_0 = 5\hbar\omega_0$, $\alpha = 0$, 0·25 and 0·5 for curves 1–3, respectively. The T_c points are marked by crosses. The dashed line shows the $K(T)$ dependence for a parabolic barrier with the same V_0 and $\hbar\omega_0$, the dashed–dotted line is the Arrhenius dependence.

quantum region. At sufficiently large γ the low-temperature limit is not reached at all. When dissipation is due to the coupling to the continuous bath spectrum with the spectral density $\rho(\omega)$, the frequency coefficient depends, in general, on frequency:

$$\gamma(\omega)=\frac{\pi}{2}\frac{\rho(\omega)}{\omega^2}\lambda^2(\omega), \tag{2.18}$$

where $\lambda(\omega)$ is the parameter of coupling to the vibration with frequency ω. In the three-dimensional lattice $\rho(\omega)\propto\omega^2$, and the case of frequency-independent (Ohmic) friction studied in [23,24] is realized when the coupling parameter λ is constant. For this reason friction remains even at $T\to 0$ as a result of coupling to the low-frequency vibrations, ensuring the decrease in K_e and T_c. The linear coupling with the bath gives rise to displacements of the equilibrium positions of vibrations Δq_k (in the mass-weighted units) during the transition. This displacement is characterized by the reorganization energy proportional to γ in the case of frequency-independent λs:

$$E_s=\frac{1}{2}\sum_k \omega_k^2(\Delta q_k)^2=\frac{1}{\pi}\omega_D\gamma b^2, \tag{2.19}$$

where b is the displacement along the reaction coordinate and ω_D is the Debye frequency. The assumption for the coupling parameters to be frequency-independent, leading to the Kramers' problem, is not likely to hold. It rather should be expected that the reaction coordinate is coupled strongly to a few vibrations from the closest neighbourhood with frequencies near ω_D, and is weakly coupled to the vibrations with longer wavelengths. Therefore, instead of introducing a phenomenological friction coefficient, a microscopic study of the multidimensional motion of the reaction complex and its environment is needed. This is the purpose which the next section is aimed at.

Comparing the above-described theoretical dependencies with experimental data one should keep in mind, in the first place, that, because of the limited temperature range available and the existence of the intermediate region, it is hard to measure $K(T)$ in both the true Arrhenius region and low temperature plateau at the same time. For this reason the experimentally measured activation energies E_a prove to be several times smaller than V_0. The behaviour of $K(T)$ in the intermediate region and dependence of T_c on the barrier shape and transfer conditions (friction coefficient), do not allow the extraction of T_c and V_0 from experimental data without additional assumptions.

In the first papers [27–29] devoted to the analysis of the experiment the values of V_0 were supposed to be the same as in the gas-phase reactions and the barrier widths were found by fitting the experimental curves $K(T)$ and theoretical dependence (2.3). For

Table 2. Effective tunnelling length for hydrogen atom in the reactions $CH_3+RH=CH_4+R\cdot$ [27]†.

Matrix	K_e, s^{-1}	T_e, K‡	V_0, kcal $(mol)^{-1}$	d, Å
CH_3OH	2×10^{-4}	45	11·9	1·08
C_2H_5OH	3×10^{-4}	47	12·1	1·04
CH_3CN	$1{\cdot}4\times10^{-5}$	44	14·3	0·93

† Symmetric Gaussian barrier.
‡ Calculation according to (1.2).

example, the results from [29] are represented in the table 2 for the reaction of abstraction of hydrogen atom by CH_3 radical from molecules of different matrices.

Although such a comparison (assuming $\gamma = 0$) gives satisfactory agreement between experiment and calculation, the d values found are in contradiction with the data on lengths and potential curves for the bonding well-known from the spectroscopy.

For the reaction $AB + C \rightarrow A + BC$ the one-dimensional model of tunnelling in a static potential supposes that transition occurs at fixed A–C distance corresponding to the initial state minimum, and the tunnelling length is equal to

$$d = R^0_{AC} - R^0_{AB} - R^0_{BC}. \tag{2.20}$$

The calculation of the PES for the methyl radical reactions analogous to the ones given in table 2 shows that the CH-bond length in transition and initial states is 1·23–1·28 Å

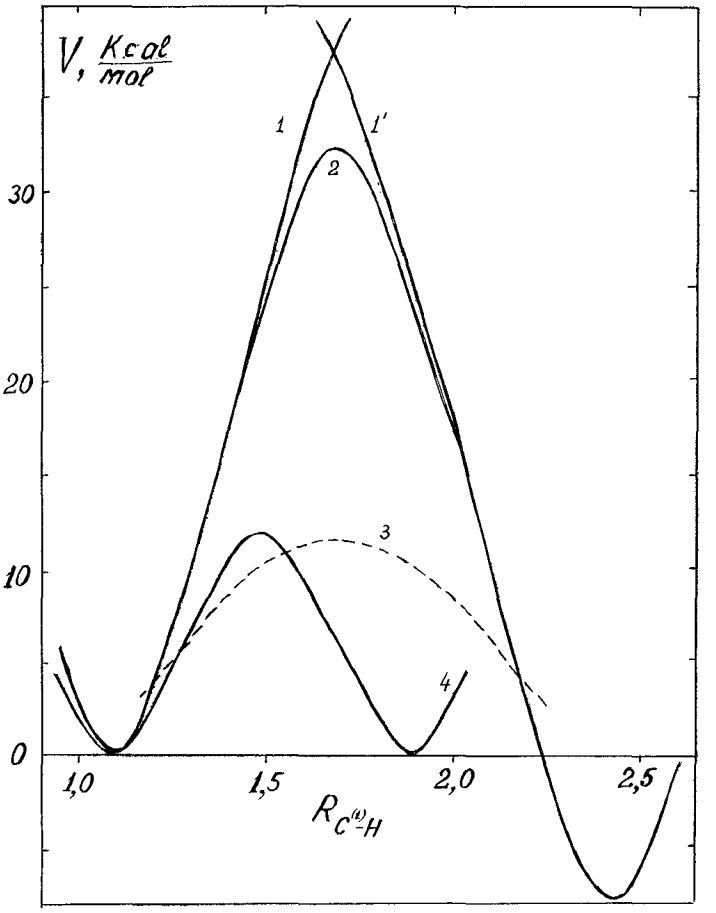

Figure 3. PES cross-sections for the reaction $C^{(1)}H_3 + C^{(2)}H_3OH \rightarrow CH_4 + CH_2OH$ ($\Delta H = -8{\cdot}1$ kcal (mol)$^{-1}$, $V_0 = 12$ kcal (mol)$^{-1}$ for the distance $C^{(1)} - C^{(2)}$ corresponding to the tunnelling distance of the hydrogen atom 1·0 Å. 1, 1′ are the Morse curves for the initial and final states; 2 is the double-well potential taking into account the adiabatic splitting borrowed from [31]; 3 is the parabolic barrier fitting expression (1·3) for the experimental dependence $K(T)$, the reference energy is the zero-point level 4·2 kcal (mol)$^{-1}$; 4 is the potential curve for passing through the saddle-point in the exchange gas-phase reaction $CH_3 + CH_4 \rightarrow CH_4 + CH_3$ of approximately the same barrier height [31].

and 1·07–1·08 Å, respectively [30]. The distance between the C atoms in the reaction complex is equal to 2·7–2·8 Å and the displacement of hydrogen atom does not exceed 0·54–0·58 Å. It is this displacement which corresponds to the barrier height measured for the gas-phase reactions. However, for these barrier parameters the value of T_c would exceed 500 K† while the observed values are $T_c \cong 50$ K. If one started from the d values calculated from the experimental data, the barrier height would go up to 30–40 kcal $(\text{mol})^{-1}$, making any reaction impossible. This disparity between V_0 and d is illustrated in figure 3 where PES cross-sections for the transition *via* the saddle-point and for the values of d found in [29] are shown.

Because of the correlation between V_0 and d, it is important for understanding the mechanism of the solid-state reactions that the van der Waals distances between the reactants in a lattice are much longer than in gas-phase reaction complexes. For instance, for the reactions in question the C–C distance corresponding to the minimum of the atom–atom potential is 3·7 Å [32], so that the displacement of the H atom in the fragment $C^{(1)}$–H...$C^{(2)}$ should exceed 1·5 Å (1·3 Å if the zero-point energy is taken into account). Therefore, to describe quantitatively the solid-state reactions it is necessary not only to explain the $K(T)$ dependencies from interrelated V_0 and d values, but also to reconcile these values with the inter-reactant distances in the lattice. Obviously, these requirements cannot be met in the framework of a one-dimensional model.

In conclusion of this section consider the relation of the rate constant to the enthalpy of the reaction ΔH. It is known that the activation energy in the Arrhenius region depends on ΔH *via* the empirical Broensted–Polanyi–Semenov rule which reads:

$$V_0(\Delta H) = V_0(0) + \alpha \Delta H, \qquad 0 < \alpha < 1. \tag{2.21}$$

Usually the symmetry coefficient α is close to 1/2. Equation (2.21) where $\alpha = 1/2$ corresponds, particularly, to the PES formed by two intersecting multidimensional paraboloids with similar frequencies. In this case the diminishing in the barrier height and the action S_Q from (2.2) at $E = 0$ are equal to [11]:

$$\begin{aligned} V_0(\Delta H) &= V_0(0)\left[1 + \frac{\Delta H}{4V_0(0)}\right]^2, \qquad -\Delta H < 4V_0(0), \\ S_Q(\Delta H) &= S_Q(0)\left\{1 + \frac{\Delta H}{4V_0(0)}\left[1 - \ln\frac{|\Delta H|}{4V_0(0)}\right]\right\}. \end{aligned} \tag{2.22}$$

Since $S_Q(\Delta H)$ drops faster than $V_0(\Delta H)$ as $-\Delta H$ increases, the crossover temperature grows with the reaction exoergicity. In the low-temperature region the rule similar to (2.21) holds: the rate constant grows exponentially with $-\Delta H$ whereas an effective symmetry coefficient at $T < T_c$ is greater than in the Arrhenius region (figure 4). The increase in α is due to both lowering and narrowing of the barrier because of more sharp descent to the product valley as $-\Delta H$ increases. This reasoning applies to the exoergic reactions. For the endoergic reactions ($\Delta H > 0$) the lower bound in the integral (1.1) should be replaced by ΔH since the tunnelling is possible only at $E \geqslant \Delta H$. Therefore, when $T < T_c$, the activation energy of endoergic reactions does not vanish but reaches its lower limit equal to $\Delta H < V_0$.

† The substantial role of tunnelling effects in the gas-phase reactions has been already noted in [6].

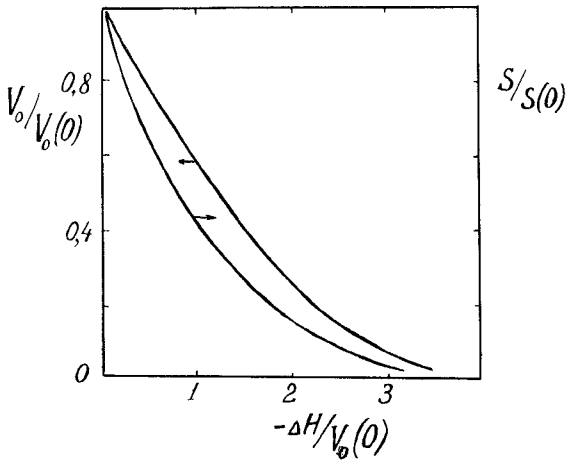

Figure 4. Rate constant plotted against the heat effect of an exoergic reaction in the Arrhenius region: $-\ln K/K_0 = V_0(\Delta H)/k_B T$ and at the low-temperature limit $-\ln K/K_0 = 2S(\Delta H)/\hbar$ for the model of one-dimensional parabolic terms.

3. Multidimensional nuclear tunnelling

As pointed out in the previous section, the model of one-dimensional tunnelling is in quantitative disagreement with molecular characteristics of reactants: if the atoms were positioned in the equilibrium sites of a lattice, the tunnelling length would correspond to the barrier so high that any reaction would be impossible. Meanwhile, the observed values of activation energies at $T > T_c$ are close to their values for the gas-phase reactions E_g in which nothing prevents the reactants from rapprochement up to the distances less than those in a lattice. The evaluation of V_0 by using (1.3) yields the values which at least do not exceed E_g. The cross-over temperatures are not in accordance with (1.2). Although there is some tendency towards decrease in T_c for heavy particle transfer, compared to the calculations, but it is far from the expected dependence $T_c \sim m^{-1/2}$. Finally, it is worth noting that the cryochemical rate constants are very sensitive to the properties of the solid state. In particular, the reaction rates in glasses differ drastically from those in crystals [11]. Hence, it follows from the experimental data that, except for the tunnelling of a particle itself (accompanied by rupture of a chemical bond in the initial state), the transition is assisted by an additional motion in the solid state (quantal below T_c). This motion brings the reactants together from the van der Waals positions up to the distances similar to those in the gas-phase reactions. The only additional motion of this type is the low-frequenty vibrations of the molecular skeleton and the intermolecular vibrations. The model incorporating the effect of these vibrations on the cryochemical reaction rate has been put forth in [33–35], which meant proceeding to the analysis of the multidimensional motion instead of a one-dimensional one. The necessity for such analysis ensues not only from the comparison of experiment with the one-dimensional model, but also from the advance of the general chemical reactions theory at large.

The model of the one-dimensional tunnelling is based on the following assumptions:

(i) The reaction coordinate is selected from the total set of the system coordinates;
(ii) The energy spectra of the initial and final states are continuous;
(iii) The thermal equilibrium continues during the transition.

All the three assumptions are, in Wigner's terminology, fundamental notions of the transition state theory [2] and hold for the classical over-barrier motion. The existence of a one-dimensional reaction path was postulated at the beginning of the 1930s by Eyring [36]. In the mid 1960s the first papers [37, 38] appeared devoted to the possibility of choosing a reaction path on the multidimensional PES, leading further (see reviews [39, 40]) to the multidimensional models for chemical conversions. Unlike the static potential $V(Q)$ in one-dimensional models, the multidimensional model deals with the dynamic barrier dependent on the vibrational coordinates. As an illustration, let us consider the collinear reaction $AB+C\rightarrow A+BC$. It is known that the classical collinear motion of the linear system ABC relative to its centre-of-mass can be reduced to the motion of the effective mass

$$m=\left(\frac{m_A m_B m_C}{m_A+m_B+m_C}\right)^{1/2} \tag{3.1}$$

in the two-dimensional potential $U(r, R)$ which is obtained from the PES $U(R_{AB}, R_{BC})$ by scaling the R_{AB} and R_{BC} coordinates and reducing the angle between the axes from $\pi/2$ to β:

$$\beta=\tan^{-1}\frac{m_B}{m}. \tag{3.2}$$

This motion is essentially two-dimensional and only for certain limits (the approximations of a slow and fast transition which will be introduced further) it can be separated to the translational motion along the reaction coordinate and transversal vibrations [39, 40]. In the event of a light atom B ($m_B \ll m_A, m_C$—such reactions are referred to as HLH), the reactant and product valleys are narrow in the (R, r) coordinates and, according to (3.2), the angle between them is small (figure 5). The motion along the valley corresponds to the respective displacement of the heavy particles A and C, while the transversal motion means vibration of the light atom near one of the heavy atoms. Since the potential profile of these fast vibrations changes but slightly over their period, the motion of B occurs at fixed values of R_{AC}, each of them corresponding to its own barrier. There is no single static barrier, and instead of the classical trajectory passing through the saddle-point, a set of the 'cutting-corner' trajectories is realized, each of which corresponding to a certain R_{AC} value. The rate constant then is determined by averaging of the transition probability over the distribution of R_{AC}, This approach has been put forward in [41] (see also [6]) and then developed in [33, 42–45] for the

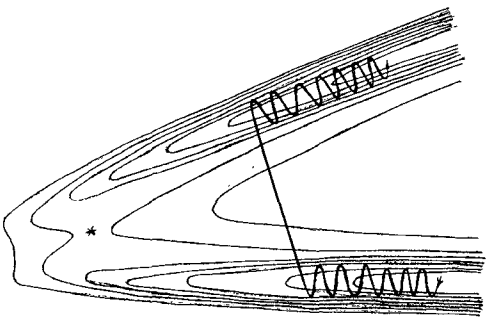

Figure 5. PES contour plot for collinear exchange reaction $AB+A\rightarrow A+BA$ for $m_B \ll m_A$. * is the saddle-point coordinate. A 'cutting corner' trajectory is shown [33, 44].

reactions of hydrogen transfer in the gas-phase reactions. As pointed out in [41], the motions cannot be treated separately when the parameter ξ, defined by (2.5), is less than unity.

As applied to the solid-phase reactions, the model described corresponds to the existence of the low-frequency intermolecular vibration A–BC bringing the reactants closer (without rupture of the bond AB) compared to their equilibrium lattice positions. This intermolecular displacement modulates the barrier corresponding to the rupture of the bond B–C and formation of the new bond A–B (figure 6). If the typical barrier frequency defined by (2.4) is greater than the frequency of the intermolecular vibration Ω (the period of motion in the barrier is less than that of longitudinal vibrations in the reactants valley)

$$\omega_B \gg \Omega, \tag{3.3}$$

the fast transition throughout the barrier takes place during which the intermolecular coordinate is fixed, as shown in figure 5. In order to get simple analytical expressions elucidating the basic features of the model, in [32] the rate constant is found for the potential formed by two parabolic terms modelling the bonds AB and BC. When the slope of the final term (AB–C) is much steeper than that of the initial one (i.e. in case of the sharp descent to the product valley), the transition probability at fixed value of intermolecular displacement q_1 is close to the probability to reach the saddle-point:

$$w(Q_0, q_1) = w_0 \exp\left[\frac{(Q_0 - q_1)^2}{\delta_0^2}\right], \tag{3.4}$$

where Q_0 is the distance between the minimum of the initial term and the barrier top at $q_1 = 0$. In the model of the fast transition one should average $w(Q_0, q_1)$ over the distribution of q_1

$$p(q_1) = \frac{1}{\delta_1 \sqrt{\pi}} \exp\left(-\frac{q_1^2}{\delta_1^2}\right). \tag{3.5}$$

The r.m.s. amplitudes of vibrations for the intra- and intermolecular coordinates (δ_0 and δ_1, respectively) are determined by the expressions:

$$\delta_0^2 = \frac{\hbar}{m\omega} \coth \frac{\hbar\omega}{2k_B T}, \qquad \delta_1^2 = \frac{\hbar}{M\Omega} \coth \frac{\hbar\Omega}{2k_B T}. \tag{3.6}$$

Equations (3.4) and (3.5) result in

$$K(T) = w_0 \frac{\delta_0^2}{(\delta_0^2 + \delta_1^2)^{1/2}} \exp\left(-\frac{Q_0^2}{\delta_0^2 + \delta_1^2}\right). \tag{3.7}$$

The relation (3.5) is equally valid for the harmonic oscillator displacement and for the Gaussian distribution of fluctuations of a random value q_1 [46]. For this reason the modulation of a barrier caused, in general, by the fluctuations of the intermolecular distances, is referred to as the fluctuational barrier preparation [9, 11]. According to (3.5), the probability of the fluctuation, for which $q_1 \cong Q_0 \gg \delta_1$, is exponentially small. However it is comparable also with the exponentially small transition probability of a barrier (3.4), so that the fluctuational barrier preparation is quite effective in the usual situation when $\delta_1 \geqslant \delta_0$ [9, 11]. The model of fluctuational barrier preparation was studied in [47, 49] for the hydrogen transfer in metals.

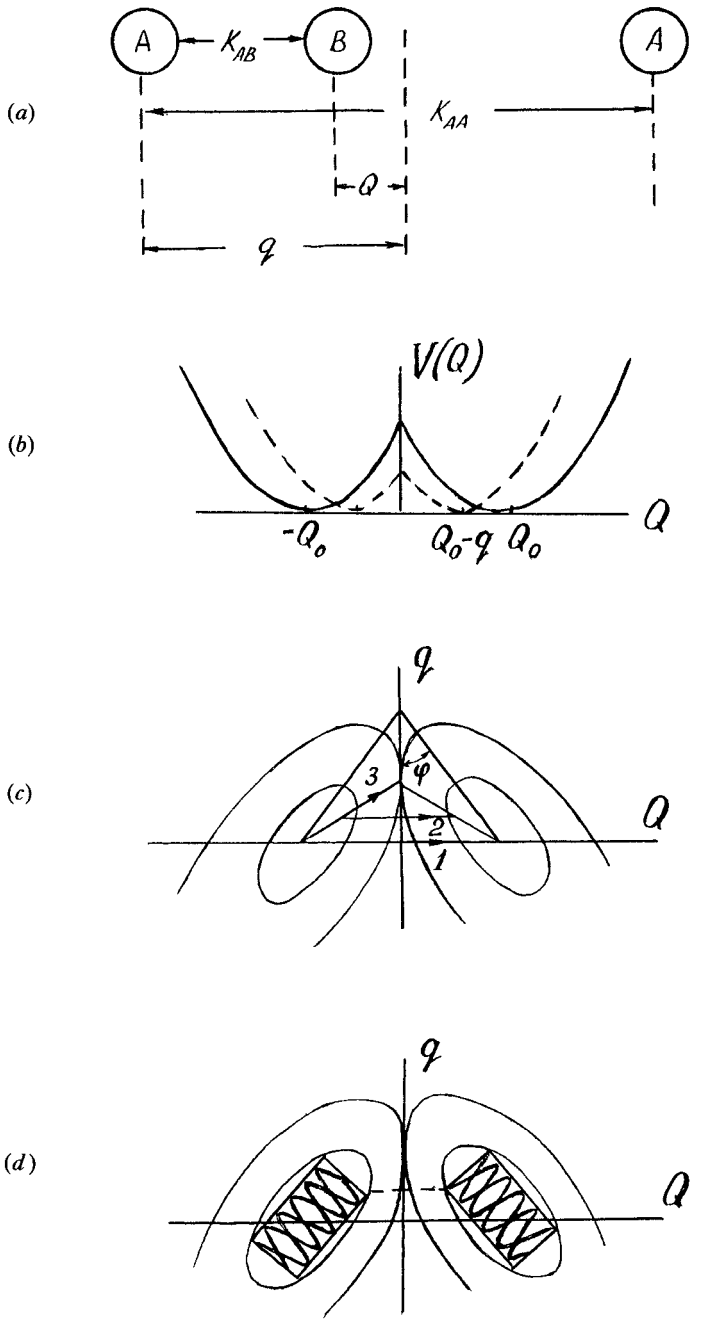

Figure 6. The model of fluctuational barrier preparation for the collinear exchange reaction AB + A → A + BA. (*a*) Coordinates and force constants. (*b*) $V(Q)$ potential at fixed intermolecular coordinate, solid and dashed lines, respectively, correspond to $q=0$ and $q>0$. (*c*) contour plots for the diabatic terms and trajectories of motion in imaginary time 1–3 for $q=0$, fast and slow transition, respectively. (*g*) Semiclassical real-time trajectories for a given energy. The dashed line shows tunnelling between the turning points [50, 56]. The angle between the valleys 2ϕ comes from the expression (3.2). Normal frequencies are $\Omega_{\pm}^2 = \omega^2[k^2+1/2(1+m/M)\pm\{[k^2+1/2(1+m/M)]^2-2k^2\}^{1/2}$, $k=2^{1/2}\Omega/\omega$.

The temperature dependences of δ_0 and δ_1 result in the three regions of $K(T)$ separated by two cross-over temperatures. The Arrhenius dependence occurs at $T > T_{c_1} = \hbar\omega/2k_B$ whereas the activation energy equals the barrier height at the saddle-point.

$$V_a = \tfrac{1}{2} m\omega^2 Q_0^2 \frac{M\Omega^2}{m\omega^2 + M\Omega^2}. \tag{3.8}$$

This transition is an over-barrier motion. Because of high velocity of the thermal motion along the valley, the relative contribution of tunnelling is small. The motion is adiabatic with respect to transversal vibrations and the adiabatic barrier is lower than the static one $V_0 = m\omega^2 Q_0^2/2$. In the intermediate region $T_{c_2} < T < T_{c_1}$ ($T_{c_2} = \hbar\Omega/2k_B$) the instanton appears. The trajectory of thermally-activated motion at energy E_a by-passes the saddle-point and is determined by excited sublevels of intermolecular vibrations. As the temperature drops, this trajectory moves away from the saddle-point whereas E_a diminishes but the barrier height in the external trajectory increases. When $T < T_c$, the quantum motion occurs for both the coordinates and only the zero-point levels take part in the transition. In this case the apparent activation energy equals zero and the maximum barrier height in the PES-cross-section along the extremal trajectory corresponds to the fast transition potential, which is higher than V_a [49]:

$$V_f = V_a\left(1 + \frac{\omega}{\Omega}\frac{\delta_1^2}{\delta_0^2 + \delta_1^2}\right). \tag{3.9}$$

A similar dynamical behaviour occurs in symmetric double-well potentials [49, 50]. The PES contour plots depicted in figure 6(*c*) are the families of concentric ellipses placed symmetrically with respect to the dividing plane. The real-time trajectories of in-well harmonic vibrations are the Lissajous figures (figure 6(*d*)) confined in the rectangle inscribed into the ellipse of the given energy [51]. Tunnelling, i.e. imaginary-time motion occurs between the turning points which are the mutual points of rectangles and ellipses. In the intermediate temperature region the instanton starts from the ellipse of energy E_a. The increase in E_a with temperature corresponds, in accordance with (2.6), to diminishing of the instanton imaginary-time period. In the case of anharmonic terms and for the non-separable variables the equipotential lines and rectangles are deformed, but the number of turning points remains the same [53, 54]. The instanton formalism for the gas-phase reactions was developed by Miller [53, 54]. A simple example of calculation the tunnelling trajectory of two-dimensional separable motion is given in [55]. The above-noted difference in initial states for the gas- and solid-phase reactions manifests in simulations of tunnelling trajectories. In the gas-phase reactions the total set of degrees of freedom consists of the singled out reaction coordinate and vibrational modes with given quantum numbers. There is no bound state for the reaction coordinate so that the motion is infinite. The wavefunctions of initial and final states are seamed on condition that the reaction coordinate and corresponding momentum are real far from the dividing plane, while the vibrational coordinates and momenta are, in general, complex in the classically available region. In the solid-phase reactions the initial and final states are bound ones so that there is no favoured degree of freedom which is to be set real. The requirement for all the coordinates and momenta to be real outside the barrier leads to the finite set of turning points in each valley, determined by the condition that the momentum equals zero.

As follows from (3.6) and (3.7), the low-temperature limit appears at $T < T_{c_2}$ whereas T_{c_2}, in contrast to T_{c_1}, has nothing to do with the static barrier. Since the frequencies of intermolecular vibrations are similar for most organic crystals, the model explains the

approximate constancy of cross-over temperature for various cryochemical reactions with tunnelling of diverse masses. When $T_{c_2} \leqslant T \leqslant T_{c_1}$, the effect of increase in the apparent activation energy can be represented as [9, 35]

$$K(T) = k_c \exp(cT). \tag{3.10}$$

The increase of the tunnelling particle (B) mass reduces both frequency and amplitude of the intramolecular vibration ($\omega \propto m^{-1/2}$, $\delta_0 \propto m^{-1/4}$), increasing the m-independent intermolecular contribution to the rate constant. For this reason $-\ln K(T)$ increases weaker than $m^{1/2}$, as m grows. This behaviour of $K(m)$ accounts for the existence of strong H/D isotope effects in the H-transfer reactions, where $\ln K \propto m^{1/2}$, and, at the same time, the low temperature rate constant limit for heavier particles transfer ($m_B/m_H \cong 10$–20), which would be impossible if that dependence $K(m)$ kept on for the same parameters of the static barrier [49]. Therefore, the model of the low-frequency fluctuational barrier preparation fits the experimental data much better than the one-dimensional model.

As the contribution of intermolecular vibration to (3.7) increases the extremal trajectory approaches the saddle-point and the barrier becomes lower. The angle between the valleys increases and ω_B diminishes. When $\omega \cong \Omega$, the fast transition approximation breaks down. Another limiting case in which the motions are separated is the slow passage [48, 49, 54] throughout the saddle point when $M/m\Omega_B$†. In the low-temperature limit below T_{c_2} the quantum intermolecular vibrations mostly contribute to overcoming the barrier (figure 7).

In the N-atom system ($N > 3$) solution of the vibrational problem yields $3N-7$ eigenfrequencies ω_k and normal vibration coordinates q_k with the equilibrium positions placed along the reaction path, so that the potential energy is of the form:

$$V(Q, \{q_k\}) = V_0(Q) + \sum_{k=1}^{3N-7} \frac{M_k}{2} \omega_k^2(Q) q_k^2. \tag{3.11}$$

In case of fast transversal motion the vibrational-adiabatic potential can be introduced [40, 58]:

$$V(Q, \{n_k\}) = V_0(Q) + \sum_{k=1}^{3N-7} (n_k + \tfrac{1}{2}) \hbar \omega_k(Q). \tag{3.12}$$

This relationship supposes that the quantum numbers of transversal vibrations remain constant as their frequencies change. For an arbitrary path, along which the energy is not minimal, the coupling to the transversal modes appears [59]. The linear coupling, i.e. having the form $\lambda_k Q q_k$ (λ is the coupling parameter), means that the transition is accompanied by a shift in the vibrational equilibrium positions. After taking up the new, non-interacting with Q vibrational coordinates, there appear additional matrix elements of the kinetic energy operator, which are determined by the curvature of the reaction path [40]. In the case of slow transition this means the change in mass of the tunnelling particle (effective instanton mass) [20, 21]. In general, linear coupling leads

† As noted in [57], the fast transition is realized in the restricted intermolecular frequency range ($\omega \gg \Omega \gg \omega_B m/M$), which is determined not only by smallness of Ω as compared to the intramolecular frequency, but by the requirement that the probability to reach the saddle points at the expense of low-frequency fluctuation ($\propto \exp(-Q_0^2/\delta_1^2)$) is lower than the tunnelling probability at small q_1. When $\Omega < \omega_B m/M$, slow transition throughout the adiabatic barrier takes place. In particular, the reactions with heavy particle transfer correspond to this limit.

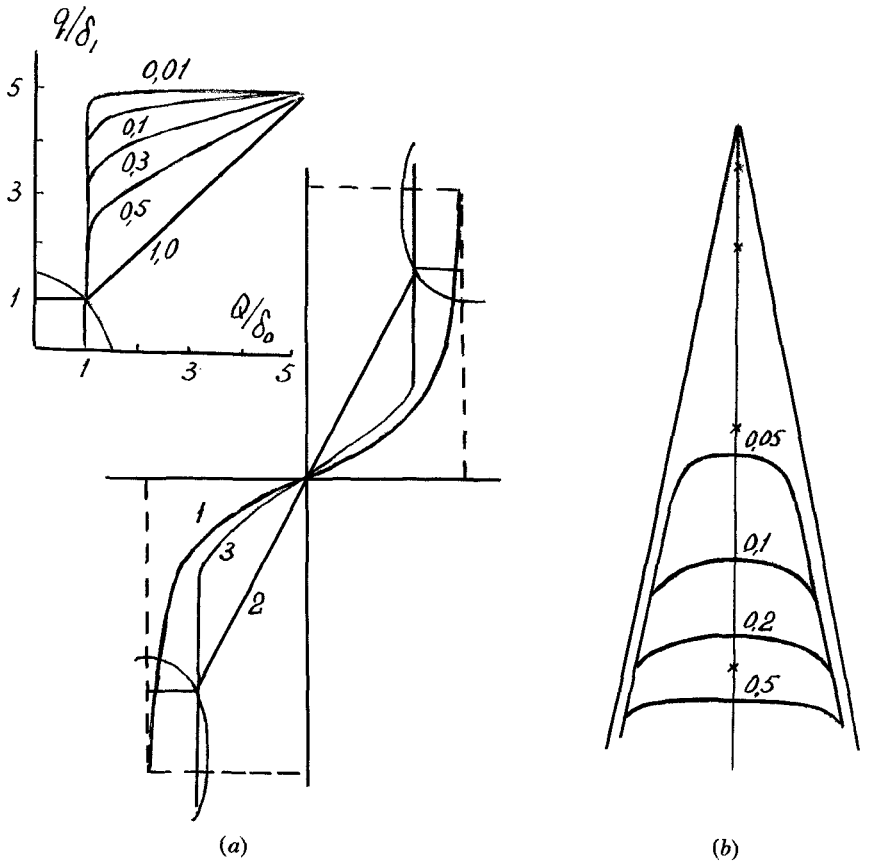

Figure 7. Contour plots for antisymmetric (*a*) and symmetric (*b*) coupling of reaction coordinate to vibration [52, 56, 66]. 1. Instanton at $T=0$; 2. periodic orbit for $n=0$; 3. trajectory [66]. $\Omega/\omega=0{\cdot}3$. Separately is shown the alteration of this trajectory for different Ω/ω_0, indicated at the curves. For symmetric coupling (the angle between the valleys is 11·5°) the trajectories [66] are shown for different Ω/ω_0. The saddle-points are marked by stars.

to the two rate-reducing effects. In the event of a fast transition the shift in equilibrium positions gives rise to multiplying the rate constant by Franck–Condon factors $\phi_k<1$. Formally, the linear coupling Qq_k corresponds to velocity-dependent friction discussed in the previous section, which always reduces the transition probability. The fluctuational barrier preparation cannot be described within this framework. To increase the transition probability it is necessary for the friction coefficient to be zero near the saddle-point. The symmetrically coupled potentials [34, 50] have this property. For example, in collinear exchange reaction the exchange of frequencies A–B and AB–A occurs, i.e. the coupling of the reaction path to the intermolecular vibration AB–A is symmetric with respect to the dividing plane, which ensures the fluctuational barrier preparation absent in the case of linear (antisymmetric) coupling. In the case of symmetric coupling the equilibrium positions do not shift so that $\phi_k=1$. Therefore, the effects of symmetrically and antisymmetrically coupled vibrations on the transition probability are opposite (figure 7). Considering multidimensional nuclear tunnelling

one cannot stick only to symmetrically coupled vibrations since the transition also involves the linearly coupled vibrations which ensure the displacement of equilibrium positions (reorganization) of both reactants and medium. In the exchange reactions the total set of vibrations can be sorted out to the symmetrically and antisymmetrically coupled ones [50, 56], which bring about the fluctuational barrier preparation and reorganization, respectively. It is shown in [56], that, although related to different-symmetry normal modes, their effects on the transition probability are not independent of each other. For example, in the fast transition limit the Franck–Condon factors for the linearly-coupled vibrations increase as the effective tunnelling length $Q_{0t} \cong Q_0\delta_1^2/(\delta_1^2 + \delta_0^2)$ decreases

$$\phi_k \simeq \exp(-C_k Q_{0t}^2), \qquad c_k = \frac{\lambda_k^2}{\omega_k^3}, \tag{3.13}$$

so that the fluctuational barrier preparation 'switches off' the reorganization of linearly-coupled modes. While reorganization reduces the transition probability up to localization in the initial well ($K_c = 0$ at $T = 0$) [60], the symmetric coupling enables finite transition rates at low temperatures.

Finding the energy spectrum for the multidimensional tunnelling is a matter of generalization of the Bohr–Sommerfeld quantization conditions for multidimensional non-separable systems. As shown in [61–63] the energy levels correspond to the classical periodic orbits, the action along which

$$\phi(E) = \int_{Q_1'}^{Q_1} 2m[E - V/(Q)]^{1/2}\,\mathrm{d}Q, \tag{3.14}$$

fulfills the equation

$$\phi(E) - \sum_{k=1}^{3N-7} (n_k + \tfrac{1}{2})\omega_k(E)T(E) = 2\pi\left(n + \frac{\lambda}{4}\right), \qquad n = 0, 1, \ldots . \tag{3.15}$$

The period of trajectory is equal to $T(E) = \hbar\,\mathrm{d}\phi/\mathrm{d}E$, λ is the number of turning points that the orbit encounters. Equation (3.15) can be rewritten

$$\phi\left[E - \sum_{k=1}^{3N-7} (n_k + \tfrac{1}{2})\hbar\omega_k\right] = 2\pi\left(n + \frac{\lambda}{4}\right). \tag{3.16}$$

Equation (3.16) demonstrates that the energy E is a sum of n quanta of the periodic motion with the period $T(E)$, and $3N - 7$ terms, each coming from the deviations from the orbit and including n_k quanta corresponding to the normal modes. The analysis [51–63] is valid for harmonic motions. The problem of quantization of anharmonic multidimensional motions has been solved in [64, 65].

Two dimensional trajectories in exchange reaction for the three-particle complex have been found in [66] in the case of a potential shaped by two strongly shifted paraboloids with the eigenfrequencies ω_0 and ω_1 ($\omega_0 \geqslant \omega_1$). Both types of coupling symmetry have been examined. The trajectory runs at first from the turning point (Q_0, Q_1) along the line $Q = Q_0$ which is the under-barrier continuation of the larger side of the rectangle, bordering the vibrations as well. Then, in a characteristic 'take-off' point (Q_0, q_1^*) the motion passes on to the classical trajectory in the upside-down potential (figure 7). The action along this trajectory is close to one calculated from (2.2). In fact, it turns out that the tunnelling occurs throughout the reduced almost one-dimensional barrier, in agreement with the model [34]. As the frequency or the quantum number of the low-frequency vibration grows, $q_1^* - Q_1$ diminishes, so that

trajectory approximates to Miller's periodic orbit [62]. When $\omega_0 \gg \omega_1$, the take-off point $q_1^\ddagger$ approaches the saddle-point. Statistically averaged trajectories correspond to the instanton. In figure 7 the two-dimensional trajectories found in [66] are compared to the instanton and periodic orbit approximations. The method put forward in [66] can be applied to finding multidimensional tunnelling trajectories on the assumption that the real terms remain parabolic up to the points $\{q_k^\ddagger\}$. In this approximation the trajectory consists of N segments. The motion along the kth segment is classical in the space of k slow degrees of freedom while the other, fast N-k degrees of freedom are frozen.

In the multidimensional system the frequency spectrum $\{\omega_k\}$ is rather dense and, according to (3.16), the energy spectrum is almost continuous, which justifies the above-formulated assumption of the model. It should be noted that in the harmonic approximation the levels with different energies E correspond to non-interacting states. Since the periodic orbits (3.16) include both in-well and sub-barrier motions, they are complex-valued. In the semiclassical approximation, when $V_0 \gg \hbar\omega_0, \hbar\omega_k$, the sub-barrier motion just slightly changes the eigenenergies in the wells. In the symmetric double-well potential the energy level of a separate well is determined by the set of quantum numbers n, $\{n_k\}$. Its tunnel splitting due to the resonant interaction with the identical state in the other well is equal to:

$$\Delta E_r = \frac{\hbar\omega_0}{2\pi} \exp\left(-\frac{1}{\hbar} S\right), \tag{3.17}$$

where ω_0 is the well frequency. The exponent (2.2) is twice as much as in (3.17). In the asymmetric double-well potential the levels corresponding to the same sets of $\{n_k\}$ differ from each other. The tunnel splitting is due to interaction of the states with $n_k^i \neq n_k^f$ for near-by energies $E_1(n^i)$ and E_2 (n^f):

$$\Delta E_{nr} = \frac{\hbar\omega_1}{2\pi} \frac{\hbar\omega_2}{2\pi} \frac{1}{|E_1 - E_2|} \exp\left(-\frac{2}{\hbar} S\right). \tag{3.18}$$

The obvious difference in ΔE in symmetric and asymmetric potentials is due to the difference in its nature: (3.17) and (3.18) arise in the first and second orders of the perturbation theory. According to (2.2), the decay probability for a metastable state is proportional to $\exp(-2S/\hbar)$. The realization of either resonant or non-resonant tunnelling depends not only on the symmetry of the potential $V(Q)$ but also on the level widths Γ, which are determined by the lifetimes of non-stationary states in relaxation processes. The relaxation is characterized, in particular, by the friction coefficient discussed above. Equation (3.17) is valid when the additional condition holds

$$\Delta E_r \gg \Gamma, \tag{3.19}$$

and corresponds to sufficiently large tunnel splittings observed in spectroscopy $\Delta E_r/2\pi\hbar c \geqslant 1\ \text{cm}^{-1}$. In most chemical reactions $\Delta E \ll \Gamma$ and resonance is disturbed even in symmetric potentials as a result of relaxation, so that the tunnelling probability $w = \Delta E/2\pi\hbar$ is described by (3.18).

As follows from figure 2, friction substantially reduces the transition probability only in case of strong coupling when $\gamma \gg \omega_b \gg \omega_0$ and vibrations along the reaction coordinate are damped. For the high-frequency intramolecular modes, among them the reaction coordinate, at $k_B T \ll \hbar\omega_0$ this condition is hardly fulfilled. On the other hand, the intermolecular vibrations promoting the transition can be strongly damped at the temperature near the Debye one, i.e. close to T_{C_2} (see, for example, [67]). For this

reason it is worthwhile to examine the reaction coordinate with $\gamma = 0$, coupled to a set of damped vibrations $\{\omega_k, \gamma_k\}$, in this way strictly incorporating interaction with vibrations in the reaction complex and phenomenologically taking into account the coupling of this complex to the environment.

The model of fluctuational barrier preparation based on the concept of promoting effect of low-frequency vibrations on the tunnelling probability, has been straightforwardly confirmed in recent experiments [68–70]. In [68, 70] the vibrational selectivity in tautomerization of tropolon has been found. The latter is due to hydrogen transfer in the fragment OH...O connected to the seven-link ring. The tunnel splitting of different vibrational sub-levels (table 3) demonstrates the increase in ΔE due to the symmetrically coupled vibrations ν_{13} and ν_{14} and the suppression of tunnelling by antisymmetrically coupled vibrations ν_{26} and ν_{39}, increasing the O–O distance. Directions of nuclear displacements are shown in figure 8. In [69] the vibrational selectivity of the two-proton tautomerization for 7-azoindole and 1-azocarbazol in excited electronic states has been studied. In the first above-mentioned compound the synchronous tunnelling two-proton transfer in the NH...N fragments leads to the widening of certain vibrational bands. This widening disappears after deuteration. As shown in figure 9, the tunnelling is accelerated by symmetric vibration with frequency 120 cm^{-1}. The widths of bands with $n = 0, 1, 2$ are equal to 5, 10 and 30 cm^{-1}, correspondingly. The bending vibration 98 cm^{-1} rather reduces the transition probability. In the second compound where the tautomerization rate equals $\sim 10^9$ s^{-1}, the relative fluorescence intensity for tautomer and dimer is determined by the ratio of rates of tunnelling and dimer fluorescence. This ratio changes by several times upon exciting the dimer to states with participation of several vibrations. The largest effect, increasing with n, has been observed for the symmetric vibration. Therefore, it is this vibration that accelerates the tunnelling. The bending vibrations suppress the transition.

In [71] the increase of the tunnelling probability in a three-atom fragment ABA, as a result of increase in the quantum number of the low-frequency A–A vibration, has

Table 3. Tunnel splittings of different vibrational sublevels in the electronically excited A^1B_2 state of tropolon molecule.

Band	Vibration frequency, cm^{-1}	Tunnel splitting, sm^{-1}	
		TrOH	TrOD
0_0^0	—	18·9†	2·2
11_0^1	511	13	—
12_0^1	640	17	—
13_0^1	414	32†	3
14_0^1	296	30·4†	11
14_0^2	2 × 296	28	13
19_0^2	2 × 269	9	—
25_0^2	2 × 171	4·2†	—
26_0^2	2 × 39	7·2†	—
26_0^4	4 × 39	4·7†	—
26_0^6	6 × 39	3·5	—
26_0^8	8 × 39	0·8	—
39_0^2	—	3·1†	

† Data from [64], other values are taken from [66].

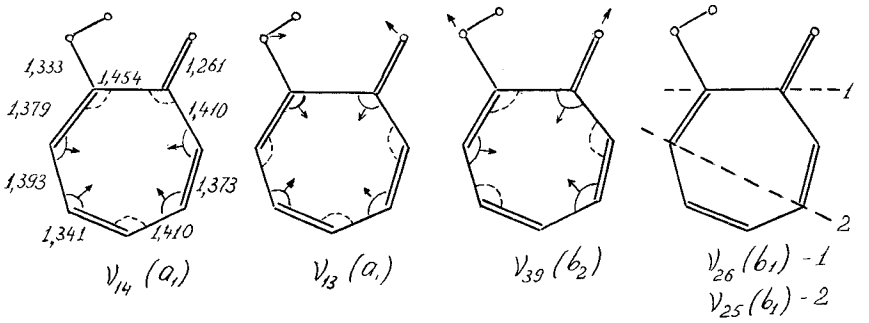

Figure 8. Normal vibrations of tropolon molecule relevant for the tunnel tautomerization. Vibration symmetry is given in brackets. For the off-plane vibrations ν_{25} and ν_{26} the plane of symmetry is shown [64]. The equilibrium bond lengths correspond to the tropolon crystal [83].

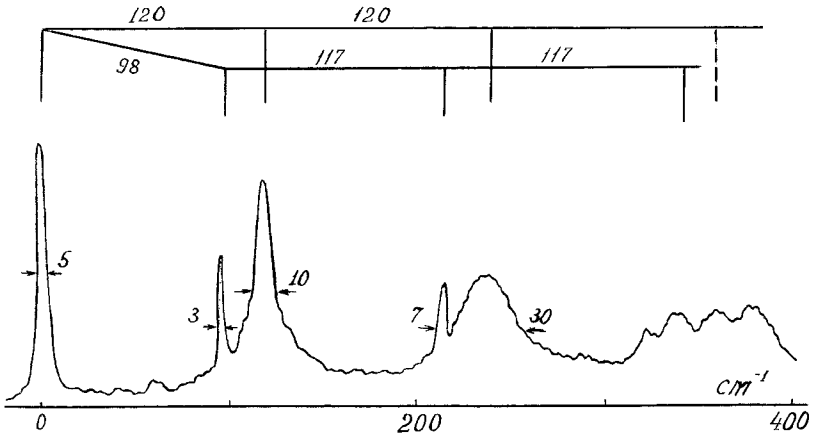

Figure 9. Laser excitation spectrum of the dimer fluorescence of 7-azoindole. The difference in the band width for the symmetric vibration 120 cm^{-1} and bending vibration 98 cm^{-1} shows that the former accelerates the rate of the tunnel two-proton tautomerization, while the latter just weakly affects it [65].

been found by straightforwardly solving the Schrödinger equation with a supercomputer. If the barrier height equals 1300 cm^{-1} (3·72 kcal $(mol)^{-1}$), the vibration frequency is 450 cm^{-1} and $m_A/m_B = 100$, then the tunnel splitting equals 111, 133, 151, 166, 193, and 202 cm^{-1} for $n = 0, 1, \ldots 5$, respectively. The two-dimensional picture of wavefunctions shows that at large ns there occurs a delocalization for the A–A distances smaller than the equilibrium one. The delocalization is due to fluctuational lowering of the barrier and, consequently, appearance of classical trajectories. This effect, caused, as shown in [56], by strong fluctuations of the barrier, reduces both V_a (i.e. activation energy in the Arrhenius region) and S (i.e. increases K_c):

$$V_a = V_0(1-B), \qquad S = S_0(1-B)^{1/2}\psi, \qquad B = \frac{\gamma^2}{2\Omega^2}, \tag{3.20}$$

where S_0 is the action in the static barrier and factor $\psi > 1$ reflects the increase in effective tunnelling mass. Expressions (3.20) hold irrespective of the static barrier form and transition conditions so that the behaviour of the transition probability as a function of m and T, discussed above, is a universal property of cryochemical exchange reactions.

The simulation in [71] performed on the brink of up-to-date computational capabilities is beyond the framework of the semiclassical approximation, since ΔE is comparable with vibrational frequencies. As far as real systems are concerned, for higher barriers and more degrees of freedom such simulations are hardly feasible. The dependence of tunnelling probability on the quantum number n for the symmetric parabolic terms in the model represented in figure 6 is of the form [66]:

$$\ln w(n) = \ln w(0) + (2n+1)\ln\left(\frac{2q_-}{\delta_{1n}}\right)^2 - \ln\left(\frac{2q_-}{\delta_{10}}\right)^2, \tag{3.21}$$

where

$$\delta_{1n}^2 = (2_n+1)\frac{\hbar}{M\Omega}$$

is the r.m.s. amplitude for the nth energy level of the symmetric mode with the frequency Ω_-,

$$q_- = Q_0 \frac{\Omega_+ \sin\varphi}{\Omega \cos^2\varphi + \Omega_+ \sin^2\varphi}$$

is the tunnelling distance for this mode. The values of Ω_-, Ω_+ and the angle between the values are defined in the caption to figure 6. It follows from comparison of (3.21) and (3.7) that $w(n) \sim (Q_0/\delta_1)^{4n}$, i.e. the vibrational selectivity increases as the transition probability drops. For greater values of K_c, compared to those studied in [68–70], equal to ca $10^{12}\,s^{-1}$, one should expect stronger effects. The vibrational selectivity grows with δ_1/δ_0, i.e. in the region of slow transition, and disappears at $T > T_{c_2}$.

4. Intramolecular transfer of hydrogen atoms

One of the most studied examples of intramolecular tunnelling is the hydrogen transfer in malonaldehyde isomerization

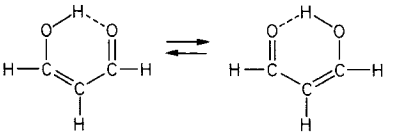

(4.1)

that leads to the tunnel splitting observable in microwave and i.r. spectra. In the ground vibration state this splitting equals 21·6 and $3\,cm^{-1}$ for the transfer of H and D, respectively [72, 73]. The calculation of the one-dimensional tunnelling probability between two equivalent equilibrium states at fixed positions of O atoms gives a ΔE value which is by almost two orders of magnitude smaller than the experimental one [74]. The reason for this discrepancy, pointed out in [75, 76], is that the transition is accompanied by substantial displacement of the heavy atoms and cannnot be reduced to the tunnelling in a static barrier. The self-consistent calculation of PES and dynamics of multidimensional tunnelling has been made in [77]. The transfer of the

hydrogen atom is brought about by a number of large-amplitude motions, including, in addition to OH-bond stretching, the bending vibrations COH and OCC and stretching vibration CO. All these vibrations supply the dynamical shortening of the tunnelling distance. The major role is played by the vibrations with frequencies 318 cm^{-1} and 1378 cm^{-1}. The tunnel splitting increases by several times with increase of their quantum numbers. The molecular skeleton deformation in the transition state is shown in figure 10 in comparison with the initial state. The tunnelling distance for the H-atom is only 0·47 Å instead of 0·85 Å in the non-deformed initial configuration. The barrier height along the PES cross-section passing through the saddle-point is equal to 6·3 kcal $(mol)^{-1}$†. The simultaneous participation in the transition of both the light mass motion (H-atom) and heavy atoms vibrations results in by-passing the saddle-point, as follows from the model of fast transition (see previous section). Contour plots are shown in figure 11. The mass-weighted coordinates q_1 and q_2 correspond to $r_1 - r_2$ and $r_1 + r_2$ (r_1 and r_2 are the distances O_1–H and H–O_2 in the fragment O_1HO_2). The configuration of heavy atoms was found by minimizing the total energy for fixed q_1 and q_2. The trajectory 122′1′ corresponds to the slow transition in the vibrational-adiabatic potential (3.12). The displacement at the segments 12 and 1′2′ is due to rapprochement of the O atoms as a result of low-frequency vibrations, while the segment 232′, including the saddle-point, corresponds to the subsequent motion of the H atom between the O atoms brought together. While moving along the extremal trajectory 13′1′, the O atoms displace much more weakly than in the case of motion throughout the saddle-point. Since the probability of realization of the nuclear trajectory with large shifts is small, the extremal trajectory 'cuts the corner', although the fast transition barrier is higher than the adiabatic one. The calculation [77] revealed an interesting property of fluctuational barrier preparation which does not follow from simple collinear models discussed in the previous section. In the latter the low-frequency vibrations reduce both tunnelling

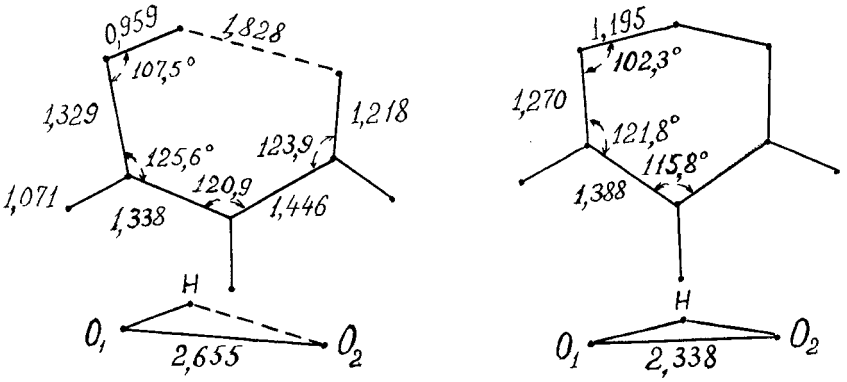

Figure 10. Malonaldehyde molecule deformation in its mirror isomerization (4.1). (*a*) is the equilibrium initial state, (*b*) transition state. The change of the O_1HO_2 is shown below. The bond lengths are given in Å. The calculation has been performed with the self-consistent field method taking into account the electronic correlations [74].

† This value corresponds to the splittings close to the observed ones (19 s m^{-1} and 1·6 s m^{-1} for H and D, respectively). The barrier height calculated in [76, 77] by various quantum-chemistry methods covers the range 6·1–10·6 kcal $(mol)^{-1}$.

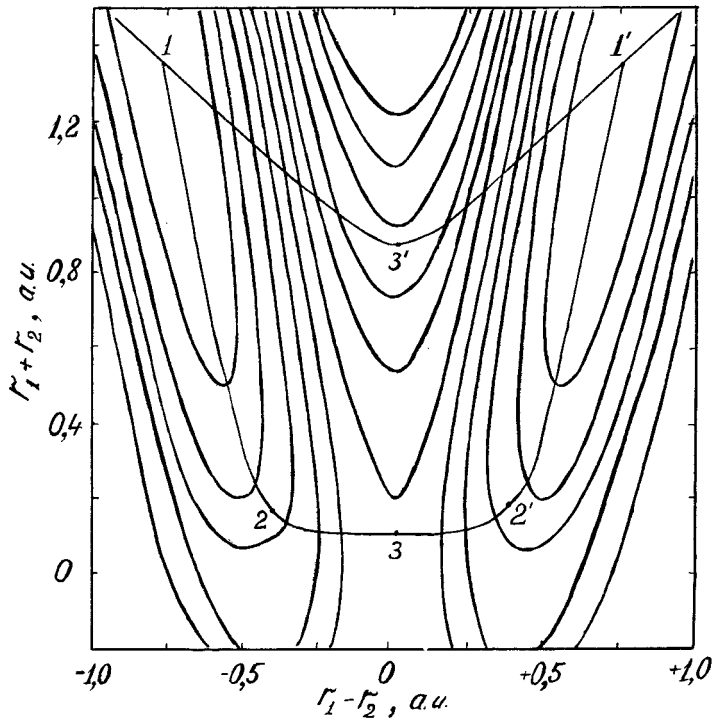

Figure 11. Contour plots for malonaldehyde isomerization. 1,1′ are the energy minima of equilibrium isomer configurations. 2,2′ are the points of greatest curvature of the minimum energy path in which the heavy nuclei shift proceeds to the hydrogen atom tunnelling. 3 is the equilibrium transition state, 3′ effective saddle-point of the fast transition potential. q_1 and q_2 are the mass-weighted coordinates [37] in the atomic units. The equipotential step is 0·63 kcal (mol)$^{-1}$.

distance and barrier height V_a so that the rate constant increases both in the Arrhenius and low-temperature regions. For a complex multidimensional motion the reduction of both parameters is not obligatory. According to [77], the skeleton vibrations reduce L but increase V_a. The barrier gets narrower but higher, so that K_c increases while $K(T)$ remains the same for $T > T_c$. Note that the results of numerical simulations [76, 77] confirm qualitative conclusions of the model of fluctuational barrier preparation [33–35, 49, 50, 56].

In [75–77] the fast resonant tunnelling is described for the malonaldehyde molecule in the gas phase. In [78], while studying the i.r. spectra of the same molecule in the noble matrices at 15–30 K, the tunnel splitting has not been observed. Its omission is caused by 'detuning' of the potential as a result of weak coupling to the environment, i.e. arising of non-resonant tunnelling when, according to (3.18), $\Delta E_{nr} \ll \Delta E_r$.

In contrast to the malonaldehyde, in the above-mentioned tropolon molecule the tunnel splitting is almost the same in both the gas phase and neon matrix [79]. Note that in both cases there is a similarity not only in ΔE_r but in the equilibrium distances in the O_1HO_2 fragment. In the ground electronic state of the tropolon molecule $\Delta E_r \leqslant 0{\cdot}17\ \text{cm}^{-1}$ ($K_c \leqslant 5 \times 10^9\ \text{s}^{-1}$) [79, 80]. The change in the angles HOC and OCC, shortening down the O_1H–O_2 distance, accounts for the lower barrier in the excited

state compared to the ground state. In the 3-isopropyl-substituted H- and D-tropolon the tunnel splitting in the S_1 state equals $58\,s\,m^{-1}$ and $14\,s\,m^{-1}$, respectively [81].

The recent analysis [82] of the i.r. tropolon spectra in the neon matrix, based on the data of [83] for the change of the bond lengths after H-atom transfer (figure 8), had shown that the displacements of non-tunnelling heavy atoms are comparable with the zero-point amplitude, or even larger. The transfer of the hydrogen is strongly coupled with the plane vibrations C=O/C–O and C–C=C/C=C–C (coordinates R and S, respectively). The projection of the three-dimensional PES $U(r, R, S)$ onto the RS plane is characterized by two saddle points. Such a configurational degeneracy of the reaction path, typical also of the two-proton transfer as well as the transfer of interstitial H atom between the neighbouring sites of the lattice, will be considered further. Because of the coupling of the H atom motion to strong skeleton deformation, the barrier is higher than for the malonaldehyde ($13{\cdot}7\,kcal\,(mol)^{-1}$). The potential asymmetry owing to the invariance of the neon matrix configuration through the transition is equal to $2–3\,s\,m^{-1}$. Unlike the excited state, in the ground state the isotope effect is small, in agreement with the model of fluctuational barrier preparation for the case when the chief contribution comes from the heavy atoms RS displacements.

In the excited state of the 2-hydroxy-4,5-benzotropon molecule immersed in an inert matrix the rate constant of the tunnelling H transfer exceeds $10^{11}\,s^{-1}$ at 10 K, which is also because of the fluctuational barrier preparation [84]. The value of K_c is smaller in the matrices with hydrogen bonds, deforming the fragment O_1HO_2. For the review of studies of fast tunnelling proton transfer in electronically-excited matrix-isolated molecules by methods of picosecond spectroscopy we refer the reader to [85].

A resonant transition with a large tunnel splitting ($\Delta E_r = 130\,cm^{-1}$) can be observed in the excited state of 9-hydroxyphenalenon in noble matrices at 4·2 K [85, 86].

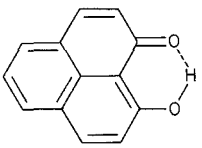

(4.2)

Insertion of a methyl group into the position 2 or 8 causes an asymmetry of the potential which equals, respectively $199\,cm^{-1}$ and $170\,cm^{-1}$ for the H and D forms. Since the asymmetry is comparable with the tunnel splitting, the fast exchange of the hydrogen atom remains [87]. The quantum-chemistry calculation of the PES shows that the O_1–O_2 distance in the transition state is by 0·21 Å smaller than in the equilibrium (2.31 Å instead of 2·52 Å), so that the tunnelling length shortens up to 0·42 Å. The shift of the atoms in the aromatic rings is not greater than 0·03 Å, i.e. the chief role in the fluctuational barrier preparation is played by bending vibrations COH and OCC. The adiabatic barrier height is equal to $5{\cdot}2\,kcal\,(mol)^{-1}$.

An example of the effect of substitutes asymmetrizing the potential is the β-hydroxyacrolein, in which the exchange rate constant for the fragment O_1HO_2 is by an order of magnitude higher than for the α-methyl-β-hydroxyacrolein [89, 90].

In the 2-hydroxyphenoxyl radicals the non-resonant transfer within the fragment O_1HO_2 occurs with the rates of 10^5–$10^7\,s^{-1}$, which ensures the changes in the hyperfine structure of the electron paramagnetic resonance (EPR) spectra [91]. The distance $O_1H...O_2$ here is much longer than in the above compounds, so that the strong angular deformation is responsible for the transfer (figure 12). The adiabatic barrier height equals $\sim 17\,kcal\,(mol)^{-1}$. The bending vibrations of the chelate ring reduce the tunnelling distance from 1·26 Å to 0·36 Å.

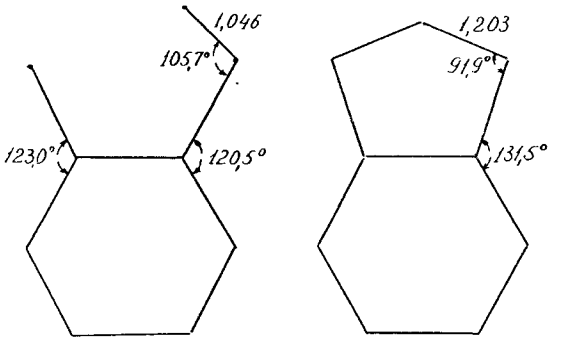

Figure 12. 2-hydroxyphenoxyl radical deformation upon transfer of the hydrogen atom, (*a*) and (*b*) are the initial and transition states, respectively.

In the 2-hydroxy-1-oxyethynil radical

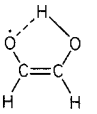

(4.3)

the transfer of the H-atom is accompanied by the rotation of OH group relative to the C–C bond in the cis-form [92].

The transfer of two hydrogen atoms (two-proton exchange) is observed in the EPR spectra of C^{13} naphtazarin crystals above $\sim 110\,K$. The rate constant equals $3 \times 10^6\,s^{-1}$ and $10^4\,s^{-1}$ for H and D, respectively [93, 94]. According to the PES calculation [95], the consecutive transfer of the H atoms *via* intermediate states B and B′ is more preferable energetically than the synchronous exchange, so that the transition states have twofold degeneracy:

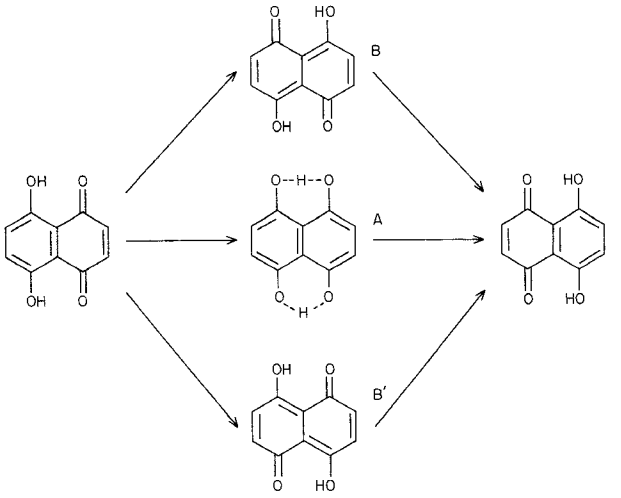

(4.4)

The adiabatic barrier in the B and B′ states (25 kcal $(mol)^{-1}$) is 3·1 kcal $(mol)^{-1}$ lower than that of the symmetric transition state A corresponding to the two-proton

exchange. As remarked in [40], the existence of more than one minimum in the transition states and, therefore, reaction path bifurcations, is a rather common event for multidimensional tunnelling. This means that at least one transversal vibration turns into a double-well potential. The PES splitting occurs, in particular, when the off-plane low-frequency vibrations take place in the reaction. As shown in [96], the behaviour of trajectories changes near T_{c_1} and T_{c_2}. The PES landscape for the model potential with two transition states

$$V(Q,q)=V_0(Q)+\tfrac{1}{2}q^2(Q^2Q_0^2)+\frac{\alpha}{4}q^4, \tag{4.5}$$

is shown in figure 13(*a*). When $Q<Q_0$, there are two minimum energy paths, along which the transversal coordinate is equal to:

$$q=\pm\left(\frac{\lambda}{\alpha}\right)^{1/2}(Q_0^2-Q^2)^{1/2}. \tag{4.6}$$

The bifurcational diagram 13(*b*) shows how the $(Q_0, 1/k_BT)$ plane breaks up into the areas with different behaviour of trajectory. In the Arrhenius region at $T>T_{c_1}$ the classical transition takes place throughout both saddle-points corresponding to the states B and B′. When $T<T_{c_2}$ the extremal trajectory is a one-dimensional instanton

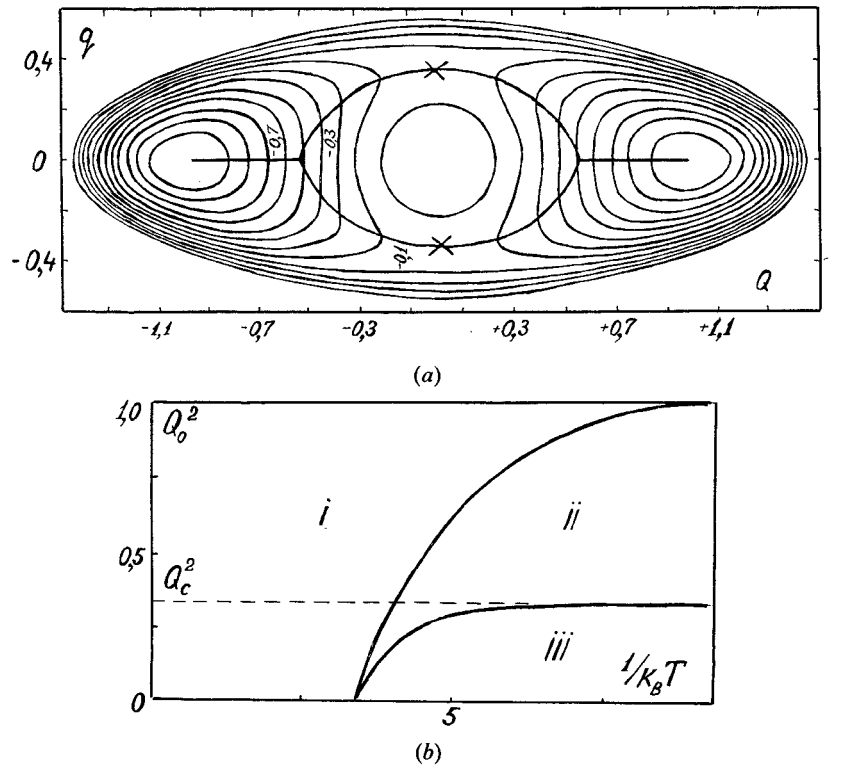

Figure 13. (*a*) Contour plot of potential with the double transition state (4.5). $V_0(Q)=Q^4-2Q^2$, $\lambda=20, \alpha=90, Q_0=0{\cdot}5$. The dashed line shows the minimum energy paths. (*b*) Bifurcational diagram in the $(Q_0^2, 1/k_BT)$ plane. Regions i, ii, and iii correspond to the Arrhenius dependence (asynchronous thermally activated transition), two dimensional tunnelling and synchronous one-dimensional tunnelling, respectively [96].

which hits the symmetric state A. The regions i and iii are divided by the region ii, in which there occurs a quantum two-dimensional motion. The values of T_{c_1} and T_{c_2} depend on the relative difference of energies in the states A and B, related to Q_0 *via* the following relationship:

$$\Delta V=\frac{V_A-V_B}{V_A}=\frac{\lambda^2}{\alpha}Q_0^4. \tag{4.7}$$

When $\Delta V\ll 1$ the region ii is sufficiently narrow ($T_{c_1}\cong T_{c_2}$), so that for the classical motion the transfer is consecutive, while the quantum motion is a two-proton transfer. The two-proton transfer changes into the consecutive motion at the critical value of parameter $Q_0^*=(2/\lambda)^{-1/4}$, i.e. when $\Delta V\geqslant 2\lambda/\alpha$.

The keto-enol tautomerization in the excited triplet state of 2-methylacetophenone is connected with the transfer of H atom in the CHO fragment:

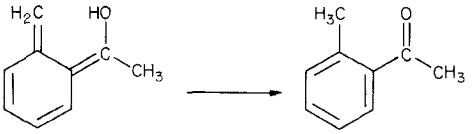

(4.8)

The tautomerization rate constant is determined by measuring the time-changing absorption of enol form, generated by flash-photolysis [97]. The measured dependencies $K_H(T)$ and $K_D(T)$ consist of an Arrhenius region ($E_a=9{\cdot}6$ kcal (mol)$^{-1}$) going over to the low-temperature plateau below 110 K, where $K_{CH}\cong 10^5\,s^{-1}$. The isotope effect grows as the temperature drops, $K_H/K_D\cong 20$ at $T=100$ K (figure 14). The fluctuational barrier preparation is due to the torsional vibrations of OH- and CH-groups as well as the oxygroup bending vibration. In the trans-enol form the transition does not occur because of the large tunnelling distance for the hydrogen atom (2·8 Å). In the cis form this length shortens up to ~ 1 Å, but the transition to this form is unfavourable energetically ($\Delta H\cong 3$ kcal (mol)$^{-1}$). In the transition state the OH bond is placed out of plane of the ring. The analysis of all these motions has not been done. In [98] it just has been shown that the experimental curves $K_H(T)$ can be described within the framework of the two-dimensional model of tunnelling for the modulating collinear vibration frequency of 120 cm^{-1} and corresponding reduced mass of $15\,m_H$. The tunnelling distance for the H atom evaluated in [98], is 1·8 Å.

The keto-enol tautomerization rate constant for 2-(2'-hydroxyphenyl)-benzoxazole in the triplet state

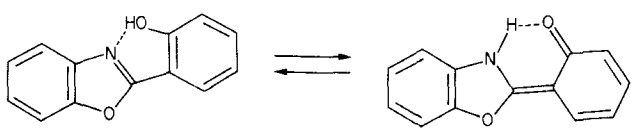

(4.9)

is characterized by similar temperature dependence and isotope effect [99].

Analogous transfer in the fragment N...OH in the lowest excited singlet state S_1 of 2,5-bis(2-benzoxazonile)-4-metoxyphenone is by several orders of magnitude faster because of the lower barrier, than in the $^3T_1$ state. The cross-over temperature is ~ 50 K, $K_c=10^{10}\,s^{-1}$, the apparent activation energy within the range of 100–200 K is 1·1 kcal (mol)$^{-1}$ [100]. The $K(T)$ dependence similar to that of reaction (4.8) has been observed in [99] for the keto-enol tautomerization of 5,8-dimethyltetralon in the $^3T_1$ state, where the H atom transfer occurs in the CH...O fragment. In [101] it has been

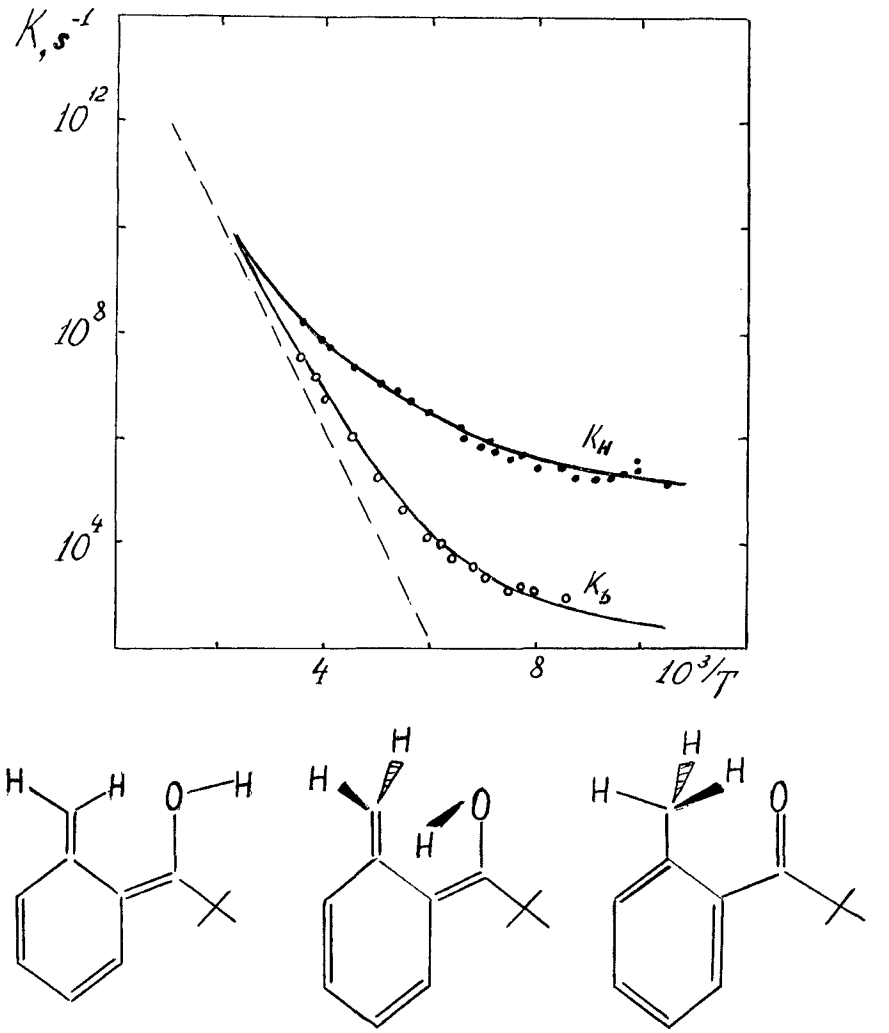

Figure 14. Temperature dependence of the rate constant of keto–enol tautomerization of 2-methylacetophenone in the lowest triplet state [92]. The configuration change as a result of transition is shown below [93].

found that the photoconversion of enamin (i) into the hexahydrocarbazole (iii) proceeds through the intermediate formation of intensively coloured zwitter-ion (ii), the decay rate of which is immediately registered through the change in the optic density:

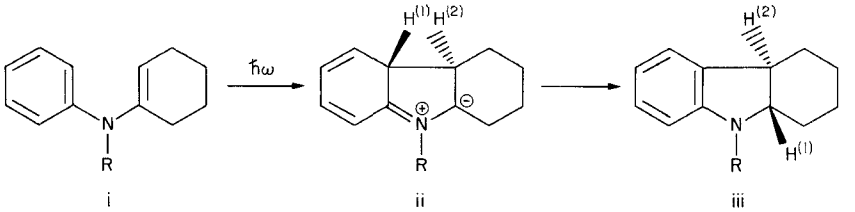

(4.10)

The change of the rate constant of the hydrogen atom transfer (conversion of ii into iii) reaches six orders of magnitude in the region 290–80 K, $K_c = 5 \times 10^{-3}\,s^{-1}$, $T_c = 100$ K, K_H/K_D increases from 10 to 5×10^3 as the temperature falls from 290 to 100 K. It is $H^{(1)}$ that is transferred since the substitution of deuterium atom for $H^{(2)}$ does not change the rate constant, while its substitution for $H^{(2)}$ has the same effect as replacing both $H^{(1)}$ and $H^{(2)}$ by D. The geometric transfer distance is much longer than that in the previous examples, exceeding 3 Å. Seemingly, the main role in the transition is played by the off-plane bending vibrations. As the authors of [98] argue, the fluctuational barrier preparation is provided by the vibrations with frequency 140 cm^{-1}. Note that the K_c value in the above-mentioned reactions ranges within ten orders of magnitude while the cross-over temperatures remain almost the same (50–100 K).

Non-Arrhenius behaviour of the isomerization rate constant of sterically hindered aryl radicals-2,4,6-tri-tert-butylphenyl (i) and 2,4,6-tri(1'-adamantyl)phenyl (ii) has been observed in [102]. In the range of 245–123 K the isotope H/D-effect increases from 40 to $\sim 10^4$, whereas the difference between the apparent activation energies for the transfer of H and D (6·2 kcal $(mol)^{-1}$ and 9·4 kcal $(mol)^{-1}$ at $T > 200$ K) substantionally exceeds the difference of zero-point energies. In the case of the H-atom transfer $T_c \cong 100$ K, $K_c \cong 10^{-2}\,s^{-1}$. According to [98], the fluctuational barrier preparation is due to the bending vibrations of C–C and C–H bonds in the butyl fragment. The effective modulating vibration frequency is 150 cm^{-1}, the mass $\sim 25\,m_H$. The transfer distance equals 1·34 Å.

The vibration-stimulated H-atom tunnelling in the sigmatropic 1,5-rearrangement of 1,3-pentadiene has been assumed on the grounds of an unusually strong H/D isotope effect in this reaction [103]. The PES [104] shows that the main contribution comes from the bending CC-bond vibrations with the effective frequency 250 cm^{-1}. The tunnelling distance totals 1·34 Å. According to the model proposed in [105], the rapprochement of CH_3 and CH_2 fragments, between which the H atom is transferred, occurs in the gauche-conformer with energy smaller than in the cis-form, considered in [104]. This rapprochement is caused by rotation through 48° relative to the CC bond. The frequency of hindered rotation assisting the tunnelling is 390 cm^{-1}. Tunnelling in the inversion of non-planar three-member ring radicals has been studied in [106–108]. According to [106], the cyclopropyl radical inversion is due to transition of an α-atom of hydrogen between the equilibrium position, in which the $C_\alpha H_\alpha$ bond forms an angle of 60° with respect to the ring plane. In the transition state the radical gets planar. The inversion barrier height for the methylcyclopropyl equals 3·1 kcal $(mol)^{-1}$. The tunnelling transition rate is large, compared to the typical EPR frequencies ($> 10^8\,s^{-1}$), even at 4·2 K. According to [107], the trajectory passing through the saddle-point includes not only the H-atom motion perpendicular to the ring plane but also the ring deformation and $C_\alpha H_\alpha$ bond stretching. Since the frequencies of enumerated vibrations are larger than that of the H_α-governing bending vibration, the transition regime is close to the adiabatic one. In the oxyranyle radical the inversion barrier height increases to 9·0 kcal $(mol)^{-1}$. The $K(T)$ dependence is found from the hyperfine EPR spectrum structure in the range of 203–105 K [108]. The cross-over temperature is 140 K, $K_c = 7 \times 10^6\,s^{-1}$. The isotope effect at 150 K equals 40.

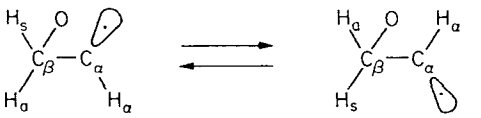

(4.11)

In the stable form the α-atom of hydrogen makes up an angle of 63° with respect to the COC plane. In the transition state with the C_{1h} symmetry the α-atom is placed in the plane. The inversion barrier is created by the angular displacement of H_α, in which the chief role is played by the low-frequency bending vibration $C_\alpha H_\alpha$ ($\nu = 883\,cm^{-1}$). The transition is escorted by change in the equilibrium positions of the ring atoms and stretching of the bond C_α–H_α. The net effect of these high-frequency vibrations is to create the adiabatic inversion barrier $V(\theta)$. The barrier forms inferred from the measured dependences $K_H(T)$ and $K_D(T)$ coincide with the calculation based on the analysis of normal vibrations in the initial and final states. The tunnelling proceeds through the one-dimensional adiabatic barrier, since there is no symmetrically coupled low-frequency vibration leading, as in previous examples, to the fast transition of a fluctuating barrier. The T_c value is in accord with expression (2.2).

Tautomerization of metal-free porphyrines (H_2P) and phtalocyanins (H_2Pc) is connected with transfer of two hydrogen atoms between equivalent positions in the square formed by four N atoms inside a planar 16-member heterocycle. In the stable trans-form the H atoms lie along the square diagonal. The energy of the cis-form, in which the atoms are positioned at one of the sides, is higher than that of the trans-form by 3–5 kcal $(mol)^{-1}$ [109]. The transition state energies for trans–cis and trans–trans isomerization, calculated in [109] by means of semi-empirical quantum-chemistry methods, are equal to $V_0 = 36$–$42\,kcal\,(mol)^{-1}$ and $V_0' = 60$–$66\,kcal\,(mol)^{-1}$, respectively. The rate constant temperature dependence for the two-proton exchange in H_2P, HDP and D_2P has been measured with nuclear magnetic resonance (NMR) methods in the interval of 160–320 K, where it grows from 10 to $10^5\,s^{-1}$ [110–114]. In the range of 95–110 K the values of K_H and K_D, measured in [115] with the 'hole-burning' method in the fluorescence spectrum, make 10^{-4}–$10^{-2}\,s^{-1}$. Comparison of data of both methods shows that the dependences $K_H(T)$ and $K_D(T)$ are not Arrhenius ones (E_a^H diminishes from $10{\cdot}4\,kcal\,(mol)^{-1}$ at $T = 200$–320 K to $6{\cdot}4\,kcal\,(mol)^{-1}$ at 95–110 K); the activation energy for the D-atom exchange is by $3{\cdot}3\,kcal\,(mol)^{-1}$ greater than for H atoms; the isotope effect is ~25 and ~250 at 250 K and 111 K, respectively. According to [111], the tautomerization at $T \geqslant 200$ K corresponds to consecutive transfer, since the rate constants for HDP and D_2P are similar, i.e. in both compounds there is a same slow stage of D transfer. The PES found in [109] has two cis-form-local minima, separated by four saddle-points from the main trans-form minima. The consecutive transfer (trans–cis, cis–trans)—because of endoergicity of the first stage—displays the Arrhenius law even for $T < T_c$. For this reason the synchronous transfer of two hydrogen atoms should prevail at sufficiently low temperatures. However, because of too high a barrier for the synchronous trans–trans transition, this region is experimentally unachievable. The computational results in [109, 117, 118] display agreement of the experimental data with the model of consecutive transfer. According to [109, 117], the tunnelling cis–trans transition is accompanied by a strong heterocycle deformation. The total reorganization energy equals $7{\cdot}4\,kcal\,(mol)^{-1}$. The upside-down barrier frequency is 2300–$2500\,cm^{-1}$ ($T_{c_1} = \hbar\omega_B/2\pi k_B \cong 550$ K).

The rate constant at $T < T_{c_1}$ can be evaluated as:

$$K = \frac{\omega_R}{2\pi} \exp\left[-\frac{2\pi}{\hbar\omega_B}(V_0 - E_{ct}) - \frac{E_{ct}}{K_B T} \right], \tag{4.12}$$

where E_{ct} is the difference of energies of cis and trans forms and V_0 is the height of the barrier dividing these states. The $K(T)$ value found from (4.12) is in agreement with

Table 4. Intramolecular tunnelling transfer of hydrogen atoms.

	Fragment	Region of T, K	$K/T/$, s^{-1}	$K_H/K_D/T, K/$	T_c, K	K_c, s^{-1}	V_0, kcal (mo
n, ground state	OH...O symm.	4·2	$3{\cdot}8 \times 10^{12}$	16	—	$3{,}8 \times 10^{12}$	5·2
und state	OH...O symm.	300	6×10^{11}	7	>300	6×10^{11}	6·3
ate, S_1-state	OH...O symm.	4·2 4·2	5×10^{9} 6×10^{11}	— 8·6	— —	5×10^{9} 6×10^{11}	— 3–5
dical ground state	OH...O symm.	170–300	6×10^{2} 2×10^{7}	140 /280/	170	10^{2}	17·0
benzoxazole ^{3}T-state	OH...N asymm.	50–200	5×10^{5} 2×10^{7}	30/200/ 300/100/	70	5×10^{5}	12·0†
nole/4-metoxyphenone S_1-state	OH...N asymm.	20–180	10^{10}–5×10^{10}	—	50	10^{10}	4·1†
ne, ^{3}T-state	OH...C asymm.	90–270	10^{5}–10^{8}	12/250/ 500/125/	100	10^{5}	12·5†
^{3}T-state	OH...C asymm.	60–200	10^{6}–2×10^{7}	300/100/	70	10^{6}	12·0†
ydrocarbazole	OH...C asymm.	70–290	5×10^{-3}–3×10^{3}	10/300/ 5×10^{3}/100/	100	5×10^{-3}	7·6†
enyl radical, ground state	OH...C asymm.	113–292	2×10^{1} 4×10^{-2}	40/245/ 10^{4}/123/	100	6×10^{-3}	9·2†
round state	inversion CH	105–203	5×10^{7}–7×10^{6}	40/150/	140	7×10^{6}	9
nd state	OH...O OH...O symm.	160, 290	10^{6}	4×10^{2}/290/	—	—	25
ound state	NH...N NH...N asymm.	95–290	10^{-6}–10^{5}	25/250/ 250/111/	90	10^{-6}	37

ted from the apparent activation energy with the H-atom zero-point energy added, which is taken to be 3 kcal $(mol)^{-1}$, L_H is the geometric

Table 5. Interreactant C–C distances and intermolecular vibration frequencies in the solid-state reactions $CH_3 + RH \rightarrow CH_4 + R$.

Matrix	R_0, Å	$\Omega\, 10^{-12}\, s^{-1}$
CH_3OH	3·66	5·7
C_2H_5OH	3·64	5·6
CH_3CN(I)†	3·82	5·3
CH_3CN(II)	3·89	4·9
CH_3NC	3·86	4·6

† I and II—are two different crystalline modifications of acetonitryle.

experiment. Owing to the skeleton vibrations, the H-atom tunnelling distance in the excited state with the energy of E_{ct} shortens up to 0·6 Å, the geometric distance being $\sim 1{\cdot}7$ Å. In the case of the trans–trans transition the barrier top is characterized by two imaginary frequencies equal to 2140–2220 cm^{-1} and 2020–2080 cm^{-1}. The transition probability proportional to $\exp(-2\pi V'_0/\hbar\omega_B)$—for found in [109] V'_0—does not exceed $10^{-14}\, s^{-1}$, so that the synchronous transfer does not occur. As shown in [96], when there are two saddle-points (figure 13), the cross-over temperature decreases as V'_0 grows. For the values V'_0/V_0 found in [109], the extremal trajectory at $T \rightarrow 0$ would remain two-dimensional with an exponentially small transition probability even in the absence of cis-form minima.

In a summary of this section we present table 4 of kinetic characteristics of the discussed reactions.

5. Intermolecular transfer of hydrogen atoms

The rate constants of transfer of the H atom between reactants situated in the neighbouring nodes of a solid-state lattice cover a vast range of values from 10^{12} to $10^{-5}\, s^{-1}$. An example of fast reaction is the two-proton transfer in the carbonic acid dimer and in the cycle dimers of nitrogen bases, in which the cycle is created owing to two intermolecular hydrogen bonds. In the excited singlet state the dimer of 7-azoindole (N_1^*) converts into the tautomer (T_1):

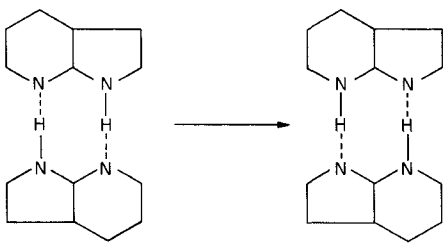

(5.1)

with a rate constant of $\sim 10^{12}\, s^{-1}$. The reaction is also observed at 4·2 K [119, 120]. The measurements of laser excitation spectra of fluorescence for the cooled supersonic jet [69] have shown that the transition is promoted by the symmetric vibrations of the intermolecular cycle with a frequency of 120 cm^{-1} (see figure 9). In the 1-azocarbazole dimer the rate constant of the two-proton transfer decreases to $\sim 10^9\, s^{-1}$ because of the asymmetry of potential. The reverse transition from the tautomer to dimer in the ground state $T_0 \rightarrow N_0$ occurs at a rate of $K \sim 10^3$–$10^5\, s^{-1}$. Non-Arrhenius dependence

of $K(T)$ is observed for $T = 170$–275 K. The isotope H/D effect is 3·2 and 14 for 273 K and 172 K, respectively [120].

In the model simulation in [71] the barrier height and H-atom vibration frequency are taken to be 3·7 kcal $(mol)^{-1}$ and 1800 cm^{-1}, respectively. The intermolecular vibration reduces the tunnelling distance from 0·8 Å to ~0·6 Å.

Two-proton exchange in various carbonic acid dimers is well-studied with NMR [121–123], non-elastic neutron scattering [123, 124] and high-resolved impurity fluorescence [125]. For different acids the cross-over temperature ranges from 40 to 160 K, K_c is (0·4–2·1) $10^9\,s^{-1}$ and the apparent activation energy at $T > T_c$ is 1–2 kcal $(mol)^{-1}$. Quantum-chemistry PES calculation [121] shows that at fixed heavy atom coordinates the barrier is higher than 30 kcal $(mol)^{-1}$. This calculation is in agreement with the data from [126] where the hydrogen bonding potential is found as a function of the O–O distance in OH...O fragments, the latter being 2·61–2·71 Å for the dimers in question. Stretching skeleton vibrations reduce this distance in the transition state to 2·45–2·35 Å, when the barrier height is less than 3 kcal $(mol)^{-1}$. It is stressed in [121] that the transfer is possible only due to the skeleton deformation shortening the distances for the hydrogen atoms transfer from 0·6–0·7 Å to ~0·3 Å. The vibrational-adiabatic potential (3.12) corresponds to a narrow and deep channel, near the bottom of which the coupling of the motion along the reaction coordinate to transversal modes is antisymmetric, so that the effective mass exceeds $2m_H$.

Crystalline fields asymmetrize the double-well potentials. The energy minima difference (which usually varies from 0·1 to 0·4 kcal $(mol)^{-1}$) is sensitive to internal and external stresses [125], so that in the perfect crystals the exchange frequency is several times as much as in the lower-quality ones. When asymmetric, the transition requires a change in the quantum numbers of vibrations coupled to the reaction coordinate. In [127] a simple model has been proposed for the transition stimulated by the resonant absorption or emission of one vibrational quantum with the energy of E_A. The rate constants for the direct and reverse transition at $E_A/k_BT > 1$ are equal to:

$$\vec{K} = K_0 N(E_A), \qquad \overleftarrow{K} = K_0[N(E_A)+1], \qquad N(E_A) = [\exp(E_A/k_BT) - 1]^{-1}, \quad (5.2)$$

where $N(E_A)$ is the equilibrium population of vibration state with the energy E_A and K_0 is determined by the coupling coefficient. The equilibration time then equals:

$$T_1^{-1} = \vec{K} + \overleftarrow{K} = K_0 \coth\left(\frac{E_A}{2k_BT}\right). \quad (5.3)$$

This expression shows that in this simple model the cross-over temperature relates to the potential asymmetry ($T_c \cong E_A/2k_B$). The model [127], as well as [98, 107, 108], is based on the weak-coupling approximation and does not take into account the change in the equilibrium positions and vibration frequencies during the motion along the reaction coordinate. Thus, the effects of reorganization and effective mass alteration, noted in section 3, cannot be accounted for in this model.

Upon replacing a pair of molecules in a benzoic acid crystal by the thioindigo molecule, there forms a dimer with very small asymmetry [125]. This has allowed us to measure for the first time the tunnel splitting in intermolecular transfer of a hydrogen atom in a crystal [128]. The splitting found with the optical 'hole-burning' method corresponds to the exchange rate constant of $8 \times 10^9\,s^{-1}$ at 1·35 K. The rate constants in other carbon acids, measured in [124] (the data is partly represented in table 6), correspond to larger asymmetries (0·15–0·65 kcal $(mol)^{-1}$) and, therefore, have lower values than in the perfect benzoic acid crystal.

Table 6. Intermolecular transfer and diffusion of hydrogen atoms.

Compound	Fragment	Region of T, K	$K(T)$, s^{-1}	K_H/K_D (T)	T_c, K	K_c, s^{-1}	V_0, kcal $(mol)^{-1}$	L_H, Å $(d, Å)$
7-azoindole ground state	NH...N	77–185	4×10^{3}–4×10^{4}	14(172)	170	4×10^{3}	—	—
dimer S_1-state	N...HN	4·2	$\sim10^{12}$	<4	—		3·7†	0·8(0·6)
Benzoic acid	OH...O	1·4	$8{\cdot}4\times10^{9}$					
(cryst.)	O...HO	298	$3{\cdot}8\times10^{10}$	—	~40	$8{\cdot}4\times10^{9}$	5·6†	0·49
terephtalic acid	OH...O	4·2–200	2×10^{9}–2×10^{10}	—	65	$2{\cdot}1\times10^{9}$	5·8†	0·47
(cryst.)	O...HO							
malonic acids	OH...O	4·2–290	5×10^{8}–2×10^{10}	—	160	5×10^{8}	6·1†	0·57
(cryst.)	O...HO							
Naphtole (S_1)-ammonia	CH...N	10–24	$4{\cdot}5\times10^{10}$	—	>24	$4{\cdot}5\times10^{10}$	3·5	0·75
Anthracene-anthraquinone radical pair	CH...O	10–270	4×10^{4}–5×10^{6}	200(<40)	60	4×10^{4}	7·5	1·3–1·5
Acrydine (^3T)—fluorene	CH...N	33–143	10^{-2}–10					
quinoxaline (^3T)—durene	CH...N	160–350	10^{-1}–10^{3}	10^{2} (240)	<120	~10^{-1}	8·5	2·2
$C\dot{H}_3$—CH_3OH	CH...C	4·2–120	10^{-4}–10^{-1}	9×10^{2}(95)	45	10^{-4}	12	1·6
$C\dot{H}_3$—C_2H_5OH	CH...C	4·2–120	10^{-5}–10^{-2}					1·6
$C\dot{H}_3$—CH_3CN	CH...C	67–120	2×10^{-5}–10^{-2}	$>2{\cdot}8\times10^{4}$ (77)	<60	~10^{-5}	14	1·6
Polyvynilacetate radical—malonic acid	CH...C	77–240	2×10^{-4}–10^{-2}	—	110	2×10^{-4}	13	—
Diphenylcarbene-methyl-cyclohexane	CH...C	108–120	5×10^{-4}–2×10^{-3}	<2	—	—	14	—
Dimethylglyoxime radical pair	OH...O	4·2–200	2×10^{-5}–10^{-2}	—	50	2×10^{-5}	14	1·1–1·2
hydrogen atom on the [110] face of W crystal	W–H–W	4·2–200	10^{-3}–3×10^{-2}	T (27)	130	~10^{-3}	7·7	2·7
hydrogen atom in H_2 crystal	$H–H_2$	1·9; 4·2	10^{-5}–10^{-4}	$\sim10^{4}$	—	—	9·4	4·6
hydrogen atom–malonic acid	CH...H	100–290	10^{-3}–5×10^{-2}	—	110	10^{-3}	~11	—

† $V_0 = E_a + \frac{\hbar\omega_B}{2}$.

The values of $K_c = 10^1$–$10^5\ s^{-1}$ and $T_c = 50$–$70\ K$ are found for the H-atom transfer from one of the neighbouring host molecules to the excited impurity molecule. In [129, 130] the abstraction of an hydrogen atom from a fluorene by the impurity acrydine molecule in the lowest triplet state has been studied. The fluorene molecule is oriented in a most favourable way for the transfer (figure 15). The formed radical pair is deactivated by the reverse transition. The H-atom abstraction by the acrydine molecules competes with the radiational deactivation (phosphorescence) of the ^3T state, and the temperature dependence $K(T)$ is inferred from the kinetic measurements in the interval of 33–143 K. At $T = 33$–$72\ K$ the expression (3.10), corresponding to $T > T_{c_2}$, is valid, while at $T > 70\ K$ the Arrhenius law holds with the activation energy of 0·33 kcal $(mol)^{-1}$ $(120\ cm^{-1})$. The value of E_a corresponds to the thermal excitation of the symmetric vibration, which is observed in the Raman spectrum of the crystal (figure 15). The shift in its frequency after deuteration shows that this is a libration, i.e., the reaction-assisting barrier fluctuations are due to the molecular rotation in the crystal. The H (D)-atom abstraction rate constants in the curene crystals by the molecules of quinoline, isoquinoline, quinoxaline and quinazoline in the excited triplet state, have been measured in [131]. In the interval of 300–160 K the activation energy drops from 3·5 kcal $(mol)^{-1}$ to 1·6 kcal $(mol)^{-1}$. Deuteration reduces the rate constants by ~ 10 times (at 250 K) whereas the activation energy builds up to 4·5 kcal $(mol)^{-1}$ (at 220–300 K). The transition occurs in the fragment CH...N, formed by a methyl group of duren and the nitrogen atom of the impurity molecule. The increase in the transfer length, following from the crystallographic data, correlates with diminishing of the rate constant. The results [131] are interpreted in the model [98] as the fluctuational barrier preparation induced by the intermolecular vibration (impurity molecule libration) with a frequency of $230\ cm^{-1}$.

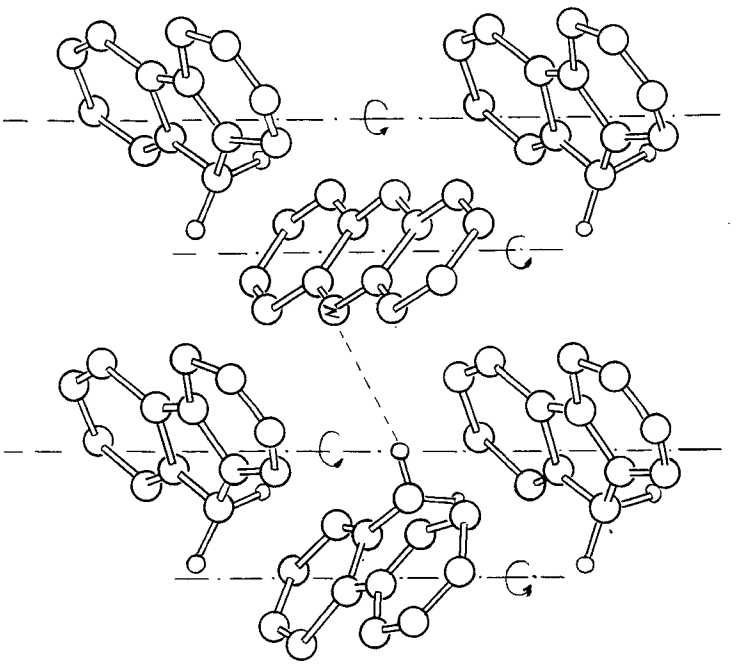

Figure 15. Position of an acrydine molecule in the fluorene crystal. The dashed line shows the direction of H-atom transfer to the impurity molecule. The arrow indicates the libration which lowers the barrier.

Hydrogen atom transfer from the anthracene molecule, excited to the higher singlet state, to the anthraquinone impurity creates a radical pair, which quenches the anthracene crystal fluorescence much stronger than the initial impurity does. The reverse transfer rate constant, found from measurements of fluorescence intensity and its characteristic time at different moments after the creation of the radical pair, varies from $10^6\,s^{-1}$ to $10^5\,s^{-1}$ in the interval of 110–65 K, $K_c = 4 \times 10^4\,s^{-1}$, $T_c = 60$ K. The K_c value drops to $\sim 10^2\,s^{-1}$ in the deuteroanthracene crystal.

The proton-transfer rate constant in the matrix-isolated complexes of α- and β-napthol with ammonia NaphOH–$(NH_3)_3$ measured in [132] with the picosecond fluorescence method, is $4{\cdot}5 \times 10^{10}\,s^{-1}$ and $4{\cdot}1 \times 10^{10}\,s^{-1}$, respectively, and does not depend on temperature at $T = 10$–24 K. The proton displacement in the fragment OH...N is ~0·75 Å. The barrier height, evaluated by use of (2.2) for the one-dimensional tunnelling, is 3·6 kcal $(mol)^{-1}$. It is worth noting that, unlike the previous cases, in this reaction a charge transfer occurs.

The abstraction of an H atom from crystalline and glass-like matrices of saturated organic compounds

$$CH_3 + RH \rightarrow CH_4 + R \tag{5.4}$$

is one of the most studied examples of the intermolecular tunnelling. The reaction (5.4) in the γ-irradiated matrices of alyphatic alcohols is registered with the EPR method via the observation of decrease in intensity of initial radical lines and increase in intensity of the matrix lines (CH_2OH and C_2H_4OH in methanol and ethanol, respectively) [29, 133–138]. The cross-over temperature is 40–50 K, $K_c = 10^{-3}$–$10^{-5}\,s^{-1}$ [139] (see table 2). The apparent activation energy at $T = 50$–100 K is far smaller ($\leqslant 2$ kcal $(mol)^{-1}$), than in the gas-phase reaction, where E_a coincides with the barrier height [140] $V_0 = 11{\cdot}5$–12·5 kcal $(mol)^{-1}$, calculated in [29, 30]. In the γ-irradiated crystalline methanol at 4·2 K the CH_3 radical dies out, forming the new radical CH_2OH, with a characteristic time of $\sim 3 \times 10^3$ s [141]. In the EPR spectrum it is observed that the initial radical pair ($\dot{C}H_3$–$\dot{C}H_3O$) converts into the stabilized pair ($\dot{C}H_2OH$–$\dot{C}H_2OH$) as a result of intramolecular (conversion of $CH_3\dot{O}$ into $\dot{C}H_2OH$) and intermolecular H transfer. By analysing the radical pair spectra, in [141] the distances between the carbon atoms in the pairs have been determined. They are equal to 5·0 Å and 6·7 Å, correspondingly. Because of the hydrogen bonding, the C–C distance between the neighbouring molecules in the methanol crystal is reduced to 4·75 Å. The formation of a water molecule and CH_3 radical through radiolysis leads to the shift of the radical along the ruptured CO bond, that results in the increase of the C–C distance in the radical pair (figure 16). Since the H atom is abstracted from the neighbouring CH_3OH molecule, the indicated displacement shortens the transfer distance making it smaller than the van der Waals radii sum.

According to [137–139], the kinetic curves in the glass matrices consist of an initial part which possess the characteristics described above, and next part of more deep conversion, which is described by the Kohlrausch law [142]:

$$R(t) = R_0 \exp\left[-\left(\frac{t}{\tau}\right)^{\alpha}\right], \tag{5.5}$$

where $R(t)$ is the CH_3 radical concentration. The parameter α in (5.5) increases with temperature and tends to unity above the glass-transition temperature ($T_g = 103$ K for methanol), where the kinetic curves become exponential [143]. It is supposed that the form of kinetic curves (5.5) is caused by variety of distances between the reactants,

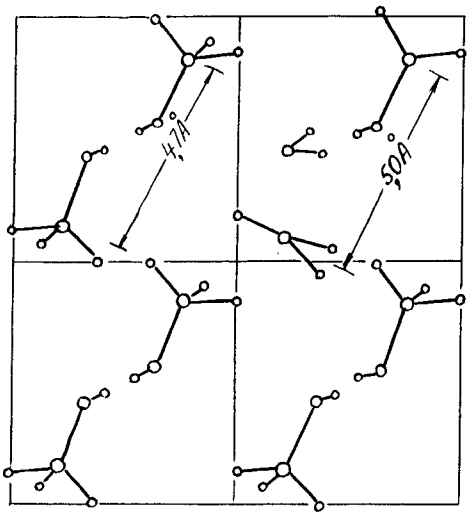

Figure 16. Primary radical pair [$\dot{C}H_2OH$–$\dot{C}H_3$] in the methanol crystal. The hydrogen atom is abstracted by the CH_3 radical from the adjacent molecule CH_3OH.

specific for disordered solids [144, 145]. This variety is characterized by the distribution of barrier parameters and, therefore, of rate constants. The existence of distances distribution and its dependence on temperature are closely connected with the processes of slowed-up relaxation in glasses. The modern state of affairs in this field is considered in [11].

In the γ-irradiated acetonitryl crystals [133] the apparent activation energy for $T = 69$–112 K increases from 0·6 to 2·3 kcal $(mol)^{-1}$. When replacing consecutively one, two and three H atoms by D in the methyl group of the acetonitryl, the rate constant of the CH_3-radical disappearance decreases by 2, 3 and $> 10^3$ times, respectively. More thorough measurements of the isotope H/D effect have shown that at 77 K its value exceeds $2{\cdot}8 \times 10^4$. An indication that the tunnelling takes place has also been obtained in the reaction of CH_3 with methyl cyanide, there E_a increases from 1·2 kcal $(mol)^{-1}$ to 4·6 kcal $(mol)^{-1}$ in the range of 77–125 K, and the disappearance of radical does not show up for a fully deuterated matrix [29].

As indicated in section 2, the reaction (5.4) has been first considered within the model of one-dimensional tunnelling [29, 134]. However, the obtained parameters of static barrier are in disagreement with both spectroscopic and crystallographic data. A satisfactory accord between experiment and theory has been achieved in the model of fluctuational barrier preparation [11, 33, 140, 146]. The C–C distances between reactants and frequencies of barrier fluctuations, found in [35, 146] from analysis of experimental dependences $K(T)$ [29], are given in table 5. As one may expect for the vibrations bringing together reactants, located in neighbouring lattice nodes, the values of Ω correspond to the Debye temperatures in typical molecular crystals. The R_0 values are close to the sum of van der Waals radii. Although the calculation is not based on the knowledge of real structure and dynamics of the crystal, these correspondences can be regarded as a ponderable testimony for the model of fluctuational barrier preparation. The values $R_0 = 3{\cdot}9$ Å and $\Omega 2{\cdot}4 \times 10^{13}\ s^{-1}$ have been obtained with a similar method for the reaction of CH_3 with CH_3OH in [139].

The transition dynamics has been studied in [33] (see also [11]). Are extremal fast transition trajectory by-passes the saddle point (figure 5) so that the height of barrier along it is $\sim 15\,\text{kcal}\,(\text{mol})^{-1}$. Owing to the intermolecular vibrations, the cutting-corner trajectory corresponds to a C–C distance of 3·0–3·1 Å, which is just 0·2–0·3 Å longer than this distance in the transition state of the same reactions in the gas phase (see figure 3). As follows from table 5 and (2.18), the transfer distance for an H atom is $\sim 1{\cdot}6$ Å and the tunnelling distance in the region of low temperatures limit falls to $\sim 0{\cdot}8$ Å.

Of course, comparison of experiment with a calculation in which R_0 and Ω are, in effect, adjustable parameters, fitting the measured and calculated curves $K(T)$ and K_H/K_D ratios, allows one only to ascertain the correctness of the qualitative description of solid-phase reactions (5.4). To progress further one needs, on the one hand, the data about reactants configuration and molecular dynamics and, on the other hand, incorporation of intramolecular vibrations, which is behond the scope of application of the double-adiabatic approximation, exploited in [33, 35, 146], since among them there are vibrations with sufficiently low frequencies close to those of intermolecular vibrations. The reaction barrier is created not only by localization of reactants in the lattice nodes, but by intramolecular reorganization as well. For example, in the reactions of the CH_3 radical the transition from the planar configuration of CH_3 to the tetrahedric one of CH_4 creates a barrier of $\sim 10\,\text{kcal}\,(\text{mol})^{-1}$ [147]. Incorporation of the total set of relevant motions can be carried out with the methods of multidimensional nuclear tunnelling [52, 75–77].

In connection with reactions (5.4) it is worth considering the relation between the kinetic and tunnel isotope effects. The former is known in the transition state theory and is due to the difference in zero-point energies in the initial state (ω_H and ω_D, respectively) which leads to the difference in the activation energies for an overbarrier transition ($E_a = V_0 - \hbar\omega/2$). The ratio K_H/K_D is independent of the barrier height and increases exponentially as temperature drops.

$$K_H/K_D = \exp\left[\frac{\hbar}{2k_B T}(\omega_H - \omega_D)\right]. \tag{5.6}$$

The relation (5.6) holds for $T > T_{c_1} = \hbar\omega_R/2\pi k_B$, where ω_R comes from (2.9) as a function of characteristic barrier frequency ω_B and friction coefficient γ. In the theory of decay of a metastable state (see section 2), the kinetic isotope effect is due to the difference in prefactors determined by (2.13). The ratio K_H/K_D grows as the temperature decreases until $T \sim T_{c_1}$ so that the large isotope effect is characteristic of smooth barriers with small frequencies compared to ω_R ($\omega_H \ll \omega_R$). The increase in the frequency coefficient diminishing ω_R widens the region of validity of (5.6). When the tunnelling transitions are prevailing ($T < T_{c_1}$), K_H/K_D values are smaller than the ones predicted by (5.6). In the low-temperature limit region ($T < \hbar\Omega/2k_B$) K_H/K_D reaches the maximal constant value determined by (3.7). The barrier fluctuations caused by ω_H-independent motions reduces the tunnel isotope effect. The stronger the fluctuation contribution (ratio δ_1^2/δ_0^2), the smaller is K_H/K_D, so that the low-temperature limit of the ratio of K_H/K_D decreases when the extremal trajectory approaches the saddle-point, i.e., for a more slow transition. For the same reason, in the intermediate region of thermal barrier fluctuations $T_{c_2} < T < T_{c_1}$ K_H/K_D is smaller than at $T < T_{c_2}$. Therefore, the temperature dependence of K_H/K_D comprises three regions: kinetic isotopic effect above T_{c_1}, more slow growth with decrease of temperature for $T_{c_2} < T < T_{c_1}$, and low temperature limit.

The exponential growth and high values of K_H/K_D at low temperatures, treated often as an evidence of tunnelling reaction mechanism, can, on the contrary, be connected with a kinetic isotope effect for $\omega_R \ll \omega_H$.

The rate constant of transfer of an H atom from the matrix of malonic acid to the polyvinylacetate macroradical reaches its low-temperature limit $K_c = 2 \times 10^{-4}\,s^{-1}$ at $T_c \cong 110\,K$ [148]. The apparent activation energy in the range of 200–240 K ($\cong 9{\cdot}1$ kcal(mol)$^{-1}$), as well as the value of K_c, corresponds to approximately the same barrier height as in the reactions of the methyl radical.

Low apparent activation energies and prefactors have been observed by means of the EPR method in the reactions of triplet diphenyl-carbene with various solid organic matrices, in which radical pairs are created:

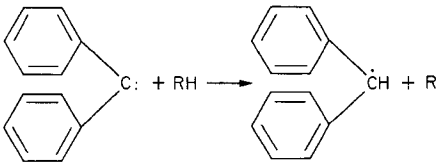

(5.7)

At $T = 77$–$150\,K$ E_a equals 2–4 kcal(mol)$^{-1}$, prefactor is 10^2–$10^5\,s^{-1}$ [149, 150], while the calculated barrier height is equal to 10–14 kcal(mol)$^{-1}$ [151]. Like in reaction (5.4), the attempt to reconcile the experimental dependences of $K(T)$ with a model of one-dimensional tunnelling in the barrier of indicated height leads to its width by far exceeding the H-atom displacement during formation of the activated complex (C–C distance is 3·0–3·2 Å, while characteristic of the transition state is $R = 2{\cdot}65$ Å [142]).

The transfer of H atom in an intermolecular fragment OH...O leads to the isomerization of the primary radical pair, created in the γ-irradiated dimethylglyoxime crystal [152]. K_c and T_c measured in [153] are equal to $10^{-5}\,s^{-1}$ and 50 K, respectively. For the temperatures above 150 K $E_a \cong 9{\cdot}9$ kcal(mol)$^{-1}$. According to the crystallographic data, the O–O distance in the dimethylglyoxime crystal equals 3·1–3·2 Å, so that the barrier for the hydrogen atom transfer would exceed 40 kcal(mol)$^{-1}$, if the intermolecular vibrations were not taken into account [126]. In the model of fluctuational barrier preparation the dependences of $K(T)$ correspond to $R_0 = 3{\cdot}17$ Å and $\Omega = 2{\cdot}9 \times 10^{13}\,s^{-1}$. The kinetic data are summarised in table 6.

The concept of tunnelling has recently been used to explain the mechanism of photodissociation of matrix-isolated molecules. Until then the photodissociation was customarily accounted for by the fact that the hot particles, created by photoexcitation above the dissociation threshold, escape from the cage and, having avoided the geminal recombination, are stabilized at matrix nodes remote from each other. As shown with the molecular-dynamical simulations [154] using the method of time-dependent self-consistent field [155], the H atoms, created upon the photodissociation of HI in the xenon matrix at 2 K, lose the energy of ~35 kcal(mol)$^{-1}$ as a result of collisions with surrounding heavy atoms much earlier (within $\sim 2{\cdot}5 \times 10^{-13}$ s) than leave the cage. Because of the fast relaxation their energy diminishes to the zero-point level (3·5 kcal(mol)$^{-1}$), which is located below the top of the barrier that the particle has to move over to get to the neighbouring intersite. Under these conditions the classical probability of the cage decay equals zero and the dissociation is solely due to the tunnel decay of the metastable state. The maximum probability to leave the cage, competing with the geminal recombination, is achieved for the times of $\sim 5 \times 10^{-12}$ s and equals $\sim 8 \times 10^{-4}$. It seems plausible that tunnelling effects play not the last role in numerous primary processes of the low-temperature radiolysis and photolysis.

6. Quantum diffusion of hydrogen

The diffusion coefficients of hydrogen atoms in metals are 10^{-10}–10^{-4} cm^2 s^{-1} in the range of 100–500 K, which is by 10–15 orders of magnitude larger than those for heavier impurities (e.g. for oxygen and nitrogen atoms). They are characterized by strong isotope H/D effects and low activation energies ($\leqslant 6$ kcal (mol)$^{-1}$) [156]. The anomalous mobility of hydrogen, deuterium and tritium atoms and muonium (with the mass of $0{\cdot}11\, m_H$) is due to vigorous jumps of these light impurities between the interstitial sites of the f.c.k. and o.c.k. lattices [157, 158]. Insertion into tetra and octahedral positions in these lattices leads to the displacement of the surrounding heavy atoms creating the energy of impurity autolocalization and potential asymmetry, since hopping into the neighbouring equilibrium position requires reorganization of the environment. Autolocalization (lattice reorganization) is similar to the formation of Landau–Pekar small-radius polaron in ion crystals [159]. The linear coupling of the particle motion to the vibrations of the initial well, ensuring asymmetry of the potential, leads to the situation in which the transition to the next well is possible only when a fluctuation creates the symmetric configuration with equivalent initial and final wells. The impurity energies in deformed lattice have been calculated in [160]. It has been shown that in the c.b.c. lattices of V, Nb, Ta, Cr, Fe the hydrogen atoms can be localized both in octa and tetrahedral positions, while in the c.f.c. lattices Al, N, Cu, Pd the hydrogen atoms can be localized only in octahedral ones. In the former case the hops occur along the lines connecting O and T positions, the typical barrier heights being 1·2–1·3 kcal (mol)$^{-1}$. In the c.f.c. lattices the barrier heights are 5–10 kcal (mol)$^{-1}$. The relative change of the lattice parameters in the first coordination sphere is 0·04–0·11, while in the second sphere it does not exceed 0·01–0·02.

Upon taking up the normal modes instead of the atom displacements, the reorganization energy can be expressed *via* the relative shifts of the equilibrium positions of acoustic vibrations. In the Debye model, on an assumption of frequency-independent friction the reorganization energy is determined by (2.19).

Since the frequencies of vibrations of H and D impurities ($\sim 10^3$ cm^{-1}) exceed the Debye frequency ω_D by almost an order of magnitude, there have been considered primarily only the jumps of a light impurity in the fixed lattice [161]. The transition probability equals the product of the square of the tunnelling matrix element, proportional to $\exp(-2S/\hbar)$ (see (2.2)), and the Franck–Condon factor dependent on the indicated displacement. For the resonant transition, in which only the zero-point vibrations take place, this factor equals:

$$\phi_0 = \exp\left(-\frac{1}{2}\sum_\omega \frac{d_\omega^2}{\delta_\omega^2}\right) = \exp\left(-\frac{5E_s}{4\hbar\omega_D}\right). \tag{6.1}$$

It follows from the (6.1) that for $k_B T \ll \hbar\omega_D$ the hopping transition is temperature-independent. Because of the presence of low-frequency vibrations, the low-temperature limit exists only below $\sim 0{\cdot}3\,\hbar\omega_D/k_B$. At higher temperatures the transitions accompanied by emission or absorption of one vibrational quantum are significant. In this case [47, 62]:

$$\phi_1 \sim \left(\frac{k_B T}{\hbar\omega_D}\right)^7 \exp\left(-\frac{5E_s}{4\hbar\omega_D}\right). \tag{6.2}$$

Finally, at $k_B T > \hbar\omega_D/2$ the Arrhenius dependence appears, characterized by the activation energy of $E_a = 1/4\ E_s$, corresponding to the thermal fluctuation driving the system through the saddle-point. The model [161, 47, 162] is very similar to that of

electron transfer in the polar medium [163–170] where, on the grounds that the electron and nuclear frequencies strongly differ from each other, the electron transfer is supposed to occur at fixed nuclear coordinates, while the slow nuclear motion (quantum below the temperature of $\hbar\Omega/k_B$ and classical in the opposite case) is favourable for the transition configuration. In [47, 162] it has for the first time been indicated that the light impurity diffusion is activated by the lattice vibrations. In order to incorporate the effect of fluctuational barrier preparation the authors have proposed to take into account the dependence of the tunnelling matrix element on heavy nuclei displacements. This idea has been developed in [171, 172]. In [35, 146] (see also reviews [9, 11]) the mentioned dependence has been represented as an expansion of the action $S(E)$ in (2.2) by the displacement powers

$$S(E,R)=S(E,R_0)+(R-R_0)\left(\frac{\partial S}{\partial R}\right)_{R=R_0}+\tfrac{1}{2}(R-R_0)^2\left(\frac{\partial^2 S}{\partial R^2}\right)_{R=R_0}, \tag{6.3}$$

which corresponds, as is clear from the discussion in section 3, to the model of the fast transition. The action of a particle hopping throughout a barrier of the height V_0 and width d during the time τ_0 is estimated as $S\cong md^2/2\tau_0+\tau_0 V_0/2$. This action is minimum for the characteristic jump time of $\tau_0\cong(md^2/V_0)^{1/2}$. If $\hbar/\tau_0\gg\hbar\omega_0$, the jump is instantaneous in the scale of characteristic vibration periods, which correspond to the fast transition condition (3.3). As noted in section 3, the fast transition potential taken on the extremal trajectory (3.9) differs from the fixed-nuclei barrier, since for the cutting-corner trajectory $R<R_0$ (see figure 6). Figure 17 shows the profiles of the barriers for the jump of a hydrogen atom between tetrahedric positions in the niobium crystal [173]. The barrier $V(Q)$ of a height of $\sim 15\,\text{kcal(mol)}^{-1}$ corresponds to the nuclear configuration in the autolocalized state. The fast transition effective barrier has a height of $9\,\text{kcal(mol)}^{-1}$, while in the case of an adiabatic transition, when at each point the minimum-energy configuration is realized, the barrier height equals only $3{\cdot}5\,\text{kcal(mol)}^{-1}$. While for muonium and hydrogen atom the transition can be believed fast, for deuterium and tritium this approximation is no longer valid. Proceeding to the

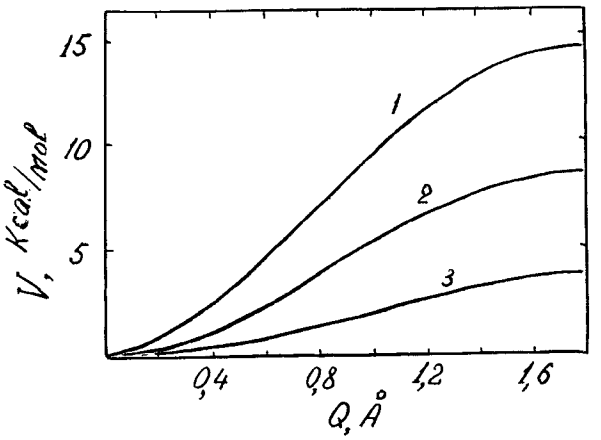

Figure 17. Potentials of slow (3) and fast (2) transition for H-atom transfer between the tetrahedral interstitial positions in the niobium crystal. The curve 1 is the potential in the non-deformed lattice.

Table 7. Tunnel matrix elements J_0 and Franck–Condon factors for diffusion of light impurities in metals.

Particle	Metal	J_0, s^{-1}	$-\ln\phi$
μ	Cu	9×10^{13}	6·1
μ	Al	$1{\cdot}5\times10^{14}$	3·2
H	Nb	9×10^{11}	3·3
D	Nb	5×10^{10}	2·9
H	$Nb(O_xH_y)$	$1{\cdot}4\times10^{12}$	3,4
D	$Nb(O_xD_y)$	9×10^{10}	3·1

slow transition for heavier particles means an effective lowering of the barrier (from V_f to V_a) because of the reorganization. For the same reason ln K grows slower than $m^{1/2}$ *as* m is increased, as pointed out in the previous section. The tunnelling matrix elements and Franck–Condon factors characterizing the diffusion of light impurities in some metals are given in table 7 [157, 158]. The parameters of jump of H and D between the equilibrium positions near admixtured oxygen atom are represented in the same table.

Until recently, hydrogen diffusion on the metal surface was considered as a result of jumps on the fixed lattice [174, 175]. The papers [176, 177] revealed the tunnelling diffusion of H and D atoms on the face [110] of tungsten and have drawn attention to the effect of lattice vibrations [178, 183]. According to [176, 177], a sharp appearance of the low-temperature limit ($D=D_c$) occurs at 130–140 K, whereas the values of D_c depends but slightly on the mass of the tunnelling particle: D_c for D and T atoms is just 10 and 15 times smaller than that for H. The value $D_c\cong2\times10^{-13}\,cm^2\,s^{-1}$ corresponds to the transition probability of $\sim10^3\,s^{-1}$ ($W_c=4D_c/d^2$ where d is the distance between equilibrium positions equal to $\sim2{\cdot}7$ Å [184]). The activation energy, characteristic of $D(T)$ above T_c, grows from 4·0 kcal $(mol)^{-1}$ to 5·8 kcal $(mol)^{-1}$, as the coverage degree is raised, and does not reveal the dependence (5.6) expected for the kinetic isotope effect. It follows from the spectrum of electron energetic losses that the hydrogen atom on the face (110) of tungsten crystal participates in the vibrations of frequencies 1310 cm^{-1}, 820 cm^{-1} and, probably, 660 cm^{-1}. The latter two vibrations are the motions along the face [185] and, therefore, can provide the fluctuational barrier preparation. The Debye frequency of the surface vibrations corresponds better to the observed value of T_c. The results [176, 177] exclude any doubt that the surface diffusion of hydrogen isotopes is quantal. However, the weak dependence of D_c on mass apparently disagrees with the one-dimensional model. In [178], by using the model chemisorption PES [184], the adiabatic transitions of a hydrogen atom between neighbouring equilibrium positions on the (100) face of W have been studied. It has been noted that the increase of coupling to the lattice vibrations and decrease of frequency of the latter enhance the transition probability. It is demonstrated in [183] that the weak dependence $D(m)$ corresponds to the slow-transition model, when effective mass, changes on the trajectory.

$$M^*=m+\sum_k\frac{Q_0^2}{M_k\Omega_k^4}\left(\frac{\partial\lambda_k}{\partial Q}\right)^2. \tag{6.4}$$

The analysis of data [176, 177] in this model has shown that the effective H atom mass spans from $10\,m_H$ to $6\,m_H$, depending on the change of transversal vibration frequency along the trajectory. Since M^* includes m just as a small component, and $S\sim M^{*1/2}$, the tunnelling matrix element changes weakly as a function of m. In the case of a slow

transition the atoms of the lattice have a time to occupy the positions in which the energy is minimum, so that the deformation of the environment follows in the particle motion. When $E_s \gg \hbar\omega_D$, i.e. in the case of strong coupling, the effective mass of the mutual motion of the particle and surrounding lattice deformation substantially exceeds m. The non-monotonic dependence of D on the coverage degree ϑ discovered in [176, 177] has been explained in [173] by the change in the adsorption potential. When some of the neighbouring nodes are occupied by the adsorbate and, hence, shifted from the equilibrium positions, there is an additional reorganization energy involved in the transition. The increase in D with ϑ for $\vartheta < 0{\cdot}5$ is due to a decrease in the vibrational-adiabatic barrier. For the further increase in ϑ the diffusion of vacancies in the two-dimensional adsorption layer replaces the H-atoms diffusion, which diminishes D. More detailed calculations within the slow-transition model have been performed in [179–182] by use of a more real PES.

In conclusion of this brief consideration we emphasize that the fast quantal diffusion of light impurities in metals is connected with overcoming wide and low barriers. The fluctuational lowering of barriers and effective mass growth, caused by low-frequency lattice vibrations, lead to the slow-transition regime despite the fact that the frequencies of these vibrations are by far lower than the typical frequencies of vibrations of an impurity near its equilibrium position.

The diffusion of H and D atoms in the molecular crystals of hydrogen isotopes has been explored in detail with the EPR method [186–194]. The atoms were generated by γ-irradiation of crystals or by photolysis of a specially admixed impurity. In the H_2 crystals the initial concentration of the hydrogen atoms 4×10^{-8} mol (cm)^2 halves during $\sim 10^4$ s at 4·2 K and 1·9 K [188, 189]. The bimolecular recombination (rate constant equals $K_H = 82\,\text{cm}^3\,\text{mol}^{-1}\,\text{s}^{-1}$) is restricted by diffusion, whereas, because of the low H concentration, each encounter of recombination partners is preceded by 10^5–10^6 hops of a length of about the lattice period. The diffusion coefficient corresponding to the measured values of K_H ($D = k_H/4\pi R_H$, R_H is the reaction diameter, supposed in [179] to be equal to 2 A) equals $2{\cdot}7 \times 10^{-16}\,\text{cm}^2\,\text{s}^{-1}$ at 4·2 K and 1·9 K. Were the H atom diffusion thermally-activated, like the molecular diffusion, the ratio of the diffusion coefficients for the given temperatures would exceed 10^{10} ($E_a = 0{\cdot}4$ kcal (mol)$^{-1}$ for the self-diffusion in H_2 at 11–14 K [195]), while the measured values coincide. The diffusion coefficient of D atoms in the D_2 crystal also is the same for 1·9 and 4·2 K. It is four orders of magnitude smaller (3×10^{20}) than the diffusion coefficient for H in H_2 [191]. In the mixed crystals of D_2 and HD (from 20 : 1 to 7 : 1) there is a decrease in the concentration of D-atoms along with the increase in that of H, so that the total concentration remains unchanged in time [190–192]. This means that the conversion is due to the exchange reaction

$$HD + D \rightarrow H + D_2, \tag{6.5}$$

with the exoergicity of 2 kcal (mol)$^{-1}$ caused by the difference in the zero-point energies. The process (6.5) does not occur until the D atom meets the HD molecule as a result of diffusion. The above-mentioned diffusion coefficient for D in D_2 is inferred from the measured rate constant of the reaction (6.5) in the same way as for H in H_2.

At $T \leqslant 11$ K the self-diffusion in the H_2 crystal is due to tunnelling of a molecule from the lattice node to the vacancy, formation of which requires 0·22 kcal (mol)$^{-1}$ [196]. For a similar mechanism the H and D diffusion would also remain thermally activated, which disagrees with the experiment. This discrepancy shows that the

mechanism of the quantum diffusion of H and D atoms is not a molecular one. In [187, 189] it has been supposed that the diffusion is caused by the exchange reactions

$$H+H_2 \rightarrow H_2+H, \qquad D+D_2 \rightarrow D_2+D, \tag{6.6}$$

as a result of which the atom moves to the nearest equilibrium position. The rate constants of reactions (6.6) are related to the diffusion coefficients by a simple formula ($K=6D/d^2V_0$, where d is the jump length equal to 4·6 Å for the H_2 crystal, V_0 is the crystal molar volume equal to 20·0 $cm^3\,(mol)^{-1}$, 20·6 $cm^3\,(mol)^{-1}$ and 22·2 $cm^3\,(mol)^{-1}$ for H_2, HD and D_2, respectively [197]). The rate constants of the reactions (6.5) and (6.6) are given in table 8.

The spatial localization of H atoms in crystals H_2 and HD has been found from analysis of the hyperfine structure of the EPR spectrum, to be caused by the interaction of the uncoupled electron with the matrix protons. The mean distance between an H atom and protons of the nearest molecules, inferred from the ratio of line intensities for the allowed (without change in the nuclear spin projections, $\Delta m_i=0$) and forbidden ($\Delta m_i=\pm 1$) transitions, equals 3·6–4·0 Å and $\sim$2·3 A° for the crystals H_2 and HD,

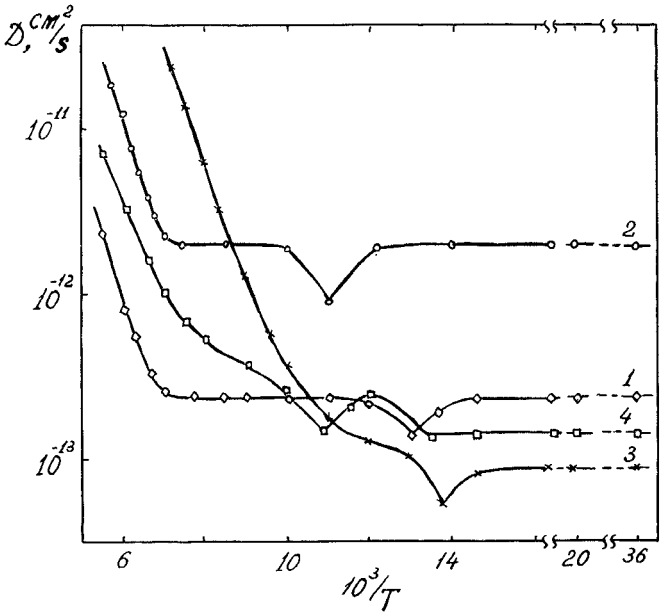

Figure 18. Temperature dependence of the surface diffusion coefficient for H (curves 1 and 2) and D (3 and 4) on [110] face of the tungsten crystal at coverage of 0·1 (curves 1,3) and 0·5 (2 and 4) [117].

Table 8. Rate constants of exchange reactions of H and D atoms at 1·9 K and 4·2 K [182]†.

Reaction	K_c $cm^3\,(mol)^{-1}\,s$	K_c/V_0 s^{-1}
$H+H_2$	1·8	0·9
$D+DH$	$2{\cdot}3\times10^{-3}$	$1{\cdot}1\times10^{-4}$
$D+D_2$	$1{\cdot}8\times10^{-3}$	$7{\cdot}8\times10^{-5}$

† The reactions $H+D_2$, H+HD are endoergic because of the difference in the zero-point energy.

the theory for half a century, further investigation is needed, involving the real crystal respectively. It follows from the comparison of the distances with parameters of the h.c.p. lattice of H_2 that the H atoms in the H_2 crystal replace the molecules in the lattice nodes, while in the HD crystal they occupy the octahedral positions.

The intermolecular distance in the H_2 crystal (3·79 Å) is almost five times as much as the H–H bond length, being close to the equilibrium distance in the linear van der Waals complex H_3 (3·5 Å) [197]. The hydrogen atom, as a substituting impurity, moves almost freely in the cavity with the radius of ~0·6 Å. This allows one, when looking for the rate constants of reactions (6.5) and (6.6), to use the gas-phase model, studied quite thoroughly (see e.g. [198]), as a first approximation. Such calculations have been performed in [199, 200]. The minimum energy of the linear H_3 complex is just by 0·055 kcal $(mol)^{-1}$ lower than that of the isolated H and H_2. The intermolecular vibration frequency is smaller than 50 cm^{-1}. The vibrational-adiabatic barrier height in the transition state is ~9·4 kcal $(mol)^{-1}$, the H–H distance 0·82 Å. In [199] this barrier has been approximated by an Eckart potential with the width of 1·5–1·8 Å. The rate constant has been calculated from (2.1) and (2.2), using the barrier height as an adjustable parameter [189], which leads to the value of V_0 similar to that of the gas-phase reaction $H + H_2$. The rate constant temperature dependence, calculated in [200], are given in figure 19. The cross-over temperature equals 25–30 K. The dependence of

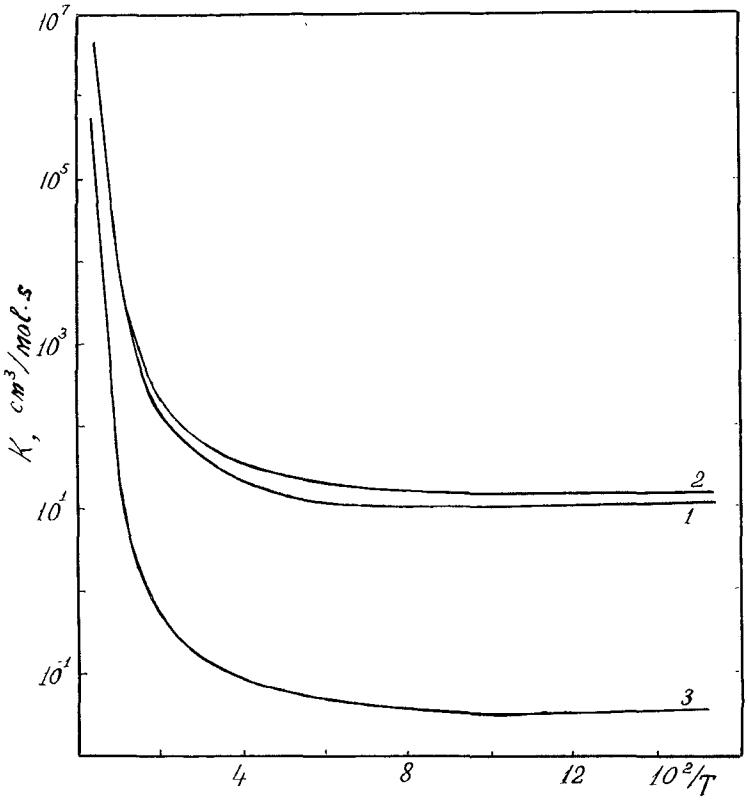

Figure 19. Temperature dependences of rate constants of the exchange reactions $H_2 + H$ (1), $H_2 + D$ (2) and $HD + D \rightarrow H + D_2$ (3) found in [200] within the method of semiclassical adiabatic trajectory with a small curvature [201].

$K(T)$ below T_c is due to the prefactor alteration because of the gas-phase model which does not take into account the zero-point vibrations of the H atom in the crystal. For the same reason the values of the constants differ by 1–2 orders of magnitude from the experimental ones. Since these exchange reactions have been one of the basic objects of dynamics. It is worth saying that the slow-transition model, upon which the results of [199, 200] are based, can prove to be insufficient because of the low frequency of the vibrations providing the fluctuational barrier preparation.

Many cryochemical solid-phase reactions of the hydrogen atom with organic compounds (see reviews [11, 202]) have been studied. The diminishing of the apparent activation energy to 1·5–2·5 kcal $(mol)^{-1}$ in the range of 100–150 K ($E_a \cong 6$ kcal $(mol)^{-1}$ at 200–250 K), which is much smaller than the barrier height (10–12 kcal $(mol)^{-1}$ [1, 30]), speaks of gradual passing from the Arrhenius dependence to the low-temperature limit in the reactions of H atom with organic molecules, among them the polymers [203]. The low-temperature limit $K_c = (0{\cdot}5\text{–}1{\cdot}0) \times 10^{-2}$ $cm^3 (mol)^{-1}$ s has been observed at $T < 110$ K for the reaction of an H atom with malonic acid [148], in which the activation energy above 250 K equals 6·2 kcal $(mol)^{-1}$.

In the methane crystal containing the ethane admixtures the H atoms react with the latter at 10–20 K, forming the C_2H_5 radicals [204]. Similar reactions $H + HR \rightarrow H_2 + R$ with saturated hydrocarbons, beginning from ethane, along with the H adding to ethylene, occur at 30–50 K in the inert gas matrices [205, 206]. These reactions are limited by hydrogen diffusion. The evaluation of the diffusion coefficient of H atom in the xenon crystals ($\sim 10^{-14}$ cm^2 s^{-1} at 50 K [206]) leads to the assumption that the transitions occur between the neighbouring interstitial positions of the h.c.k. lattice (the jump length is ~4·4 Å [207]), separated by wide and low barriers, the fluctuations of which are caused by the low-frequency vibrations of a crystal. Within the framework of the above-discussed resonant mechanism (see (6.1)), if the xenon Debye temperature ($\vartheta_D = \hbar\omega_D/k_B$) equals 55 K [207], it could be assumed that T_c for the hydrogen diffusion in the crystal is ~20 K.

7. Inversion and tunnel rotation

The inversion splitting in the NH_3 molecule is one of the best known spectroscopic apearances of the tunnel effect. The planar structure corresponds to the energetic barrier of 5·94 kcal $(mol)^{-1}$, which separates the equilibrium pyramid-shaped mirror-symmetric configurations. The inversion splitting ω_i is related to the stretching vibration frequency in the equilibrium configurations, equal to 950 cm^{-1} and 745 cm^{-1} for NH_3 and ND_3, respectively, as:

$$\omega_i = \omega_0 \exp\left(-\frac{1}{\hbar}S\right). \tag{7.1}$$

ω_i equals 0·8 cm^{-1} and 36·5 cm^{-1} in the ground and first vibrational state, respectively (see e.g. [208]). The inversion is due to the tunnelling of the reduced mass

$$M = 3m_H(m_N + 3m_H \sin^2\alpha)/(m_N + 3m_H) = 2{\cdot}54\, m_H$$

(α is the equilibrium pyramid angle 21·8°). The tunnelling distance, corresponding to the relative displacement of the N atom in the H_3 plane between the potential minima, equals 0·77 Å. The inversion splitting in the ND_3, where the tunnelling mass is 4·45 m_H, is equal to 0·053 cm^{-1} and 3·9 cm^{-1} for $n = 0$ and $n = 1$, respectively. The influence of rotation on the inversion spectrum is similar to the above-discussed fluctuational barrier preparation and appearance of the reorganization energy. Both effects are

caused by changing of the potential due to the centrifugal forces. The rotation around the symmetry axis flattens the pyramid and diminishes the barrier, while rotation around the perpendicular axis increases the barrier. Note, that the ND_3 inversion is the tunnelling of sufficiently heavy mass throughout the barrier of typical height for the radical chemical reactions, with the probability of $\omega_i/\omega_0 \sim 10^{-3}$. For this reason it is natural that in the cryochemical reactions, the measured constants of which are 5–10 orders of magnitude smaller than ω_i (even allowing for the fact that the transition probability is proportional to $\sim\exp(-2S/\hbar)$ rather than $\exp(-S/\hbar)$), the tunnelling of reduced masses of $(15\text{–}20)m_H$ is possible.

The studies of the high-resolution i.v. spectra of the admixtured molecule NH_3 in the crystals of inert gases and nitrogen at helium temperatures [209, 210] have shown that the crystalline-field-induced asymmetry of the double-well potential reduces ω_i by 1–2 orders of magnitude. In the N_2 crystal at 5·5 K ω_i equals 0·017 cm^{-1} and 1·46 cm^{-1} for $n=0$ and $n=1$.

The torsion vibrations of a methyl group in the potential

$$V(\phi)=\frac{V_0}{2}(1+\cos 3\phi), \tag{7.2}$$

with the C_3 symmetry have the frequency $\omega_r=(K_r/I_r)^{1/2}$, where K_r is the force constant, $I_r=I_1I_2/(I_1+I_2)$ is the reduced moment of inertia, I_1 and I_2 are the moments of inertia for CH_3 and the rest of the molecule, with respect to the C_3-rotation axis. The hindered-rotation barrier height is given to the relationship:

$$V_0=\frac{2}{g}I_r\omega_r^2. \tag{7.3}$$

The tunnel rotation splits the ground state of the torsion vibration into the singlet state A and doublet state E. Their energy difference for sufficiently high barriers ($V_0/\hbar\omega_r \geqslant 2$) can be found within the WKB approximation [211] yielding (7.1) with

$$S=\int_0^{\phi_0}\left\{2I_r\left[V(\phi)-\frac{\hbar\omega_r}{2}\right]\right\}^{1/2}\mathrm{d}\phi, \tag{7.4}$$

where $\phi_0=1/3\cos^{-1}\hbar\omega_r/V_0$ is the turning point for the energy $\hbar\omega_r/2$. As follows from comparison of (7.4) and (2.2), the tunnel rotation of the end CH_3 group of a large molecule, when $I_r\cong I_1$, is equivalent to the transfer of the reduced mass $M\cong 3m_Hm_c/(3m_H+m_C)=2{\cdot}4$ ($M=4{\cdot}0$ for CD_3) through the distance 1·74–1·79 Å. The tunnelling distance is substantially larger than that in the hydrogen transfer reactions, so that the tunnel rotation is observable owing to lower barriers.

The intensive studies of tunnel rotation of CH_3 in molecular crystals and glasses performed mostly with the methods of inelastic neutron scattering and weak field NMR [212, 213], allows the tunnel frequencies to be found within the range from 10^5 to $10^{11}\,s^{-1}$, the influence of intra and intermolecular vibrations on the barrier form and height can be explored.

As distinct from the tunnelling of the hydrogen atom considered in the previous section, when the crystalline fields create an asymmetry of the potential E_1-E_2, in the case of tunnel rotation $E_1-E_2=0$, i.e. the barrier fluctuations and interaction of the rotator with the environment do not break the resonance of initial and final states. For this reason the tunnel rotation is coherent and is described by (7.1) rather than (3.18). The intra and intermolecular interactions create shape and width of the spectral lines.

In the crystals of *n*-alkanes with even numbers of carbon atoms the end methyl groups are packed in the parallel planes and have rotation axes directed similarly. The tunnel rotation frequency, $(3{\cdot}00 \pm 0{\cdot}04) \times 10^5\ s^{-1}$ in the crystals C_6–C_{18}, corresponds to the barrier height of $\sim 3{\cdot}4$ kcal $(mol)^{-1}$ [214], which is close to that observed in the isolated molecules of ethane and propane. In the *n*-alkane crystals with odd number of carbon atoms the axes of end methyl groups are not parallel so that there are two tunnel rotation frequencies, $\sim 1{\cdot}4 \times 10^5\ s^{-1}$ and $3{\cdot}4 \times 10^5\ s^{-1}$, the first of them being observable when the number of C atoms is less than 11. In the crystals of ketones ω_t depends on the number of CH_2 fragments dividing CH_3 and CO groups. For $l = 0$ ω_t reaches 10^8–$10^9\ s^{-1}$ whereas V_0 decreases to 0·8–1·0 kcal $(mol)^{-1}$, while for $l > 4$ it is the same as in the crystals of *n*-alkanes [215]. In the acetylacetone crystal, as a result of existence of keto and enol forms

(7.5)

there are two tunnel rotation frequencies, $1{\cdot}01 \times 10^{10}\ s^{-1}$ and $2{\cdot}3 \times 10^8\ s^{-1}$, corresponding to the barrier heights of 0·45 kcal $(mol)^{-1}$ and 1·18 kcal $(mol)^{-1}$ [216]. In the acetophenone crystal $\omega_t = 1{\cdot}78 \times 10^8\ s^{-1}$, the barrier height equals 1·26 kcal $(mol)^{-1}$ [217]. Larger barrier height in comparison with the 2-keton crystals [215] is due to the interaction of the hydrogen atoms of the CH_3 group with the phenyl ring (H–H distance is 1·83 Å) and neighbouring molecules. The calculation based on the atom–atom potentials method [32] shows that the major contribution comes from the intramolecular interaction [217].

In the isolated nitromethane molecule the CH_3 group rotates almost freely [208]; the barrier in the crystal is created by the intermolecular interaction and can be described as

$$V(\phi) = \frac{V_3}{2}(1 - \cos 3\phi) + \frac{V_6}{2}[1 - \cos(6\phi + \delta)], \tag{7.6}$$

where $V_3 = 0{\cdot}586$ kcal $(mol)^{-1}$, $V_6 = -0{\cdot}356$ kcal $(mol)^{-1}$, $\delta = 30°$ [218]. The contribution to $V(\phi)$ of electrostatic and dispersional interactions, found in [218] with the method of [219], comes at most from dispersional interaction of the hydrogen atoms with nine nearest molecules placed at about 4–5 Å. The interactions potential, apart from ϕ, depends also on the rotation angles of the CH_3NO_2 in the lattice. Describing the rotations of the environment by a single angle ϑ, the authors of [218] have constructed a two-dimensional potential $V(\phi, \vartheta)$, the cross-sections of which for different ϑs are given in figure 20. The experimental values ω_t (table 9) correspond to $V(\phi)$ at $\phi = \vartheta$, i.e., to the slow transition of the adiabatic barrier rapidly modulated by torsion vibrations of surrounding methyl groups. The amplitude of these vibrations at 4·2 K is 0·27 rad and 0·22 rad for the crystals CH_3NO_2 and CD_3NO_2, respectively. The temperature dependence of $\delta^2(T)$ is well described by the harmonic-oscillator relation (3.6) up to 120 K. The r.m.s. amplitude of H and D atoms in zero-point torsion vibrations ($T \leqslant 30$ K) is 0·30 Å and 0·35 Å and goes up to $\sim 0{\cdot}5$ Å at 120 K. Because of large-amplitude motions the tunnel rotation frequencies are very sensitive to internal and external stresses. In the CH_3NO_2 and CD_3NO_2 crystals ω_t (at $n = 0$) increases by 1·5 and 2·0 times at pressure of 4·2 kbar [220]. Since complete deuteration of the hydrogen-content organic crystals, as a rule, reduces the specific volume by $\sim 0{\cdot}5\%$

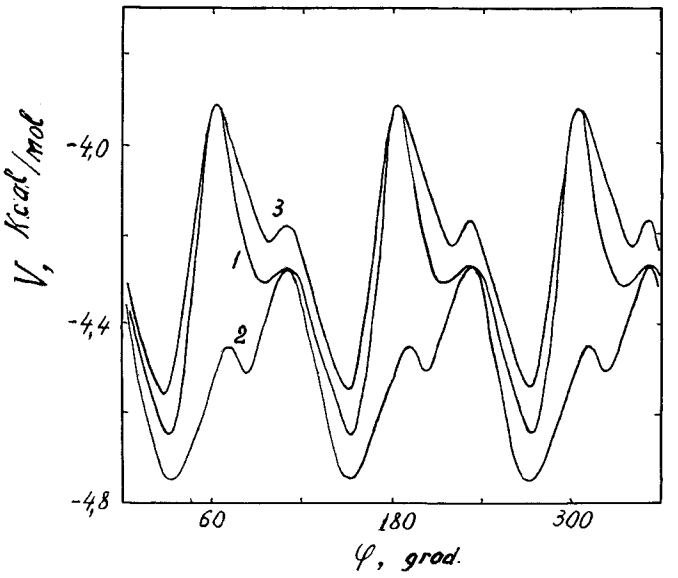

Figure 20. The hindered rotation potential of a methyl group in the nitromethan crystal for different angles of the molecule rotation with respect to its environment. 1. $\varphi=\vartheta$, 2. $\vartheta=0$, 3. $\vartheta=60°$ [218].

[221], which is equivalent to the compressing by external pressure of ~0·5 kbar [222], the matrix deuteration increases the frequencies of tunnel rotation. The tunnel rotation of two non-equivalent CH_3 groups in the α-form of the crystalline toluene is characterized by the frequencies $6{\cdot}3\times10^9\,s^{-1}$ and $6{\cdot}9\times10^9\,s^{-1}$ [223, 224]. Like in the nitromethane crystal, the barrier is created by the intermolecular interaction and ω_t grows with increasing pressure.

Besides the above-considered rotation, the torsion vibrations of the tetrahedric molecules (like CH_4) and ions (like NH_4^+) in crystalline fields of different symmetry have been studied in detail. The three-axial tetrahedron vibrations in the tetrahedric surroundings are characterised by three energy levels A, T and E with the tunnel splitting $2\omega_t$ and ω_t. The potential has 12 equivalent minima [225, 226]. The dependence of ω_t/B ($B=\hbar^2/2I$ is the rotational constant) on the barrier height has been found in [226].

The temperature dependence of the rotation rate $\omega_t(T)$ comes from the statistical averaging of the tunnelling frequencies over the spectrum of libration levels. When $k_BT\sim\hbar\Omega$, the main contribution comes from the levels $n=0$ and $n=1$ with the tunnel splittings ω_{t_0} and ω_{t_1}, respectively:

$$\omega_t(T)=\omega_{t0}\left[1-\exp\left(-\frac{\hbar\Omega}{k_BT}\right)\right]+\omega_{t1}\exp\left(-\frac{\hbar\Omega}{k_BT}\right). \tag{7.7}$$

When $\hbar\Omega\ll V_0$, the librations are almost harmonic and $\omega_t(T)$ is proportional to the r.m.s. amplitude [227] behaving according to (3·6). The dependence (7.7) agrees with the experimental data and shows that the cross-over temperature for the tunnel rotation as associated with $\hbar\Omega/k_B$. In figure 20, borrowed from [227], the curve $\omega_t(T)$ for the methane crystal is given. The activation energy is $70\,cm^{-1}$, the libration frequencies being 50 and $92\,cm^{-1}$ [228].

Table 9. Barrier height and tunnel rotation frequency ($n=0$) in molecular crystals.

Crystal	ω_B, s^{-1}	V_0, kcal $(mol)^{-1}$
4-methylpirydin	$1{\cdot}25\times10^{11}$	0·064
lithium acetate	$6{\cdot}05\times10^{10}$	0·184
plumbum acetate	$1{\cdot}09\times10^{10}$	0·436
nitromethane	$8{\cdot}4\times10^{9}$	0·768
toluole	$6{\cdot}05\times10^{9}$	0·520
ammonia acetate	$3{\cdot}94\times10^{9}$	0·610
3-methylbenzoic acid	$3{\cdot}63\times10^{9}$	0·624
2,5-dimethylpirydine	$3{\cdot}46\times10^{9}$	0·632
4-methylbenzoic acid	$3{\cdot}15\times10^{9}$	0·652
2,6-dimethylpirydine	$2{\cdot}98\times10^{9}$	0·660
3-methylpirydine	$2{\cdot}42\times10^{9}$	0·698
pentamethylbenzole	$1{\cdot}52\times10^{9}$	0·788
sodium acetate	$1{\cdot}40\times10^{9}$	0·804
2-hexanole	$1{\cdot}40\times10^{9}$	0·810
zinc acetate	$1{\cdot}20\times10^{9}$	0·836
methyliodide	$5{\cdot}90\times10^{8}$	1·148
magnesium acetate	$4{\cdot}36\times10^{8}$	1·052
dimethylacetylene	$4{\cdot}11\times10^{8}$	—
3,5-dimethylpirydine	$3{\cdot}9\times10^{8}$	1·078
4-toluoleacetic acid	$2{\cdot}83\times10^{8}$	1·150
methylmalonic acid	$1{\cdot}60\times10^{8}$	1·240
tetramethylgermanium	$7{\cdot}5\times10^{7}$	1·470
copper acetate	$7{\cdot}3\times10^{7}$	1·482
hexamethylbenzole	$1{\cdot}2\times10^{7}$	2·030
3-pentalone	$3{\cdot}6\times10^{6}$	2·34
acetophenone	$3{\cdot}4\times10^{6}$	2·36
3-hexanole	$2{\cdot}4\times10^{6}$	2·43
4-heptanole	$4{\cdot}8\times10^{5}$	3·00
n-hexane	$2{\cdot}98\times10^{5}$	3·4
n-octane	$3{\cdot}00\times10^{5}$	3·4
n-decane	$3{\cdot}01\times10^{5}$	3,4
n-dodecane	$3{\cdot}01\times10^{5}$	3·4
n-heptane	$1{\cdot}46\times10^{5}$	—
	$2{\cdot}98\times10^{5}$	—
n-nonane	$1{\cdot}34\times10^{5}$	—
	$2{\cdot}99\times10^{5}$	
n-undecane	$3{\cdot}36\times10^{5}$	3·4

The thermal excitation of the upper libration levels, increasing $\omega_t(T)$, reduces the tunnel splittings in the spectra of NMR and inelastic neutron scattering, without widening of the lines, which is accounted for by the opposite ordering of the sublevels A and E (in one-axial rotation) for the ground ($n=0$) and first excited ($n=1$) states [229, 230].

The tunnel rotation frequencies (at $T<T_c$) in different compounds range from 10^5 to 10^{12} s^{-1}. Some values of ω_t and V_0, taken from the cited papers, are given in table 9.

8. Heavy particles transfer

As shown in section 3, when the tunnelling mass grows, the regime of transition of the multidimensional barrier tends to be slow, and the extremal trajectory approaches the minimum energy path passing through the saddle-point. The transition can be thought of as a one-dimensional tunnelling in the vibrational-adiabatic barrier (3.12),

and an estimation of K_c and T_c can be obtained upon substitution of the parameters of this barrier for (1.2) and (1.3). It follows from these expressions that K_c hits the interval available for measurements if, as the mass m is increased, the barrier parameters are decreased so that the quantity $d(V_0 m/m_H)^{1/2}$ remains approximately invariant. Since the existing spectral methods allow to measure the tunnel splittings greater than $\sim 10^8\,s^{-1}$, it follows from the data on H atoms exchange reactions (table 4 and 6) that the tunnelling exchange of particles with the reduced masses $m/m_H = 5$–10 is possible only for exotic cases of very high and narrow barriers. The only example known to date involving the tunnelling exchange reaction with heavy particles is automerization of cyclobutadiene [231–235]. The interest in this reaction has been kindled after discovering its anomalous negative activation entropy at 250–270 K [231]. The automerization barrier arises, when passing from the initial rectangular configuration with the alternating bonds of lengths 1·56 Å and 1·33 Å to the transition square configuration with the bond length 1·45 Å, and has the height $\sim 10\,kcal\,(mol)^{-1}$ (according to different methods it ranges from 8 to $12\,kcal\,(mol)^{-1}$ [235]). The transition occurs through the minimum energy path on the two-dimensional PES $U(X_1, X_2)$. The coordinates X_1 and X_2 are the linear combinations of lengths of the bonds C–C (r_1) and C–C (r_2). The reduced tunnelling mass equals

$$m = \frac{2(m_c + m_H)}{(1+\sin\alpha)^2} = 6,53 m_H, \tag{8.1}$$

where $\alpha = 81{\cdot}24°$ is the central angle leaning on the shortest side of the initial rectangle configuration. Owing to the weakness of coupling of the reaction coordinate to other vibrations, the one dimensional model is a good approximation giving a sufficiently accurate result. The ground state splitting is $4{\cdot}2\,cm^{-1}$ in $^{12}C_4H_4$, and it falls to $2{\cdot}35\,cm^{-1}$ for $^{13}C_4D_4$. Because of the weak coupling to the transversal vibrations ω_t changes but slightly for excited levels: 4·2, 4·6 and $5{\cdot}1\,cm^{-1}$ for $n = 0, 1, 2$, respectively. Since the barrier is narrow, even at 350 K the tunnelling rate is by three orders of magnitude greater than the rate of thermally-activated automerization.

The tunnelling transition in the optically active conformers of (4,4,4)-propellahexaene (three six-member carbon rings connected by the common simple CC bond) has been studied in [236]. This compound is in the form of racemic mixture, but, according to the NMR data, the racemization time exceeds 10^{-6} s. As calculated in [236], the barrier height equals $1{\cdot}86\,kcal\,(mol)^{-1}$, the vibration frequencies in the minimum of the term and in the upside-down barrier are $85\,cm^{-1}$ and $68\,cm^{-1}$, respectively. The parameters $dm^{1/2}$ characterizing the tunnelling length in the mass-weighted coordinates is 4·5 $Am_H^{1/2}$. The rate constant found is $6 \times 10^{-3}\,s^{-1}$.

The tunnelling intramolecular rearrangement carbocation of 2-norbornyl was considered in connection with the symmetry of its NMR spectrum persisting up to 4·2 K, which means that the rate of transition between the two asymmetric structures

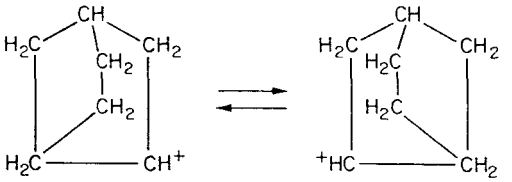

(8.2)

is over $10^9\,s^{-1}$ [237, 238]. According to the calculations in [239, 240], the barrier here is higher than 1 $kcal\,(mol)^{-1}$, which rules out the possibility of an over-barrier transition

with the indicated rate; the frequency of vibrations in the minimum of the double-well potential equals $200\,cm^{-1}$. The CH_2-group displacement length is $\sim 0{\cdot}8$ Å.

The rate constant low-temperature limit for the isomerization of the biradical of 1,3-cyclopentadiyl to the bicyclo-(2, 10)-pentan

(8.3)

has been found in [241]. At $T_c = 15\,K$ $K_c = 6 \times 10^{-4}\,s^{-1}$. Above 20 K the apparent activation energy equals $2{\cdot}3\,kcal\,(mol)^{-1}$, and the small value of the prefactor, according to the discussion in section 2, indicates the tunnelling character of the transition. The smallness of the isotope effect in the reaction (8.3) shows that the contribution of individual hydrogen atom displacements to this reaction is immaterial. This is due to the off-plane bending vibration of the five-member ring. The experimental value of K_c corresponds to the tunnelling of the reduced mass $\sim 7m_H\,(1/2\,(m_C + 2m_H))$, associated with this vibration, throughout a parabolic barrier with the halfwidth 0·6 Å, which is approximately equal to the relative displacement of the CH_2 group for formation of the four-member ring.

In [242, 243] the desorption of the boron ions $^{10}B^{3+}$ from the surface of a non-crystalline metal in strong electric fields has been studied. The activation energy characterizing the desorption rate temperature dependence is $3\,kcal\,(mol)^{-1}$ at $T120$ K, diminishing to $0{\cdot}25\,kcal\,(mol)^{-1}$ in the range of 60–100 K, which corresponds to the tunnelling throughout a barrier with the width 0·3 Å for the mass $10\,m_H$. The tunnel mechanism of the molecular nitrogen dissociative adsorption on metals (W, Re, Fe) has been studied in [244] with the molecular dynamics methods. The two-dimensional model potential surface, the coordinates of which are the N–N length and the distance from the N_2 centre-of-mass to the metal surface, consists of two valleys corresponding to the molecule weakly bonded with the surface (initial state) and strongly bonded atoms. A narrow and high ($\sim 10\,kcal\,(mol)^{-1}$) barrier makes the tunnelling transition more possible than the activated one for the temperatures below 300 K. The saddle-point is shifted to the reactants valley so that the N–N bond stretches just slightly in the transition state (1·14 Å), as compared to the initial length 1·10 Å. The transition is driven by the low-frequency vibration Me–N_2 with the r.m.s. amplitude 0·055 Å ($\Omega = 355\,cm^{-1}$), the displacement along this coordinate equals 0·23 Å.

In the numerous studies of the i.r. spectra of the matrix-isolated reactants (see, for example, [245, 246]) there have been discovered a number of chemical conversions. Among them, from the point of view of the present review, the reactions NO with O_2 [247, 248] and O_3 [249] are of interest. In the former reaction there has been observed the oxidizing of the cis-dimer $(NO)_2$ in solid oxygen at 13–29 K. The dimer has been created at 35 K as a result of NO diffusion. The reaction product is N_2O_4 in the electronically-excited state, converting them, in the opinion of Smith and Guillory [248], into the iso-form of $ONONO_2$. The transition state structure is supposedly of the form:

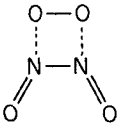

(8.4)

The rate constant for ^{14}NO and ^{15}NO at 13 K is $8 \times 10^{-4}\,s^{-1}$ and $5{\cdot}2 \times 10^{-4}\,s^{-1}$, respectively. The isotope effect, low activation energy (0·1 kcal(mol)$^{-1}$ against 0·65 kcal(mol)$^{-1}$ in the gas-phase reaction) and anomalously low prefactor ($\sim 10^{-2}\,s^{-1}$) testify to the tunnelling mechanism of this reaction. Chemiluminescent gas-phase reaction

$$NO + O_3 \rightarrow NO_2 + O_2 \tag{8.5}$$

with the enthalpy $-47{\cdot}1$ kcal(mol)$^{-1}$ has the activation energy 2·3 kcal(mol)$^{-1}$. Investigation of this reaction in the N_2 matrix at 10–20 K has shown that the apparent activation energy is smaller than 0·11 kcal(mol)$^{-1}$, $K = 1{\cdot}4 \times 10^{-5}\,s^{-1}$ at 12 K. The experiments on ozone enriched with ^{18}O has revealed no isotope effect. The structure of the van der Waals 1 : 1 complexes of NO–O_3 has been studied in [250]. In the planar complex with symmetric position of the NO molecule relative to the O_3-symmetry axis the distance between the centres-of-mass of O_3 and NO is $R_{12} = 2{\cdot}30$ Å, the bonding energy 2·42 kcal(mol)$^{-1}$. In the complex in which NO-bond is perpendicular to the O_3 plane and $R_{12} = 2{\cdot}15$ Å, the bonding energy goes up to 2·73 kcal(mol)$^{-1}$. The potential energy surface of the gas-phase reaction (8.5) has been calculated in [251] with the semi-empirical LEPS method (see, e.g., [1, 252]). The vibrationally-excited products in the ground electronic state are created when the end O atom is abstracted from the O_3 molecule as a result of approach of the NO molecule at an ONO angle of 110°. The height of the reaction path barrier equals 3·57 kcal(mol)$^{-1}$. The activation energy 2·13 kcal(mol)$^{-1}$ is close to the measured one. In the transition state the saddle-point is shifted towards the reactants valley and the distances R_{OO} and R_{NO} are equal, respectively, to 1·277 Å and 1·957 Å, while the equilibrium bond lengths in O_3 and NO are 1·272 Å and 1·150 Å. Comparison of the geometry of the first van der Waals complex with the transition-state arrangement shows that the package of the reactants provides the same attack angle as in the gas phase reaction. The O–O bond stretching does not exceed 0·2 Å. The relative displacement of O–NO in the barrier is 0·45 Å. Seemingly, the fluctuational barrier preparation is due to the intermolecular vibrations as well as the hindered rotation with the above-mentioned low barrier. Because of low frequencies of these vibrations the low temperature limit has not been reached even at 10 K.

The rebinding of CO and O_2 ligands to the complex-creating Fe ions of the heme group of myoglobin after the rupture of the coordination bond induced by the laser photolysis, has been studied in [253–256]. The formation of F–CO and Fe–O_2 bonds has been registered by the restoration of absorption spectrum of the initial compound in a wide range of times ($10^{-6}\,s^{-1}$–10^3 s) and temperatures (2–100 K). T_c and K_c are $\sim$20 K and $\sim 10^{-1}\,s^{-1}$. The apparent activation energy at 30–100 K is 0·9 kcal(mol)$^{-1}$. A qualitative structure model has been proposed in [255, 256]. Before the photolysis the 6-coordinated Fe^{2+} ion locates in the heme plane. The rupture of the coordination bond not only leads to the displacement of a ligand but also rebuilds all the coordination sphere. As a result, the Fe^{2+} ion leaves the plane. Opposite exoergic rebinding of the ligand requires surmounting a barrier that separates the initial configuration from the one created after photolysis. As shown in [257], the change in Fe–CO bond length upon photodissociation of carboxyhemoglobin does not exceed 0·1 Å, so that the mentioned barrier is created at most on account of reorganization of many bonds in the heme (see also [258]).

The reactions of organic radicals with chlorine

$$R + Cl_2 \rightarrow RCl + Cl \tag{8.6}$$

have been explored in [259–263] by combining spectrophotometric measurements of chlorine consumption and EPR-observation of the fall-off in the free radicals concentration after Cl_2 photolysis, inducing the formation of R. The radicals in the RH $+Cl_2$ mixtures appear as an outcome of succession of fast cage reactions after Cl_2 photolysis ($Cl_2^{h\omega}\rightarrow Cl_2^*$, $Cl_2^*\rightarrow Cl^*+Cl^*$, $RH+Cl^*\rightarrow R+HCl$) and react with the surrounding molecules, so that the reaction (8.6) can occur in clusters ($RH{-}Cl_{2n}$) at $n\geqslant 2$ and shows up only if the molar concentration of chlorine in the mixture (C) is greater than 0·1. When $C>0{\cdot}5$, the chain growth takes place. It is restricted by the cluster size and the reaction (8.6) is the growth-limiting stage [262]. The $K(T)$ dependence includes an Arrhenius region (60–90 K) in which the activation energy (2–4 kcal $(mol)^{-1}$) is 1·5–2 times as much as that in the gas phase reactions with the same reactants. The low-temperature plateau occurs below 40–50 K where K_c equals $5\times10^{-3}\,s^{-1}$ and $2\times10^{-2}\,s^{-1}$ for the radicals of *n*-butylchloride [259] and methylcyclohexane [260], respectively. The reaction barrier corresponds to the inter-reactant distance 2·7–2·8 Å, while for the van der Waals distance between them (3·4–3·5 Å) the K_c would be by 15 orders of magnitude smaller than the observed value. Consequently, the reaction (8.6) becomes possible only due to the low-frequency intermolecular and bending vibrations (see the next section). The value of T_c in the reaction (8.6) for the mixture of Cl_2 with methane spans from 30 K to 55 K, depending on the structural non-equilibricity of the glass-like mixture [263]. As the mixture equilibrates, the Arrhenius-region activation energy ($T\leqslant 60$ K) increases from 2·4 kcal $(mol)^{-1}$ to 6·4 kcal $(mol)^{-1}$. The sharp dependence of rate constants for the low-temperature reactions on relative arrangement of atoms in the neighbouring nodes, which, in turn, results from the non-equilibrium glass structure, is an origin of specific critical behaviour observed in the glass-like reactant mixtures (see the review [264]). The same dependence accounts for the jumps in the rate constants near the structural phase transitions [34, 265].

The considered data are collected in table 10. Since most reactions are exoergic and the tunnelling lengths $dm^{1/2}$ are much smaller than the reduced geometrical displacements of the heavy particles, the $dm^{1/2}$ values are given. The chain reactions discussed in the next section are also included in the table. Comparison to the H-atom transfer (tables 4 and 6) and tunnel rotation (table 9) shows that the increase in the tunnelling particle mass does not lead to a substantial decrease in the cross-over temperature T_c. It is a straightforward consequence of the fluctuational barrier preparation (see section 3). The decrease in the tunnelling length and vibrational-adiabatic barrier height ensures the exoergic tunnel reactions with the masses transferred $m/m_H\leqslant 20$.

9. Low-temperature chain reactions

The chain polymerization of formaldehyde turned out to be the first example of a chemical conversion for which the rate constant low-temperature limit has been discovered [266, 267]. Upon γ-irradiation the growth of chain with the length from 10^3 (4·2 K) to 10^7 (77 K) has been observed with a calorimeter with the time-constant 0·3 s. The rate constant of a one link growth, found from the kinetic post-polymerisation curves, is invariant in the interval 4·2–12 K where $K_c=1{\cdot}6\times10^2\,s^{-1}$. Above 20 K the apparent activation energy goes up to 2·3 kcal $(mol)^{-1}$ at 140 K, where $K\sim10^5\,s^{-1}$. A detailed analysis of the experimental data has been given in [8, 9, 11, 268–270]. The polymerization of crystalline and amorphous formaldehyde, initiated by the photodissociation of β-naphtol admixture, has been observed then in [271, 272] at $T\geqslant 20$ K. As the photodissociation leads to the proton transfer, the data [271, 272] testify to the cation polymerization mechanism. In [273–275] the conversions in the mixtures of

Table 10. Tunnelling reactions of heavy particles.

Reaction	T_c, K	K_c, s^{-1}	m/m_H	V_a, kcal $(mol)^{-1}$	$dm^{1/2}$, Å $m_H^{1/2}$
cyclobutadyene automerization	>350	$1{\cdot}2\times10^{11}$	6·53	~9·5	0·59
automerization of 2-norbornyle cation	—	10^9	~7	1·0	2·1
electrofield desorption of boron cation	110	—	10	3·3†	0·95
rebinding of CO–Fe in myoglobin	20	10	(19)	1·6†	~2·2
chain polymerization of formaldehyde $(CH_2O)_{n-1}CH_2OH^+ + CH_2O\ (CH_2O)_nCH_2OH^+$	12	$1{\cdot}6\times10^2$	14	~2·3	2·2
chain haloidation and hydrohaloidation of ethylene					
$C_2H_4Br+HBr \quad C_2H_sBr+Br$	50	20	—	~1·6	—
$C_2H_4Cl+Cl_2 \quad C_2H_4Cl_2+Cl$	45	12	17·3	1·6	2·3
$C_2H_4Br+Br_2 \quad C_2H_4Br_2+Br$	45	8	—	~1·6	—
$(NO)_2+O_2 \quad N_2O_4$	<13	8×10^{-4}	—	2·5†	—
$NO+O_3 \quad NO_2+O_2$	<12	$1{\cdot}4\times10^{-5}$	(10)	~6‡	1,4
$R+Cl_2 \quad RCl+Cl$	40–50	10^{-3}–10^{-2}	(17)	2–3	(2·4)
Isomerization of 1,3-cyclopentadyile radical	15	6×10^{-4}	(14)	3·3†	2·2

† The sum of the activation and longitudinal zero-point energies.

‡ The sum of the activation energy in gas-phase reaction and bonding energy in the van der Waals complex.

formaldehyde and chlorine, initiated by the photolysis of the latter, have been studied with the i.r.-spectroscopy methods at 18–95 K. The products of conversion are formylchloride HCOCl and oligomer $(H_2CO)_v$. Below 70 K $v = 5$–10 and quantum yield of the oligomer does not depend on temperature, and the time of chain growth does not exceed 2 s, i.e. $K_c \geqslant 2{\cdot}5\,s^{-1}$. Above 70 K the slow chain growth also occurs ($v = 50$ at 90 K) and is subject to the Arrhenius dependence with $E_a = 3{\cdot}9$ kcal (mol)$^{-1}$ for $T = 75$–95 K. The chain growth is driven by the proton transfer:

$$(CH_2O)_{v-1}CH_2OH^+ + CH_2O \rightarrow (CH_2O)_vCH_2OH^+. \qquad (9.1)$$

The primary cation CH_2OH^+, along with HCOCl, is created in the cage reaction under Cl_2 photolysis.

Thus, results obtained in different laboratories and with different methods reveal the existence of a completely unusual chemical conversion, polymerization at very low temperatures. A similar effect has been found in the γ-irradiated acrylonitrile and acrolein [276].

The mechanism of ion polymerization in the crystals of formaldehyde [277, 278] rests on the Semenov's assumption [279] that solid-phase chain reactions are possible when the arrangement of the reactants in a crystal prepares the future chain configuration. The monomer crystals capable of low-temperature polymerization fulfill this condition. In the initial equilibrium state the monomer molecules locate in the lattice nodes and the creation of a chemical bond requires surmounting a high barrier. However, upon creation of the primary dimer cation the active centre shifts to the intersite and the barrier for the next link connection diminishes. Since the internode distance in the monomer lattice is much greater than that between the polymer chain links, the chain end-group has to shift towards the next monomer link, as a result of the previous reaction act. This displacement along with the reorientation of the monomer link lead to the formation of a low-barrier configuration facilitating the next reaction act. According to the calculations of different configurations [278], the formaldehyde molecule turns by the angle ~45° with respect to its axis for the connection to the chain. The C–O–C angle in the cation is close to 180° and decreases to 120° after connection of the next link, which associates with the barrier 2–3 kcal (mol)$^{-1}$. As a result of the two mentioned motions (rotation of the monomer molecule and isomerization of the end-group of cation) the connection act corresponds (at $T < T_c$) to the tunnelling of the CH_3 group through the distance 0·6 Å. The growth of long chains according to the considered mechanism is realized only in one of the possible crystalline structures of formaldehyde. In the other structures the chain length is limited by the number of 'suitably packed' molecules and is under 8–10. Since the calculated [277, 278] structures differ from the one that recently has been found experimentally [280], the proposed mechanism needs corrections. As noted in [275], a fast growth of chain consisting of 5–7 links can occur in the structurally selected groups, where the intermolecular distance is shortened to ~2·75 Å compared to the van der Waals one (3·22 Å).

The chain ethylene hydrobromination upon the HBr decomposition initiated by γ-irradiation proceeds according to the scheme:

$$Br + C_2H_4 \rightarrow C_2H_4Br, \qquad C_2H_4Br + HBr \rightarrow C_2H_5Br + Br. \qquad (9.2)$$

Both the chain-growth reactions are exoergic. The low-temperature rate constant limit $K_c = 20\,s^{-1}$ is achieved at $T < T_c \cong 50$ K [281–283]. The weak isotope effect (the rate constant for $C_2D_4 + DBr$ is only 1·5–2 times smaller than for $C_2H_4 + HBr$) shows that the transfer of hydrogen atoms does not limit the reaction rate.

The growth of long chains ($\nu \geqslant 10^2$) in the mixed 1:1 crystals of ethylene with chlorine and bromine at 20–70 K has been observed in [284] after the halogen impulse photolysis, $K_c = 8\text{–}12\,s^{-1}$, $T_c = 45$ K. The chain growth occurs according to the radical mechanism, the limiting stage is reaction (8.6). Above 90 K the chief process is the spontaneous binding of a halogen with the ethylene, forming 1,2-gauche-dihaloethane which, above 115 K, converts into the trans-form [285, 286]. The latter is formed immediately in the radical chain growth at lower temperatures [284]. A specific feature of the mixed halogen-ethylene crystals is the alternating quasi-one-dimensional reactants arrangement which is due to the donor–acceptor interaction [287, 288]. The spatial specificity of the low-temperature chain reaction in such crystals is due to the fact that the radical, created after connection of the halogen atom to ethylene, turns solely into the trans-form $C_2H_4Cl_2$ (or $C_2H_4Br_2$), abstracting the second halogen atom from the neighbouring molecule:

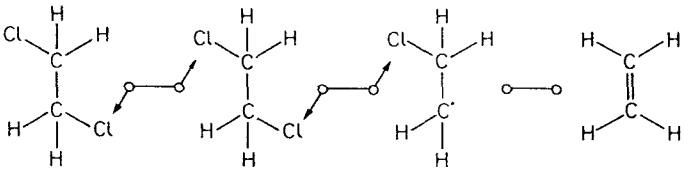

(9.3)

In fact, the mixed crystal is a 'primer' for the chain solid-phase conversion which provides the spatial transfer of a free valency which is not connected with the translational displacement of molecules comparable with the lattice period. As shown in [284], the chain length at $T < T_c$ is determined by the structural quality of the crystal, i.e. it is limited by presence of defects that violate the arrangement of reactants favourable for the reaction. Variation of the crystal growth conditions allows a change

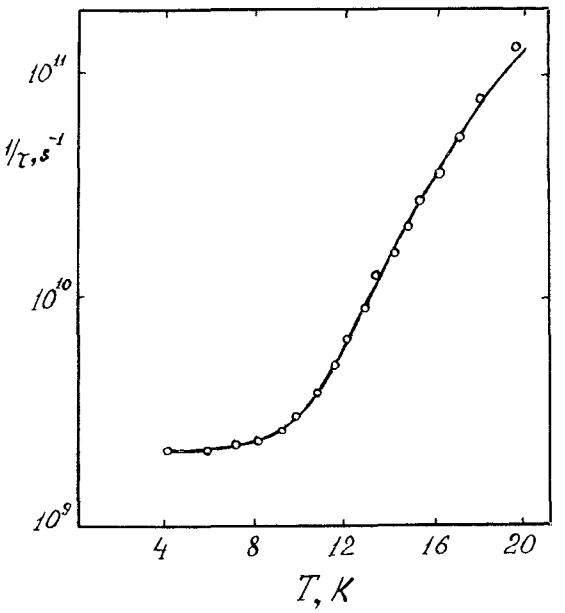

Figure 21. Temperature dependence of the torsion reorientation rate in the methane crystal $1/\tau = 10{\cdot}22 + 1870\exp(-100/T))\,10^{10}\,s^{-1}$ [227].

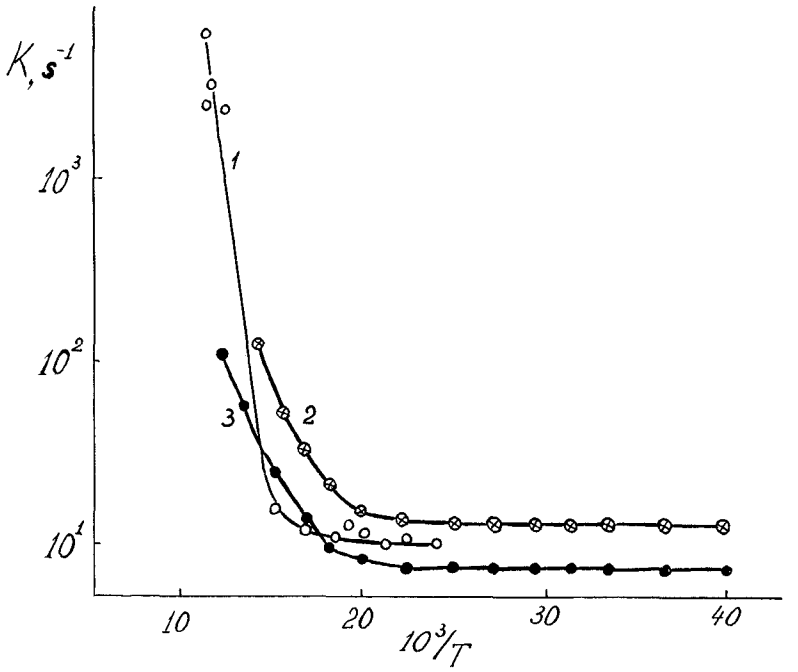

Figure 22. The temperature dependences of the chain growth rate constants of hydrobromination (1), chlorination (2) and bromination (3) of ethylene in mixed 1 : 1 crystals of the reactants.

in the chain length from 50 to 250. The change in v is accompanied by the proportional change in the chain growth time τ, which justifies inferring the rate constant from the kinetic curves ($K = v/\tau$), i.e., the following condition is met: the chain initiation (formation of primary radical) is faster than its growth.

The $K(T)$ dependences for the reactions of C_2H_4 with HBr, Cl_2 and Br_2 practically coincide (figure 22), despite the difference in the reactant masses, if the contribution of the molecular mechanism to the first reaction near 90 K (which increases the apparent activation energy) is taken into account. For 50–80 K $E_a \cong 1$ kcal(mol)$^{-1}$, coinciding with the E_a for the gas-phase reaction of C_2H_4Cl with Cl_2 [289].

The rate constants of the reaction (8.6) in the mixed crystals are $\sim 10^3$ times greater than in the isolated clusters (see section 8), which has been accounted for in [57, 290] by the correlated chain growth: the local deformation arising as a result of previous acts of conversion substantially shortens the inter-reactant distance. This effect, along with the above-considered fluctuational barrier preparation, ensures the anomalously high rates of the chain solid-state reactions at $T < T_c$. Following [57, 290], consider in more detail the results of simulation of the chain growth in the $C_2H_4 : Cl_2$-crystal, since this example reveals most spectacularly the two major peculiarities of the chain solid-state reactions in the region of the low-temperature limit: the chain growth acceleration by the static deformation and low frequency vibrations.

According to the X-ray data [287], the axis of the molecule Cl_2 is perpendicular to the double-bond, and the distance between the molecules is much shorter than in usual molecular crystals. In the 1 : 1 complex structure, calculated in [291], the distance from the nearest chlorine atom to the C–C axis is 3·0 Å, which is by 0·5–0·6 Å shorter than for

the van der Waals contact. The crystal structure has been calculated with the same method as in [277], by means of the minimization of the potential energy represented in the form of atom–atom potential sum, as a function of Euler angles and centre-of-mass coordinates of the molecules. The found triclinic face-centred lattice ($a=4{\cdot}9$ Å, $b=4{\cdot}0$ Å, $c=7{\cdot}0$ Å, $\alpha=121°$. $\beta=97°$, $\gamma=91°$) in which the ethylene molecules locate in nodes, while the chlorine molecules are directed along the shortest diagonal (d_1) of the *ac* plane, is shown in figure 23. This configuration manifests appreciable overlap of the van der Waals radii. The chain growth leads to the creation of a chain of the trans-dichlorethane directed along d_1. The two radicals situated at the chain ends take part in the reaction (8.6) with the neighbouring chlorine molecules. The structure of such an extended defect has been calculated on assumption that only the nearest neighbourhood of the chain was deformed, while the rest of the crystal remained fixed. The energy of the appeared local deformation of the radical surroundings is 3–4 kcal $(mol)^{-1}$. The free-volume deficit created in the chain growth is due to disappearance of the donor–acceptor complexes, instead of which the trans-dichlorethane molecules appear positioned in equilibrium at van der Waals distances. The strongest deformation occurs at the ends of the chain since the atom–atom potential Cl–Cl acting between the $C_2H_4Cl_2$ molecules is much more rigid than the C–Cl potential between radical and Cl_2. The deformation shortens the C–Cl distance (between the reactants) to 3·20 Å instead of the van der Waals radii sum 3·60 Å. In the created compact reactional complex the motion along the reaction coordinate interacts with three normal vibrations: the stretching of the bond Cl–Cl with the force constant $k_1=3\times10^5$ dyn $(cm)^{-2}$, frequency $\nu_1=560\,cm^{-1}$ and zero-point amplitude $\delta_1=0{\cdot}03$ Å;

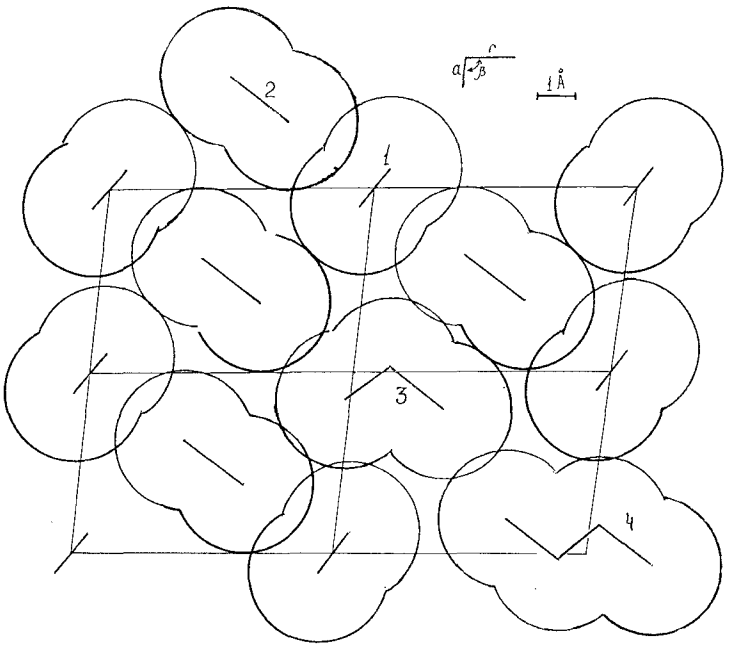

Figure 23. The reactants arrangement in the ac-plane of ethylene–chlorine 1:1 crystal. (1) ethylene molecule (HCH plane is perpendicular to the ac-plane). (2) Cl_2 molecule, (3) H_2C–CH_2Cl radical, (4) transdichloroethane molecule. The circles show the van der Waals radio. The H atoms are not shown.

bending of C–C–Cl in the radical ($k_2 = 4 \times 10^4$ dyn (cm)$^{-2}$ with respect to the C–C bond length, $\nu_2 = 400\,\text{cm}^{-1}$, zero-point displacement of CH_2 fragment towards Cl_2 $\delta_2 = 0{\cdot}07$ Å); intermolecular vibration ($k_3 = 5 \times 10^3$ dyn (cm)$^{-2}$, $\nu_3 = 47\,\text{cm}^{-1}$, $\delta_3 = 0{\cdot}15$ Å). The potential energy surface is three-dimensional since the C–Cl (r_2) is a result of interplay among the components of displacements in the bending (Q_2) and intermolecular (Q_3) vibrations:

$$U(r_1, r_2) = U[r_1, r_2(Q_2, Q_3)], \tag{9.4}$$

where r_1 is the Cl–Cl distance. The PES (9·4) has been calculated in [57, 290] with the LEPS (London–Eyring–Polany–Sato) method for the isolated reactant pair $C_2H_4Cl + Cl_2$ with the crystalline potential added. The barrier found in this way is 2 kcal (mol)$^{-1}$, in satisfactory agreement with experiment. It should be emphasized that the low barrier occurs due to the mentioned static rapprochement of the reactants, as a result of previous acts of the chain growth. Had the C–Cl distance been retained to be 3·6 Å, the 'crystalline' barrier height would exceed 7 kcal (mol)$^{-1}$, which made the tunnelling impossible. Because of strong exoergicity of the reaction, the potential energy surface $U(r_1, r_2)$ is characterized by an (early descent) to the product valley and, since $k_1 \gg k_2, k_3$, the Cl–Cl distance remains nearly invariant while moving from the initial state minimum ($r_2 = 3{\cdot}2$ Å) up to the point $r_2 = 2{\cdot}30$ Å, which is placed at the slope to the products valley and corresponds to the initial energy. Such a situation is characteristic of each of the three mentioned ethylene reactions and, in particular, ensures the H–Br bond in the reactional complex with C_2H_4Br being practically at equilibrium all the way through the barrier. This accounts for the absence of the isotope effect in the second reaction (9.2). Approximate constancy of r_1 in the barrier allows us to represent the PES in the coordinates Q_2 and Q_3, with a small variation of r_1 in the reaction path being taken into account. The cross-section $U(Q_2, Q_3)$ is demonstrated in figure 24 in the Smith-Delves coordinates [39], $q_2 = \lambda Q_2$, $q_3 = \lambda^{-1} Q_3$, $\lambda = (m_{Q_2}/m_{Q_3})^{1/4}$, in which the kinetic energy $T = m/2(\dot{q}_2^2 + \dot{q}_3^2)$ describes the motion of an effective mass $m = (m_{Q_2} m_{Q_3})^{1/2} = 17{\cdot}3\, m_H$ (m_{Q_2} and m_{Q_3} are the reduced masses of the bending and intermolecular vibrations, respectively). The angle between the reactant and product valleys is $\beta = \sin^{-1}(m_{Q_2}/m_{Q_3})^{1/2} = 31°$. Thus, the motion in the reaction path s is at most contributed by the low-frequency intermolecular displacement ($\omega_s \cong \nu_3$ at the initial minimum) while the transversal vibrations have high frequencies (which are close to ν_1 and ν_2 in the initial state), since $\omega_2 \gg \omega_s$, the extremal trajectory corresponds to the vibrational-adiabatic motion. In [57] it is shown how the slow transition potential

$$V_{sl} = V(s) + \frac{m}{2} \sum_k \omega_{\perp k}^2 q_{\perp k}^2 \tag{9.5}$$

transforms into the vibrational-adiabatic one (3.12). The tunnelling probability at $T = 0$ equals:

$$K_c = \frac{\Omega}{2\pi} \left(\frac{S_0}{2\pi\hbar} \right)^{1/2} \exp\left(-\frac{2}{\hbar} S_a \right), \tag{9.6}$$

where

$$\Omega_0^2 = \frac{1}{m} \left(\frac{\partial^2 V/s)}{\partial s^2} \right)_{s = s_1}$$

is the longitudinal vibration frequency in the initial state,

$$s_0 = \int_{s_1}^{s_2} [2mV/s)]^{1/2}\, ds, \qquad S_a = \int_{s_1}^{s_2} [2mV_a/s)]^{1/2}\, ds. \tag{9.7}$$

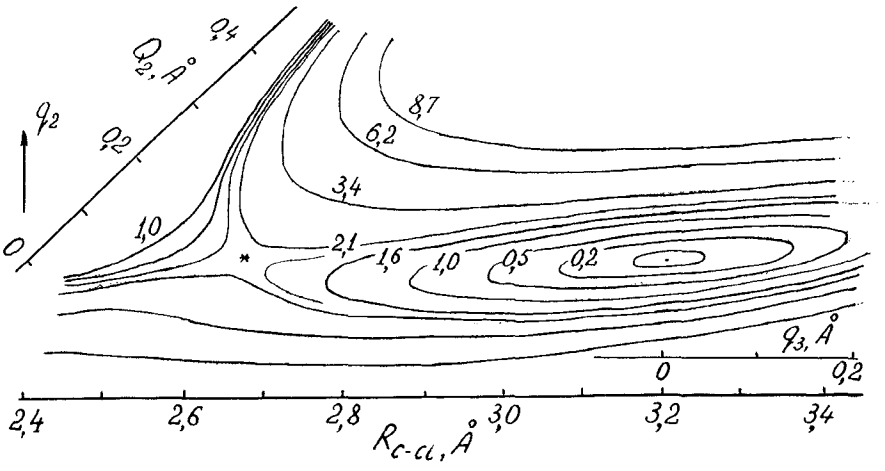

(a)

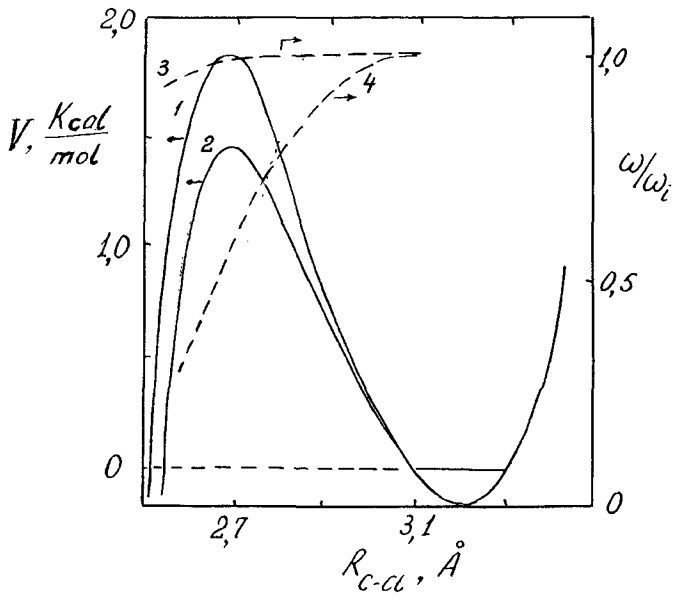

(b)

Figure 24. (*a*) Contour plot $U(Q_2, Q_3)$ for collinear reaction C_2H_4Cl with Cl_2 in crystal. The dashed line shows the extremal trajectory passing through the saddle-point *. (*b*) Bare (1) and vibrational-adiabatic (2) barriers in the reaction path. Change in the frequencies of the stretching Cl–Cl (3) and bending C–C–Cl (4) vibrations. In accordance with (9.7), the zero potential corresponds to the zero-point energy of the longitudinal vibrations in the minimum of the term.

S_0 and S_a are the actions in the bare ($V(s)$) and vibrational-adiabatic barriers, respectively (s_1, s_2 and s'_2 are the turning points coming from conditions $V(s_1)=V(s_2)=V_a(s'_2)=0$). The reaction barriers $V(s)$ and $V_a(s)$ along with the transversal vibration frequencies as functions of s are given in figure 24. The reduction of the latter near the turning point s'_2, where the product valley sharply widens (see figure 23), reduces the adiabatic barrier height by $\sim 0{\cdot}5$ kcal $(\text{mol})^{-1}$, its width diminishes to 0·55 Å. The rate constant found by using (9.6) and (9.7) $K_c = 10^2\,\text{s}^{-1}$ is in agreement with the experimental results.

10. Conclusions

Since the discovery of the rate constant low-temperature limit less than twenty years have passed. The further studies have shown that such a dependence of $K(T)$ is inherent in very different chemical reactions (from intramolecular rearrangements with H-atom transfer to the chain reactions with transfer of much heavier fragments). The numbers of examples of the low-temperature limit grows steadily, which allows us to speak of universality of this phenomenon.

The present review is the most complete analysis of the low-temperature conversions caused by heavy particle tunnelling. The specific features of these reactions are due to the existence of bound initial states, the effect of reactant packing in solids and its change as a result of previous acts of conversion and involvement of low-frequency intra and intermolecular motions of the tunnelling particle environment. These properties closely connect the low-temperature chemistry with the physics of point and extended defects in crystals and non-crystalline solids. It could be said that this area is a boundary between the modern solid state physics and chemical physics of elementary processes.

The appreciable progress in the low-temperature chemistry of the last decade is, in the first place, due to the development of the concept of multidimensional nuclear tunnelling. This concept has appeared independently in the theories of gas-phase and solid-phase reactions and by now it is ascertained by the necessity of their use to describe the conversions occurring at very low rates at energies close to the zero-point ones, when the tunnelling, from a small correction, turns into the main contribution to the transition probability. Reactions in both gas phase and in the van der Waals and matrix-isolated reactant complexes are now being studied under conditions of low initial reactants energies. The low-temperature chemistry step by step fills up the gap between the chemistry of gas and solid-phase reactions. On the way of comparison of kinetic characteristics in different aggregate states and at interfaces at equally low energies appearance of quantitative dynamical models incorporating the totality of reactant and environment motions can be expected.

The advance of experimental methods of measurement of small tunnel splittings, along with improvement in the time resolution and sensitivity of kinetic methods, makes possible the studies of low-temperature reactions in a very wide range of rate constants from 10^{-5} to $10^{12}\,\text{s}^{-1}$.

References

[1] EYRING, H., LIN, S. H., and LIN, S. M., 1983, *Basic Chemical Kinetics* (New York: Wiley).
[2] WIGNER, E. P., 1932, *Z. phys. chem.* B., **19**, 1903.
[3] BELL, R. P., 1935, *Proc. Roy. Soc.* A., **139**, 466; 1935, *Ibid.*, **148**, 241; 1937, *Ibid.*, **158**, 128.
[4] BELL, R. P., 1973, *The Proton in Chemistry* (Ithaca, New York: Cornell University Press).
[5] BELL, R. P., 1980, *The Tunnel Effect in Chemistry* (London: Chapman & Hall).

[6] JOHNSTON, H. S., 1960, *Adv. chem. Phys.*, **3,** 131.
[7] GOLDANSKII, V. I., 1959, *Dokl. Akad. Nauk USSR*, **124,** 1261; *Ibid.*, **127,** 1037 (in Russian).
[8] GOLDANSKII, V. I., 1979, *Nature*, **279,** 109.
[9] GOLDANSKII, V. I., TRAKHTENBERG, L. I., and FLEROV, V. N., 1989, *Tunneling Phenomena in Chemical Physics* (New York: Gordon and Breach).
[10] JORTNER, J., and PULLMAN, B. (Editors), 1986, *Tunnelling*, (Dordrecht: Reidel).
[11] GOLDASNKII, V. I., BENDERSKII, V. A., and TRAKHTENBERG, L. I., 1989, *Adv. Chem. Phys.*, **75,** 349.
[12] MILLER, W. H., and GEORGE, T. F., 1972, *J. chem. Phys.*, **56,** 5668.
[13] WEINER, J. H., 1978, *J. chem. Phys.*, **68,** 2492.
[14] VAINSHTEIN, A. I., ZAKHAROV, V. I., NOVIKOV, V. A., and SHIFMAN, M. A., 1982, *Usp. Phys. Nauk*, **136,** 553 (in Russian).
[15] LARKIN, A. I., and OVCHINNIKOV, YU. N., 1984, *JETP.*, **86,** 719.
[16] KRAMERS, H., 1940, *Physica*, **7,** 284.
[17] MELNIKOV, V. I., and MESHKOV, S. V., 1986, *J. chem. Phys.*, **85,** 1018.
[18] DAKHNOVSKII, YU., I., and OVCHINNIKOV, A. A., 1986, *Himicheskaya fizika*, **5,** 36 (in Russian).
[19] POLLAK, E., 1986, *J. chem. Phys.*, **85,** 865.
[20] GALDEIRA, A. O., and LEGGETT, A. J., 1986, *Ann. Phys. (N.Y)*, **149,** 347.
[21] SETHNA, J. P., 1981, *Phys. Rev. B*, **24,** 698.
[22] HANGGI, P., 1986, *J. statist. Phys.*, **42,** 105.
[23] GRABERT, H., OLSCHOWSKI, P., and WEISS, U., 1987, *Phys. Rev.* B, **36,** 1931.
[24] GRABERT, H., and LINKWITZ, S., 1988, *Phys. Rev.* B, **37,** 963.
[25] HANGGI, P., TALKNER, P., and BORKOVEC, M., 1990, *Rev. mod. Phys.*, **62,** 251.
[26] AFFLECK, I. K., 1981, *Phys. Rev. Lett.*, **46,** 388.
[27] LE ROY, R. J., SPRAQUE, E. D., and WILLIAMS, F., 1972, *J. phys. Chem.*, **76,** 546.
[28] PACEY, P. D., 1979, *J. chem. Phys.*, **71,** 2966.
[29] LE ROY, R. J., MURAI, H., and WILLIAMS, F., 1980, *J. Am. Chem. Soc.*, **102,** 2325.
[30] SANA, M., LERRY, G., and VILLAVECES, J. L., 1984, *Theor. chim. acta.*, **65,** 109.
[31] HIPES, P. G., and KUPPERMAN, A., 1986, *J. phys. Chem.*, **90,** 3630.
[32] PERTSIN, A. J., and KITAIGORODSKY, A. I., 1987, *The atom–atom potential method. Application to organic molecular solids* (Berlin: Springer), Ch. 3.
[33] OVCHINNIKOVA, M. YA., 1979, *Chem. Phys.*, **36,** 15.
[34] BENDERSKII, V. A., GOLDANSKII, V. I., and OVCHINNIKOV, A. A., 1980, *Chem. Phys. Lett.*, **73,** 492.
[35] TRAKHTENBERG, L. I., KLOCHIKHIN, V. L., and PSHEZHETSKII, S. YA., 1982, *Chem. Phys.*, **69,** 121.
[36] EYRING, H., and POLANYI, M., 1931, *Z. phys. Chem.* B, **12,** 279.
[37] HOFACKER, G. L., 1963, *Z. Naturforsch.* B, **189,** H. 607.
[38] MARCUS, R. A., 1966, *J. chem. Phys.*, **45,** 4493, 4500; 1968, *Ibid.*, **49,** 2610.
[39] BAER, M., 1982, *Adv. chem. Phys.*, **49,** 191.
[40] MILLER, W. H., 1983, *J. phys. Chem.*, **87,** 3811.
[41] JOHNSTON, H. S., and RAPP, D., 1961, *J. Am. Chem. Soc.*, **83,** 1.
[42] MILLER, W. H., 1975, *J. chem. Phys.*, **63,** 1166.
[43] TRUHLAR, D. G., and KUPERMANN, A., 1971, *J. Am. Chem. Soc.*, **93,** 1840.
[44] BABAMOV, V. K., and MARCUS, R. A., 1981, *J. chem. Phys.*, **74,** 1790.
[45] BABAMOV, V. K., LOPEZ, V., and MARCUS, R. A., 1983, *J. chem. Phys.*, **78,** 5621.
[46] LANDAU, L. D., and LIFSHITZ, E. M., 1958, *Statistical Physics* (London: Pergamon).
[47] FLYNN, C. P., and STONEHAM, A. M., 1970, *Phys. Rev.* B., **I,** 3967.
[48] KAGAN, YU. M., and KLINGER, M. I., 1974, *J. Phys.*, C., **7,** 2791.
[49] BENDERSKII, V. A., GOLDANSKII, V. I., and MAKAROV, D. E., 1990, *Dokl. Akad. Nauk USSR*, **311,** 626.
[50] BENDERSKII, V. A., GOLDANSKII, V. I., and MAKAROV, D. E., 1990, *Chem. Phys. Lett.*, **171,** 91.
[51] ARNOLD, V. I., 1978, *Mathematical Methods of Classical Mechanics* (New York: Springer Verlag).
[52] MACRY, N., and MILLER, W. H., 1989, *J. chem. Phys.*, **91,** 7026.
[53] MILLER, W. H., 1975, *J. chem. Phys.*, **62,** 1899; 1975, *Ibid.*, **63,** 996.
[54] MILLER, W. H., 1979, *J. chem. Phys.*, **83,** 960.

[55] ALTKORN, R. I., and SCHATZ, G. C., 1980, *J. chem. Phys.*, **72,** 3337.
[56] BENDERSKII, V. A., and GOLDANSKII, V. I., and MAKAROV, D. E., 1991, *Chem. Phys.*, **154,** 407.
[57] BENDERSKII, V. A., GOLDANSKII, V. I., MAKAROV, D. E., and MISOCHKO, E. YA., 1991, *Chem. Phys. Lett.*, **179,** 334.
[58] GARRETT, B. C., and TRUHLAR, D. G., 1979, *J. phys. Chem.*, **83,** 188, 1079.
[59] MILLER, W. H., HANDY, N. C., and ADAMS, J. E., 1980, *J. chem. Phys.*, **72,** 99.
[60] DAKHNOVSKII, YU. I., OVCHINNIKOV, F. F., and SEMENOV, M. B., 1988, *Molec. Phys.*, **63,** 497.
[61] GUTZWILLER, M. C., 1971, *J. Math. Phys.*, **12,** 343.
[62] MILLER, W. H., 1979, *J. phys. Chem.*, **83,** 960.
[63] MILLER, W. H., 1975, *J. chem. Phys.*, **63,** 996.
[64] MASLOV, V. P., and FEDORUK, M. V., 1976, *Quasiclassical Approximation for the Quantum Mechanics Equations* (Moscow: Nauka).
[65] PECHUKAS, P., 1972, *J. Chem. Phys.*, **57,** 5577.
[66] BENDERSKII, V. A., GOLDANSKII, V. I., and MAKAROV, D. E., 1991, *Chem. Phys.*, **159,** 29.
[67] PRASAD, P. N., 1980, *Molec. Crystals liq Crystals*, **58,** 39.
[68] REDINGTON, R. L., CHEN, Y., SCHERER, G. J., and FIELD, R. W., 1988, *J. chem. Phys.*, **88,** 627.
[69] FUKE, K., and KAYA, K., 1989, *J. phys. Chem.*, **93,** 614.
[70] SEKIYA, H., NAGASHIMA, Y., and NISHIMA, Y., 1990, *J. chem. Phys.*, **92,** 5761.
[71] SATO, N., and IWATA, S., 1988, *J. chem. Phys.*, **89,** 2932.
[72] BANGHCUM, S. L., SMITH, Z., WILSON, E. B., and DUERST, R. W., 1984, *J. Am. Chem. Soc.*, **106,** 2260.
[73] TURNER, P., BANGHCUM, S. L., COY, S. L., and SMITH, Z., 1984, *J. Am. Chem. Soc.*, **106,** 2265.
[74] DE LA VEGA, J. R., 1982, *Accts. Chem. Res.*, **15,** 185.
[75] BICERANO, J., SCHAEFER, H. F., and MILLER, W. H., 1983, *J. Am. Chem. Soc.*, **105,** 2550.
[76] CARRINGTON, T., and MILLER, W. H., 1986, *J. chem. Phys.*, **84,** 4364.
[77] SHIDA, N., BARBARA, P. F., and ALMLOF, J. E., 1989, *J. chem. Phys.*, **91,** 4061.
[78] FIRTH, D. W., BARBARA, P. F., and TROMMSDORF, H. P., 1989, *Chem. Phys.*, **136,** 349.
[79] ROSETTI, R., and BRUS, L. E., 1980, *J. chem. Phys.*, **73,** 1546.
[80] ALVES, A. C. P., HOLLAS, J. M., MUSA, H., and RIDLEY, T., 1985, *J. molec. Spectrosc.*, **109,** 99.
[81] SEKIYA, H., TAKESUE, H., NISHIMURA, Y., LI, Z-H, and MORI, F., 1990, *J. chem. Phys.*, **92,** 2790.
[82] REDINGTON, R. L., 1990, *J. chem. Phys.*, **92,** 6447.
[83] SHIMANOUCHI, H., and SASADA, Y., 1973, *Acta crystallogr.* B, **29,** 81.
[84] JANG, D. J., BRUKER, G. A., and KELLEY, D. F., 1986, *J. phys. Chem.*, **90,** 6808.
[85] BARBARA, P. F., WALSH, P. K., and BRUS, L. E., 1989, *J. phys. Chem.*, **93,** 29.
[86] ROSETTI, R., HADDON, R. C., and BRUS, L. E., 1980, *J. Am. Chem. Soc.*, **102,** 6913.
[87] ROSETTI, R., RAYFORD, R., HADDON, R. C., and BRUS, L. E., 1981, *J. Am. Chem. Soc.*, **107,** 4303.
[88] KUNZE, K. L., and DE LA VEGA, J. R., 1984, *J. Am. Chem. Soc.*, **106,** 6528.
[89] FLUDER, E. V., and DE LA VEGA, J. R., 1978, *J. Am. Chem. Soc.*, **100,** 5265.
[90] ROWE, W. F., and DUERST, R. W., 1976, *J. Am. Chem. Soc.*, **98,** 4021.
[91] LOTH, K., GRAF, F., and GUNTHARD, H., 1976, *Chem. Phys.*, **13,** 95.
[92] GRAF, F., LOTH, K., RUDIN, M., FORSTER, M., HA, T-K., and GUNTHARD, H. H., 1977, *Chem. Phys.*, **23,** 327.
[93] SHIAN, W-I, DUESTLER, E. N., PAUL, I. C., and CURTIN, D. Y., 1980, *J. Am. Chem. Soc.*, **102,** 4546.
[94] BRATAN, S., and STROHBUSH, F., 1980, *J. molec. Struct.*, **61,** 409.
[95] DE LA VEGA, J. R., BUSH, J. H., SCHAUBLE, J. H., KUNZE, J. H., and HAGGART, B. E., 1982, *J. Am. Chem. Soc.*, **104,** 3295.
[96] BENDERSKII, V. A., GOLDANSKII, V. I., and MAKAROV, D. E., 1991, *Chem. Phys. Lett.*, **186,** 517.
[97] GRELLMANN, K-H., WELLER, H., and TAUER, E., 1983, *Chem. Phys. Lett.*, **95,** 195.
[98] SIEBRAND, W., WIDMAN, T. A., and ZGIERSKI, M. Z., 1984, *J. Am. Chem. Soc.*, **106,** 4083.
[99] GRELLMANN, K-H., MORDZINSKI, F., and HEINRICH, A., 1989, *Chem. Phys.*, **136,** 201.
[100] MORDZINSKI, A., and KUHNLE, W., 1986, *J. phys. Chem.*, **90,** 1455.

[101] BARTELT, G., EYCHMULLER, A., and GRELLMANN, K. H., 1985, *Chem. Phys. Lett.*, **118,** 568.
[102] BRUNTON, G., GRILLER, D., BARKLAY, L. R. C., and INGOLD, K. U., 1976, *J. Am. Chem. Soc.*, **98,** 6803.
[103] DEWAR, M. J. S., MERZ, K. M., and STEWART, J. J. P., 1985, *J. chem. Soc. Chem. Commun.*, **00,** 166.
[104] ZEBRETTO, F., and ZGIERSKI, M. Z., 1989, *Chem. Phys.*, **130,** 45.
[105] CHANTRANUPONG, L., and WILDMAN, T. A., 1990, *J. Am. Chem. Soc.*, **112,** 4151.
[106] DEYCARD, S., HADHES, L., LUSZTYK, J., and INGOLD, K. U., 1987, *J. Am. Chem. Soc.* **109,** 4954.
[107] ZEBRETTO, F., ZGIERSKI, M. Z., and SIEBRAND, W., 1989, *J. Am. Chem. Soc.*, **111,** 2799.
[108] DEYCARD, S., LUSZTYK, J., INGOLD, K. B., ZEBRETTO, F., ZGIERSKI, M. Z., and SIEBRAND, W., 1988, *J. Am. Chem. Soc.*, **110,** 6721.
[109] SMEDARCHINA, Z., SIEBRAND, W., and ZEBRETTO, F., 1989, *Chem. Phys.*, **136,** 289.
[110] HENING, J., and LIMBACH, H. H., 1979, *J. chem. Soc. Farad. Trans.* II, **75,** 752.
[111] SCHLABACH, M., WEHRLE, B., and LIMBACH, H. H., 1986, *J. Am. Chem. Soc.*, **108,** 3856.
[112] CROSSLEY, M. J., FIELD, L. D., and HARDING, M. M., 1988, *J. Am. Chem. Soc.*, **109,** 2335.
[113] FRYDMAN, L., OLIVIERI, F. C., and DIAZ, L. E., 1988, *J. Am. Chem. Soc.*, **110,** 336.
[114] LIMBACH, H. H., HENNIG, J., GERRITZER, D., and RUMPEL, H., 1982, *Farad. Disc. Chem. Soc.*, **74,** 229.
[115] BUTTENHOFF, T. J., and MOORE, C. B., 1988, *J. Am. Chem. Soc.*, **110,** 8336.
[116] VOLKER, S., and VAN DER WAALS, J. H., 1976, *Molec. Phys.*, **32,** 1703.
[117] SARAI, A., 1982, *J. chem. Phys.*, **76,** 5554.
[118] MERZ, K. M., and REYNOLDS, C. H., 1988, *J. Chem. Soc. Chem. Commun.*, **00,** 90.
[119] INGHAM, K. C., and EL-BAYOUMI, M. A., 1974, *J. Am. Chem. S.*, **96,** 1674.
[120] TOKUMURA, K., WOTANABE, Y., and ITOH, M., 1986, *J. phys. Chem.*, **90,** 2362.
[121] MEIER, B. H., GRAF, F., and ERNST, R. R., 1982, *J. chem. Phys.*, **76,** 767.
[122] NAGAOKA, S., TERAO, T., IMASHIRO, F., SAIKA, N., HIROTA, N., and NAYASHI, S., 1983, *J. chem. Phys.*, **79,** 4694.
[123] IDZIAK, S., and PISLEWSKI, N., 1987, *Chem. Phys.*, **III,** 439.
[124] HORSEWILL, A. J., and AIBOUT, A., 1989, *J. Phys. Condens. Matter.*, **I,** 9609.
[125] RAMBAUD, C., OPPENLANDER, A., TROMMSDORFF, H. P., and VIAL, J. C., 1990, *J. Luminescence,* **45,** 310.
[126] SAITON, T., MORI, K., and ITON, R., 1981, *Chem. Phys.*, **60,** 161.
[127] SKINNER, J. L., and TROMMSDORFF, H. P., 1988, *J. chem. Phys.*, **89,** 897.
[128] OPPENLANDER, A., RAMBAND, C., TROMMSDORFF, H. P., and VIAL, J. C., 1989, *Phys. Rev. Lett.*, **63,** 1432.
[129] PRASS, B., COLPA, J. R., and STEHLIK, D., 1988, *Chem. Phys.*, **88,** 191.
[130] PRASS, B., COLPA, J. R., and STEHLIK, D., 1989, *Chem. Phys.*, **136,** 187.
[131] HOSHI, N., YAMANCHI, S., and HIROTA, N., 1990, *J. phys. Chem.*, **94,** 7523.
[132] BRUCKER, G. A., and KELLEY, D. F., 1989, *Chem. Phys.*, **136,** 213.
[133] SPRAGUE, E. D., and WILLIAMS, F., 1971, *J. Am. Chem. Soc.*, **93,** 787.
[134] CAMPION, A., and WILLIAMS, F., 1972, *J. Am. Chem. Soc.*, **94,** 7633.
[135] LE ROY, A. R. J., SPROGUE, E. D., and WILLIAMS, F., 1972, *J. phys. Chem.*, **16,** 545.
[136] HUDSON, P. L., SHIOTANI, M., and WILLIAMS, F., 1977, *Chem. Phys. Lett.*, **48,** 193.
[137] BOLSHAKOV, B. V., and TOLKACHEV, V. A., 1976, *Chem. Phys. Lett.*, **40,** 486.
[138] BOLSHAKOV, B. V., STEPANOV, A., A., and TOLKACHEV, V. A., 1980, *Int. J. Chem. Kin.*, **12,** 271.
[139] DOBA, T., INGOLD, K. U., SIEBRAND, W., and WILDMAN, T. A., 1984, *J. phys. Chem.*, **88,** 3165.
[140] FURUE, H., and PACEY, P. D., 1986, *J. phys. Chem.*, **90,** 397.
[141] TORIYAMA, K., and IWASAKI, M., 1979, *J. Am. Chem. Soc.*, **101,** 2516.
[142] KLAFFER, J., and SHLESINGER, M. E., 1986, *Proc. Natl. Acad. Sci. U.S.A.*, **83,** 848.
[143] ZASKULNIKOV, V. M., VYAZOVKIN, V. L., BOLSHAKOV, B. V., and TOLKATCHEV, V. A., 1981, *Int. J. Chem. Kin.*, **13,** 707.
[144] KLOCHIKHIN, V. A., and TRAKHTENBERG, L. I., 1984, *Zh. Fiz. Him.*, **58,** 2877 (in Russian).
[145] BURSHTEIN, A. I., KLOCHIKHIN, V. A., and TRAKHTENBERG, L. I., 1984, *Himicheskaya Fizika,* **3,** 155 (in Russian).
[146] TRAKHTENBERG, L. I., 1982, *Himicheskaya Fizika,* **1,** 53.
[147] WALCH, S. P., and DINNING, T. H., 1980, *J. chem. Phys.*, **72,** 3221.

[148] DUBINSKAYA, A. M., 1975, *Vysokomol. Soed.* A, **17,** 815.
[149] SENTHILNATHAN, V. P., and PLATZ, M. S., 1982, *J. Am. Chem. Soc.*, **102,** 7637.
[150] PLATZ, M. S., SENTHILNATHAN, V. P., WRIGHT, B. B., and MCCUROLY, C. W., 1982, *J. Am. Chem. Soc.*, **104,** 6494.
[151] BAUSCHLITHER, C. W., BENDER, C. F., and SCHAEFER, H. F., 1976, *J. Am. Chem. Soc.*, **98,** 3072.
[152] YAKIMCHENKO, O. E., and LEBEDEV, Ya.S., 1971, *Int. J. Radiat. Phys. Chem.*, **3,** 17.
[153] TORIYAMA, K., NUNOME, K., and IWASAKI, M., 1977, *J. Am. Chem. Soc.*, **99,** 5823.
[154] GERBER, R. B., and ALIMI, R., 1990, *Chem. Phys. Lett.*, **173,** 393.
[155] GERBER, R. B., BUCH, V., and RATNER, M. A., 1982, *J. chem. Phys.*, **77,** 3022.
[156] VOLNL, J., and ALEFELD, G., 1978, *Hydrogen in Metals*, Topics in Appl. Phys. V. 28, p. 321 (Berlin: Springer Verlag).
[157] FUKAI, Y., and SUGIMOTO, H., 1985, *Adv. Phys.*, **34,** 263.
[158] RICHTER, D., 1986, *Hyperfine Inter.*, **31,** 168.
[159] PEKAR, S. I., 1953, *Usp. Fiz. Nauk.*, **50,** 197 (in Russian).
[160] PUSKA, M. J., and NIELMIEN, R. M., 1984, *Phys. Rev.* B., **29,** 5382.
[161] HOLSTEIN, T., 1959, *Ann. Phys.* (N.Y.). **8,** 325, 343.
[162] STONEHAM, A. M., 1972, *Berichte Bunsengeselsch. Phys. Chem.*, **76,** 816.
[163] KUBO, R., and TOYAZOWA, Y., 1955, *Progr. theor. Phys.*, **13,** 160.
[164] LEVICH, V. G., and DOGONADZE, R. R., 1959, *Dokl. Akad. Nauk. USSR*, **124,** 123 (in Russian).
[165] MARCUS, R. A., 1964, *Ann. Rev. Phys. Chem.*, **15,** 155.
[166] OVCHINNIKOV, A. A., and OVCHINNIKOVA, M.Ya., 1969, *Zh. Exp. Theor. Fiz.*, **56,** 1278 (in Russian).
[167] DOGONADZE, R. R., and KUZNETSOV, A. M., 1975, *Prog. Surf. Sci.*, **6,** 1.
[168] OVCHINNIKOV, A. A., and OVCHINNIKOVA, M.Ya., 1982, *Adv. quant. Chem.*, **16,** 161.
[169] ULSTRUP, J., 1979, *Charge Transfer Process in Condensed Media.* (Berlin: Springer Verlag).
[170] BOCKRIS, J. O. M., and KHAN, S. U.M., 1979, *Quantum Elektrochemistry* (New York: Plenum).
[171] EMIN, D., BASKES, M. I., and WILSON, W. D., 1979, *Phys. Rev. Lett.*, **42** 791.
[172] DHAWAN, L. L., and PRAKASH, S., 1984, *J. Phys.* F, **14,** 2329.
[173] CHAKRABORTY, B., HEDEGARD, P., and NYLENS, M., 1988, *J. Phys.* C, **21,** 3437.
[174] TULLY, J. C.,1980, *Ann. Rev. Phys. Chem.*, **31,** 319.
[175] EHRLICH, G., and STOLT, K., 1980, *Ann. Rev. Phys. Chem.*, **31,** 603.
[176] DIFOGGIO, R., and GOMER, R., 1982, *Phys. Rev.* B, **25,** 3490.
[177] WAND, S. C., and GOMER, R., 1985, *J. chem. Phys.*, **83,** 4193.
[178] JAQUET, R., and MILLER, W. H., 1985, *J. phys. Chem.*, **89,** 2139.
[179] LAUDERDALE, J. G., and TRUHLAR, D. G., 1985, *Surf. Sci.*, **164,** 558.
[180] TRINGIIDES, M., and GOMER, R., 1986, *Surf. Sci.*, **166,** 440.
[181] AUERBACH, A., FREED, K. F., and GOMER, R. 1987, *J. chem. Phys.*, **86,** 2356.
[182] TRUONG, T., and TRUHLAR, D. G., 1987, *J. phys. Chem.*, **91,** 6229.
[183] MUTTALIB, K. A., and SETHNA, J., 1985, *Phys. Rev.* B, **32,** 3462.
[184] MCGREERY, J. H., and WOLKEN, G. 1975, *J. chem. Phys.*, **63,** 2340.
[185] BLANCHET, G. B., DINAVCLO, N. J., and PLUMMER, E. W., 1982, *Surf. Sci.*, **118,** 496.
[186] KATUNIN, A.Ya., LUKASHEVICH, I. I., OROZMAMATOV, S. T., SKLAROVSKII, V. V., SURAEV, V. V., FILIPPOV, V. V., and SHEVTSOV, V. A., 1981, *Pis'ma Zh. Exp. Teor. Fiz.*, **34,** 375.
[187] IVLEV, A. V., KATUNIN, A. YA., LUKASHEVICH, I. I., SKLAROVSKII, V. V., SURAEV, V. V., and FILIPOV, V. V., 1983, *Pis'ma Zh. Exp. Teor. Fiz.*, **38,** 317.
[188] ITSKOVSKIH, A. S., KATUNIN, A. YA., and LUKASHEVICH, I. I., 1986, *Zh. Exp. Teor. Fiz.*, **91,** 1832.
[189] MIYAZAKI, T., LEE, K-P., FUEKI, K., and TAKEUCHI, A., 1984, *J. Phys. Chem.*, **88,** 4959.
[190] MIYAZAKI, T., and LEE, K-P., 1986, *J. Phys. Chem.*, **90,** 400.
[191] LEE, K-P., MIYAZAKI, T., FUEKI, K., and GOTOH, K., 1987, *J. phys. Chem.*, **91,** 180.
[192] MIYAZAKI, T., IWATA, N., LEE, K-P., and FUEKI, K., 1989, *J. phys. Chem.*, **93,** 3352.
[193] MIYAZAKI, T., IWATA, N., FUEKI, K., and HASE, H., 1990, *J. phys. Chem.*, **94,** 1702.
[194] MIYAZAKI, T., 1991, *Chem. Phys. Lett.*, **182,** 35.
[195] WEINHAUS, F., MEYER, H., and MYERS, S. M., 1973, *Phys. Rev.* B, **7,** 2960.
[196] EBNER, C., and SAND, C. C., 1972, *Phys. Rev.* A, **5,** 2625.
[197] SILVERA, L. F., 1980, *Rev. mod. Phys.*, **52,** 393.

[198] VORONIN, A. I., and OSHEROV, V. I., 1990, *Dynamics of Molecular Reactions* (Moscow: Nauka).
[199] TAKAYNAGI, T., MASAKI, N., NAKATURA, K., OKAMOTO, M., and SATO, S. 1987, *J. chem. Phys.*, **86,** 6133.
[200] HANCOCK, G. C., MEAD, C. A., TRUHLAR, D. G., and VARANDAS, A. J. S., 1989, *J. chem. Phys.*, **91,** 3492.
[201] SKODJE, T., TRUHLAR, D. G., and GARRETT, B. C., 1982, *J. chem. Phys.*, **77,** 5955.
[202] DUBINSKAYA, A. M., 1990, *Sov. Sci. Rev.* B. *Chem.*, **14,** 37.
[203] DUBINSKAYA, A. M., and BUT'AGIN, P. YU., 1973, *Dokl. Akad. Nauk. USSR*, **211,** 141.
[204] TORIYAMA, K., IWASAKI, M., and NUNOME, K., 1979, *J. chem. Phys.*, **71,** 1698.
[205] TORIYAMA, K., IWASAKI, M., and NUNOME, K., 1980, *J. chem. Phys.*, **84,** 2374.
[206] IWASAKI, M., TORIYAMA, K., NUNOME, K., and FUKAYA, M., 1981, *J. phys. Chem.*, **85,** 1326.
[207] POLLACK, G. L., 1964, *Rev. mod. Phys.*, **36,** 748.
[208] TAUNS, CH., and SHAVLOV, D., 1959, *Radiospectroscopy* (Moscow: Inostr. Lit.).
[209] GIRARDET, C., ABOUAF-MARGUIN, L., GAUTHIER-ROY, B., and MAILLARD, D., 1984, *Chem. Phys.*, **89,** 415. 431.
[210] GIRARDET, C., and LAKHLIFI, A., 1985, *J. chem. Phys.*, **83,** 5506; 1989. *Ibid.*, **91,** 1423.
[211] PETERNELJ, J., and JENCIE, I., 1989, *J. Phys.* A., **22,** 1941.
[212] CLOUGH, S., HORSENWILL, A. J., and MCDONALD, P. J., 1985, *Phys. Rev. Lett.*, **55,** 1794.
[213] JANIC, J. A., 1980, *Phys. Rep.*, **66,** 20.
[214] ABED, K. J., and CLOUGH, S., 1987, *Chem. Phys. Lett.*, **142,** 209.
[215] ABED, K. J., CLOUGH, S., HORSEWILL, A. J., and MOHAMMED, M. A., 1988, *Chem. Phys. Lett.*, **147,** 624.
[216] HORSEWILL, A. J., ALSANOOSI, A. M., and CARLILE, C. J., 1987, *J. Phys.* C. **20,** L 869.
[217] ALSANOOSI, A. M., HORSEWILL, A. J., and CLOUGH, S., 1989, *J. Phys. Condens. Matter.*, **1,** 643.
[218] CAVAGNAT, D., and PESQUER, M., 1986, *J. phys. Chem.*, **90,** 3289.
[219] CAILLET, J., and CLAVERIC, P., 1975, *Acta crystallogr.* A, **31,** 448.
[220] CAVAGNAT, D., TREVINO, S. F., and MAGERL, A., 1989, *J. Phys. Condens. Matter.* **I,** 10047.
[221] KOONER, Z. S., and VAN HOOK, W. A., 1988, *J. chem. Phys.*, **92,** 6414.
[222] CROMER, D. T., RYAN, R. R., and SCHIFFERL, D., 1985, *J. phys. Chem.*, **89,** 2315.
[223] CAVAGNAT, D., MAGERL, A., VETTIER, C., and CLOUGH, S., 1986, *J. Phys.* C., **19,** 665.
[224] CAVAGNAT, D., LASCOMBRE, J., LASSEGUES, J. C., HORSEWILL, A. J., HEIDEMANN, A., and SUCK, J. B., 1984, *J. Phys.* (Paris), **45,** 97.
[225] SMITH, D., 1975, *J. chem. Phys.*, **63,** 5003.
[226] HULLER, A., and RAICH, J., 1979, *J. chem. Phys.*, **71,** 3851.
[227] PUNKINEN, V., 1980, *Phys. Rev.* B, **21,** 54.
[228] SMITH, D., 1990, *J. Chem. Phys.*, **93,** 10.
[229] ALLEN, P. S., 1974, *J. Phys.* C, **7,** L22.
[230] CLOUGH, S., 1976, *J. Phys.* C, **9,** L523.
[231] WHITMAN, D. W., and CARPENTER, B. K., 1982, *J. Am. Chem. Soc.*, **104,** 6473.
[232] CARPENTER, B. K., 1983, *J. Am. Chem. Soc.*, **105,** 1701.
[233] HUANG, M. J., and WOLFSBERG, M., 1984, *J. Am. Chem. Soc.*, **106,** 4039.
[234] DEWAR, M. J. S., MERZ, K. M., and STEWART, J. J. P., 1984, *J. Am. Chem. Soc.*, **106,** 4040.
[235] CARSKY, P., BARTLETT, R. J., FITZGERALD, G., NOGA, J., and SPIRKO, V., 1988, *J. chem. Phys.*, **89,** 3008.
[236] ZEBRETTO, F., and ZGIERSKI, M. Z., 1989, *Chem. Phys.*, **130,** 45.
[237] YANNONI, C. S., MACHO, V., and MYHRE, P. C., 1982, *J. Am. Chem. Soc.*, **104,** 7380.
[238] MYHRE, P. C., MCLAREN, K. L., and YANNONI, C. S., 1985, *J. Am. Chem. Soc.*, **107,** 59.
[239] FONG, F. K., 1974, *J. Am Chem. Soc.*, **96,** 7638.
[240] BRICKMAN, J., 1981, *Ber. Bunsenges. phys. Chem.*, Bd. **85,** S. 106.
[241] BUCHWALTER, S. L., and CLOSS, G. H., 1979, *J. Am. Chem. Soc.*, **101,** 4688.
[242] MENAND, A., and KINGHAM, D. R., 1984, *J. Phys.* D., **17,** 203.
[243] MENAND, A., and KINGHAM, D. R., 1985, *J. Phys.* C, **18,** 4539.
[244] HOASE, G., ASSCHER, M., and KOSLOFF, R., 1989, *J. chem. Phys.*, **90,** 3346.
[245] FREI, H., FREDIN, L., and PIMENTEL, G. C., 1981, *J. chem. Phys.*, **74,** 397.
[246] FREI, H., and PIMENTEL, G. C., 1983, *J. chem. Phys.*, **78,** 3698.
[247] SMITH, G. R., and GUILLORY, W. A., 1977, *J. molec. Spectrosc.*, **68,** 223.
[248] SMITH, G. R., and GUILLORY, W. A., 1977, *Int. J. Chem. Kin.*, **9,** 953.

[249] LUCAS, D., and PIMENTEL, G. C., 1979, *J. phys. Chem.*, **83,** 2311.
[250] ARNOLD, C., GETTYS, N. S., THOMPSOK, D. L., and RAFF, L. M., 1986, *J. chem. Phys.*, **84,** 3803.
[251] VISWANATHAN, R., and RAFF, L. M., 1983, *J. phys. Chem.*, **87,** 3251.
[252] SUZAKAWA, H. H., and RAFF, L. M., 1975, *J. chem. Phys.*, **62,** 3743, 4727.
[253] AUSTIN, R. H., BEESON, K. W., EISENSTEIN, L., FRAUNFELDER, H., and GUNSALUS, I. C., 1975, *Biochem.*, **14,** 5355.
[254] ALBERDING, N., AUSTIN, R. H., CHAN, S. S., EISENSTEIN, L., FRAUNFELDER, H., GUNSALUS, I. C., and NORDLUNG, T. M., 1976, *J. chem. Phys.*, **65,** 4701.
[255] ALBERDING, N., AUSTIN, R. H., BEESON, K. W., CHAN, S. S., EISENSTEIN, L., FRAUNFELDER, H., and NORDLUNG, T. M., 1976, *Science*, **192,** 1002.
[256] ALBERDING, N., CHAN, S. S., EISENSTEIN, L., FRAUNFEDLER, H., GOOD, D., GUNSALUS, I. C., NORDLUNG, T. M., PERUTZ, M. F., REYNOLDS, A. H., and YUE, K. T., 1980, *Phys. Rev. Lett.*, **44,** 1156.
[257] CHANCE, B., FISCHETTI, R., and ROWERS, L., 1983, *Biochem.*, **22,** 3820.
[258] DEBRUNNER, P., and FRAUNFELDER, H., 1982, *Experience in Biochemical Perception.* (New York: Academic), 326.
[259] MISOCHKO, E. YA., FILIPPOV, P. G., BENDERSKII, V. A., OVCHINNIKOV, A. A., BARKALOV, I. M., and KIRUKHIN, D. P., 1980, *Dokl. Akad. Nauk USSR.*, **253,** 163.
[260] FILIPPOV, P. G., MISOCHKO, E.YA., KULIKOV, A. V., BENDERSKII, V. A., and OVCHINNIKOV, A., 1981, *Dokl. Akad. Nauk. USSR*, **256,** 1173.
[261] BENDERSKII, V. A., MISOCHKO, E.Ya., OVCHINNIKOV, A. A., and FILIPPOV, P. G., 1983, *Zh. Fiz. Khim.*, **57,** 1079 (in Russian).
[262] BENDERSKII, V. A., MISOCHKO, E.Ya., and FILIPPOV, P. G., 1986, *Himicheskaya Fizika*, **5,** 955 (in Russian).
[263] BENDERSKII, V. A., TITOV, V. A., and FILIPPOV, P. G., 1984, *Dokl. Akad. Nauk USSR*, **278,** 1157.
[264] BENDERSKII, V. A., OVCHINNIKOV, A. A., and FILIPPOV, P. G., 1988, *Reactivity of Solids*, **4,** 228.
[265] DAKHNOVSKII, Y. I., OVCHINNIKOV, A. A., and BENDERSKII, V. A., 1982, *Chem. Phys.*, **66,** 93.
[266] KIRUKHIN, D. P., KAPLAN, A. M., BARKALOV, I. M., GOLDANSKII, V. I., 1972, *Dokl. Akad. Nauk USSR.*, **206,** 147.
[267] KIRUKHIN, D. P., KAPLAN, A. M., BARKALOV, I. M., and GOLDANSKII, V. I., 1972, *Vysokomol. Soed.* A, **14,** 2115.
[268] GOLDANSKI, V. I., 1975, *Uspekhi Himii*, **44,** 2121.
[269] GOLDANSKII, V. I., 1976, *Ann. Rev. Phys. Chem.*, **27,** 85.
[270] GOLDANSKII, V. I., 1979, *Nature*, **279,** 109.
[271] GERASIMOV, G. N., and ABKIN, A. D., 1984, *Him. Fiz.*, **1,** 181.
[272] DOLOTOV, S. M., YUZHAKOVA, O. A., GERASIMOV, G. N., and ABKIN, A. D., *Vysokomol. Soed.*, **25,** 585.
[273] MANSUETO, E. S., JU, C. Y., and WHIGHT, C. A., 1989, *J. Phys. Chem.*, **93,** 4404.
[274] MANSUETO, E. S., and WHIGHT, C. A., 1989, *J. Am. Chem. Soc.*, **111,** 1900.
[275] MISOCHKO, E., YA., BENDERSKII, V. A., GOLDANSKII, V. I., and KONONIKHINA, V. V., 1991, *Dokl. Akad. Nauk USSR.*, **316,** 403.
[276] GERASIMOV, G. N., DOLOTOV, S. M., and ABKIN, D. A., 1980, *Int. J. Radiat. Phys. Chem.*, **15,** 405.
[277] BASILEVSKY, M. V., GERASIMOV, G. N., and PETROCHENKO, S. I., 1982, *Chem. Phys.*, **72,** 349.
[278] BASILEVSKY, M. V., GERASIMOV, G. N., and PETROCHENKO, S. I., 1984, *Him. Fiz.*, **3,** 162.
[279] SEMENOV, N. N., 1960, *Himiya i Tehnologiya Polimerov*, **7–8,** 196 (in Russian).
[280] WENG, S-X, TORRIE, B. H., and POWELL, B. M., 1989, *Molec. Phys.*, **68,** 25.
[281] KIRYUKHIN, D. P., BARKALOV, I. M., and GOLDANSKII, V. I., *Dokl. Akad. Nauk USSR*, **238,** 388.
[282] KIRYUKHIN, D. P., BARKALOV, I. M., and GOLDANSKII, V. I., 1979, *J. Chim. Phys.*, **76,** 1013.
[283] BARKALOV, V. I., GOLDANSKII, V. I., KIRYUKHIN, D. P., and ZANIN, A. M., *Chem. Phys. Lett.*, **73,** 273.
[284] TITOV, V. A., FILIPPOV, P. G., MISOCHKO, E.Ya., USMANOV, R. D., and BENDERSKII, V. A., 1986, *Dokl. Akad. Nauk USSR*, **290,** 1414.
[285] KIMELFELD, J. M., LUMER, E. V., and SHWEDCHIKOV, A. P., 1973, *Chem. Phys. Lett.*, **21,** 429.

[286] SERGEEV, G. B., SMIRNOV, V. V., and SHILINA, M. I., *Dokl. Akad. Nauk USSR*, **274,** 123.
[287] HASSEL, O., and ROMMING, C., 1962, *Quart. Rev.*, **14,** 1.
[288] FREDIN, L., and NELANDER, B., 1973, *J. molec. Struct.*, **16,** 205.
[289] CHILT, G., GOLDFINGER, P., HUYBRECHTS, G., MARTINES, G., and VERBEC, G., 1963, *Chem. Rev.*, **63,** 355.
[290] BENDERSKII, V. A., GOLDANSKII, V. I., and MISOCHKO, E.Ya., 1990, *Dokl. Akad. Nauk USSR*, **311,** 1148.
[291] STEPANOV, N. F., GISNINA, O. E., SERGEEV, G. B., and SMIRNOV, V. V., *Teor. Exp. Him.*, **14,** 809 (in Russian).